THE ELECTRICAL PROPERTIES OF RUTHENIUM-ALUMINIUM ALLOYS

by Ernest Gregory Smith

A thesis submitted to the Faculty of Engineering, University of Cape Town in part fulfilment of the requirements for the degree of Master of Science (Applied Science)

Department of Materials Engineering
University of Cape Town
January 1995

Abstract

The electrical properties of platinum, gold-palladium and a selection of alloys from the ruthenium-aluminium system have been studied at high temperatures (up to 1000°C). The majority of the ruthenium-aluminium alloy compositions studied lie near or in the ruthenium aluminide phase field. Ruthenium aluminide is a B2 structure intermetallic which is suited to high temperature applications because in addition to a high melting point (2060°C), oxidation resistance to 1200°C and high temperature strength, it is also relatively ductile at room temperature. The possibility of high temperature electrical applications required an investigation of the electrical properties of ruthenium-aluminium alloys as compared to platinum and gold-palladium. Two sets of apparatus, capable of measuring the resistivity and thermo-e.m.f. to high temperatures, were constructed and used to obtain the first experimental results for the electrical properties of ruthenium-aluminium alloys. Chemical analysis of these alloys has been performed for the first time, and together with energy dispersive spectroscopy, has revealed a composition at which there is a resistivity minimum and a positive thermo-e.m.f maximum, which appears to be associated with the formation of the ordered ruthenium aluminide phase. The resistivity and the temperature dependence of resistivity of some ruthenium-aluminium alloys are similar to that of platinum, the least resistive of the three materials investigated.

Acknowledgements

The following people have assisted me and are due thanks:

My supervisor, Dr Candace Lang, for many useful discussions and guidance. Dr Lang's enthusiasm and positive attitude greatly assisted the completion of this degree, not to mention the initiative shown in setting the project in motion.
Dr Herman Steyn and Dr Michael Cortie of the Council for Mineral Technology (MINTEK), for their encouraging attitude, interest and practical assistance.

Dr John Tapson, of the Department of Electrical and Electronic Engineering, Dr Richard Doyle, of the Interdisciplinary Research Centre in Superconductivity at the University of Cambridge, Andrew Dacre of Sasol, and my brother, Quinton Smith, of Plessy SA for their help with the design and construction of the electronic circuitry.

My father, Frederick Smith of Dorbyl Marine, for astute comments on the design of the apparatus and contribution to the construction of the furnace loading mechanism.
Glen Newins (workshop), for patience, commitment to quality and doing it right first time. Nicholas Dreze (workshop) for skill in turning intricate designs into reality.
Gary Hockney of Ceramiart Dental Laboratories for generously donating time and superb skills to producing the intricate alumina components required, without which this project would never have succeeded.

My brother, Bernard Smith of Innovex Computer Consultants, who assisted me with the computing.
Mrs J.D. Sharland and Mrs A.C. Ball, administrators who were efficient and friendly.
My fiancé, Sandra Emms, of AECI's Materials Department, for getting me interested in Materials Engineering in the first place and providing me with the motivation for completing this degree timeously.
My fellow students in the Materials Engineering Department, for making the department a pleasant place to be.
The financial support of MINTEK and the Foundation for Research Developement is gratefully acknowledged.

Dedicated to my parents , Fred and Magdalene Smith, for their interest, support and the opportunities they have given me.

Table of Contents

1. Introduction

Ruthenium-aluminium alloys are suited to high temperature applications in view of their high melting point and oxidation resistance[1]. Confidential industrial trials indicated that ruthenium-aluminium alloys could compete with platinum and gold-palladium as a high temperature electrical material. In order to confirm ruthenium-aluminium alloys as a competitor for platinum and gold-palladium a knowledge of its electrical properties at high temperatures was required. The electrical properties of ruthenium-aluminium alloys have not been the subject of any published study and a knowledge of these properties was required in order to optimize ruthenium-aluminium alloys for high temperature electrical applications. The electrical properties of ruthenium-aluminium alloys were studied and compared to those of platinum and gold-palladium for this thesis.

A review of the relevant literature has been conducted in Chapter Two. The ductility of ruthenium-aluminium alloys relative to other intermetallics[i] has caused its microstructure, electronic structure, mechanical properties and oxidation resistance to be studied for mechanical applications[2]. This forms the basis of a review of ruthenium-aluminium alloys which concentrates on the electronic structure and oxidation resistance as is appropriate to high temperature electrical applications. Resistivity and thermo-e.m.f. in metals, alloys and intermetallics are reviewed so as to introduce ideas relevant to this study. A prerequisite to the work presented was the selection of methods to measure the properties and the design and construction of the required apparatus. A review of the methods selected is included in the literature review.

In order to optimize ruthenium-aluminium alloys it was necessary to determine the dependence of the properties of interest on composition. Previously workers have had to rely on nominal compositions owing to the extreme chemical resistance of ruthenium-aluminium alloys which prevents the dissolution required for chemical analysis[3]. In

Chapter Three (Experimental Methods) a chemical analysis is reported and a comparison with energy dispersive spectroscopy is made. The processing route of ruthenium-aluminium alloys is also reported.

It was felt necessary to devote a separate chapter to detailing the construction of the apparatus in view of the design innovations that had to be made in order to i) apply the selected methods to the ruthenium-aluminium alloys and ii) be able to use the laboratory bench furnaces available. The brittleness of ruthenium-aluminium alloys is a determining factor in preparing experimental specimens, the variety of shapes and dimensions of specimens being limited by the machining constraints that apply to brittle specimens. The specimen stage design had to allow for this and the design had to be such that the probes and conductors could be orientated to minimise the effect of electrical noise in the furnace environment. The design also had to accommodate the spring loading mechanism which was necessary to allow for expansion and ensure good electrical contact. The problems that were encountered in building the apparatus and the design solutions found are detailed in Chapter Four.

The results obtained for the well documented materials such as platinum and gold-palladium indicated that the equipment designed and constructed was accurate. The electrical properties of ruthenium-aluminium alloys were then measured at various compositions and over a wide range of temperature (20°C to 1000°C for resistivity and to 400°C for thermo-e.m.f.). This represents the first study of the electrical properties of ruthenium-aluminium alloys.

The resistivity of ruthenium-aluminium alloys is found to be similar to that of platinum and to have a similar dependence on temperature. The dependence of resistivity on composition in ruthenium-aluminium alloys is as expected for a binary transition metal aluminide, showing a resistivity minimum near 50 atomic % aluminium. Thermo-e.m.f. is at a maximum at the same composition as that at which the resistivity minimum occurs, which corresponds to the formation of the ordered ruthenium aluminide phase.

2. Literature Review

There are three themes in this literature review: i) the three materials: platinum (transition metal), gold-palladium (transition metal alloy) and ruthenium aluminide (transition metal intermetallic), ii) the electrical resistivity and thermo-e.m.f. of these types of materials and iii) the methods of measuring these electrical properties. The review covers pure metals, alloys and intermetallics. Models which relate the electronic structure of materials to the thermo-e.m.f. and resistivity, and the dependence of these properties on temperature and composition are reviewed. The theoretical background to the experimental methods used completes the literature review.

2.1 Resistivity and thermo-e.m.f. in metals

Pure metals are reviewed prior to reporting the dependence on temperature and composition of resistivity and thermo-e.m.f. for gold-palladium. Issues pertinent to the resistivity and thermo-e.m.f. of intermetallics are highlighted by reviewing the electrical properties of three transition metal intermetallics: cobalt aluminide, nickel aluminide and iron aluminide. Finally the present knowledge of the atomic and electronic structure of ruthenium aluminide is presented as a basis for the later discussion of the electrical properties of ruthenium-aluminium alloys.

2.1.1 Pure metals

Platinum, a transition metal with a high density of d electrons at the Fermi energy, and copper, a simple metal with only s electrons at the Fermi energy, have different electrical properties. Copper is included in this review, as discussing differences in the electronic structure between copper and platinum introduces ideas helpful to later discussion.

2.1.1.1 Electronic structure of platinum and copper

In Table 2.1 the electrical properties of platinum are seen to differ from the electrical properties of copper and this is a consequence of the different electronic structure of the two metals.

Table 2.1: Electrical properties of platinum and copper

Metals	Electronic Structure	Resistivity (μΩcm)	Thermo-e.m.f. (μV/K)	dρ/dT (μΩcm/K)
platinum	s and d electrons at Fermi energy	10.6 (20°C)[4]	-4 (0°C)[5]	0.0332
copper	only s electrons at Fermi energy	1.7 (20°C)[4]	1.8 (27°C)[6]	0.0076

An idealised schematic diagram, showing the variation of the density of states with energy of copper, is shown in Figure 2.1. This shows that the Fermi energy of copper falls exclusively in the s band. Copper conforms to the simple metal model in that there are only s electrons at the Fermi energy. This results in a nearly spherical Fermi surface as shown in Figure 2.2.

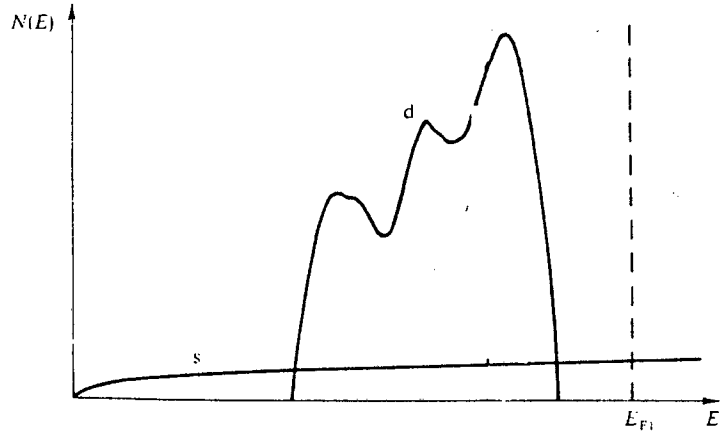

Figure 2.1: Schematic variation of density of states with energy for a simple metal such as copper (after Rossiter[7]).

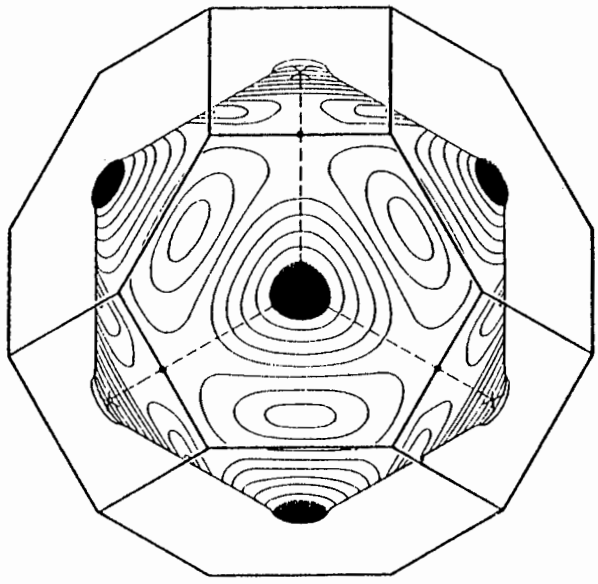

Figure 2.2: Schematic diagram of the Fermi surface for copper (after Ziman[8]).

An idealised schematic diagram showing the variation of density of states with energy for platinum is shown in Figure 2.3. A salient feature is the overlap of s and d electron bands at the Fermi energy showing that both are present at the Fermi surface. This is characteristic of a transition metal. This complicates the Fermi surface, making it non-spherical as shown in Figure 2.4. Platinum is classified as a non-simple metal due to its complicated electronic structure.

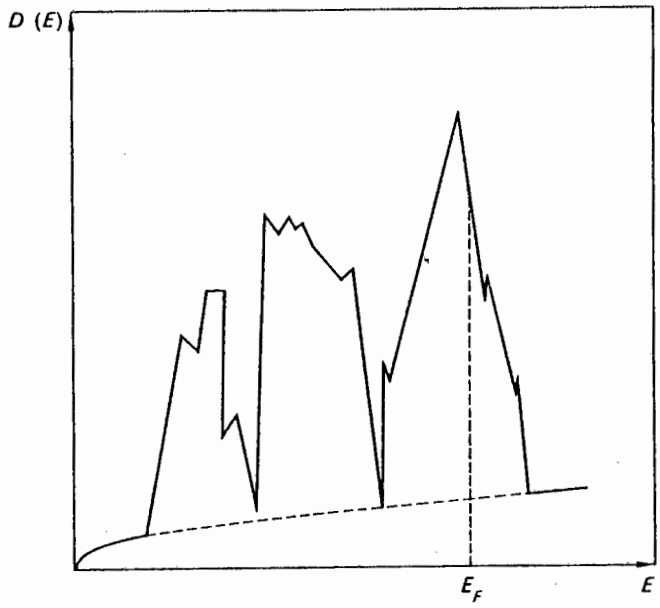

Figure 2.3: Schematic variation of density of states with energy for a transition metal such as platinum (after Dugdale[12]).

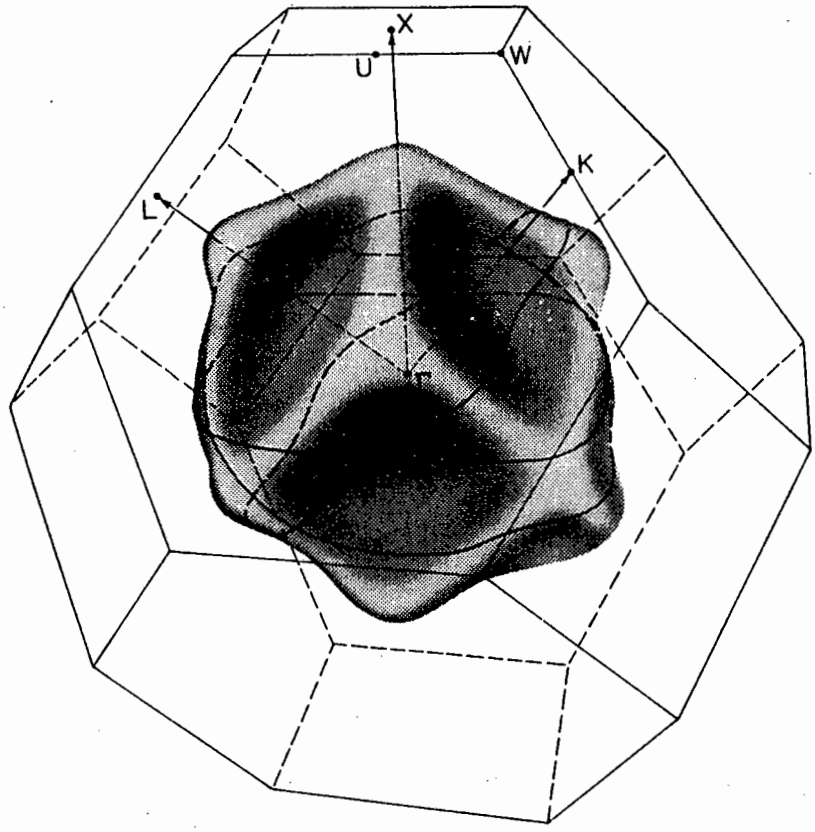

Figure 2.4: Schematic diagram of Fermi surface of platinum (after Ketterson and Windmiller[9]).

2.1.1.2 Resistivity of platinum and copper

The scattering of conduction electrons, i.e. those near the Fermi energy, causes a material to be electrically resistive. There are two main contributions to scattering as is expressed in the following equation:

$$\rho = \rho_i + \rho_{ep}(T) \qquad \text{Equation 2.1}$$

The first term in equation 2.1 arises from impurities, dislocations, grain boundaries or any other lattice defects which disrupt the periodic variation of the potential in the lattice, creating scattering sites. This term is independent of temperature provided that the structure is not susceptible to temperature induced transformations. As temperature increases from absolute zero packets of thermal vibrations (phonons) travel through the lattice and also scatter electrons. This is termed an electron-phonon interaction and is represented by the second term. As temperature increases the value of this term increases.

When modelling the residual resistivity of simple metals such as copper versus transition metals such as platinum the following equation is appropriate:

$$\rho_i = \rho_{s-s} + \rho_{s-d} \qquad \text{Equation 2.2}$$

where ρ_{S-S} is the contribution to resistivity from scattering s electrons to s states,

and ρ_{S-d} is the contribution to resistivity from scattering s electrons to d states

In a simple metal there are only s electron states at the Fermi energy (see Figure 2.1) thus the only scattering which can occur is s-s scattering. In a transition metal the presence of vacant d states at the Fermi energy (see Figure 2.3) allows s-d scattering and the probability of this scattering is proportional to the density of d states at the Fermi energy. The s-d scattering substantially increases the resistivity as d electrons have a greater effective mass than s electrons and thus less mobility. This is the reason for the high resistivity of platinum relative to copper.

The difference in the electrical resistivity of platinum and copper extends to the dependences of their resistivities on temperature as can be seen in Table 2.1. The temperature dependence of resistivity in platinum and copper is linear, with a slight downward curve at higher temperatures for platinum. The platinum resistivity curve is steeper than that of copper and this can also be related to the occurrence of s-d scattering in platinum.

The curve in Figure 2.5 shows the contribution to the temperature dependence of a transition metal such as platinum from s-d scattering by comparing platinum (s-s and s-d scattering) to a noble metal such as gold (s-s scattering only). This extra contribution accounts for the greater temperature dependence of platinum when compared to copper.

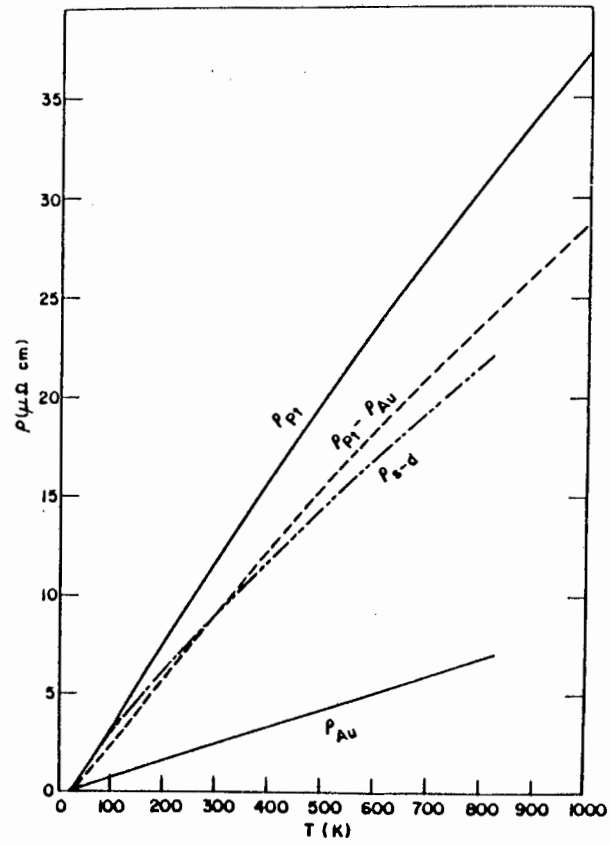

Figure 2.5: Dependence of resistivity on temperature for platinum compared with that of a noble metal such as gold (after Fradin et al[10]).

2.1.1.3 Thermo-e.m.f. of platinum and copper

The thermo-e.m.f. values of copper and platinum are substantially different. At room temperature the following equation, derived by Mott[11], is valid:

$$S = \frac{-\pi^2 kT}{3|e|}\left[\frac{\partial \ln \sigma(E)}{\partial E}\right]_{E=E_F} \qquad \text{Equation 2.3}$$

where S is the absolute thermo-e.m.f.

e is the magnitude of the electronic charge

k is the Boltzmann constant

T is the temperature

σ(E) is the electrical conductivity as a function of electron energy

The conductivity derivative[5] can be written as follows:

$$\frac{\partial \ln \sigma(E)}{\partial E} = \frac{\partial \ln \Lambda}{\partial E} + \frac{\partial \ln \mathbf{A}}{\partial E} \qquad \text{Equation 2.4}$$

where Λ is the mean free path of the electron

A is the area of Fermi surface not in contact with the Brillouin zone boundary

For platinum it can be assumed that the first term in equation 2.4 dominates the conductivity owing to i) the strong influence of s-d scattering on the conductivity and ii) the fact that the Fermi surface of platinum is seen in Figure 2.4 not to be in contact with the Brillouin zone boundary and therefore the influence of the second term is zero. Since Λ is shorter for a higher probability of scattering we find, for a transition metal such as platinum.

$$\Lambda \propto \frac{1}{N_d(E_F)} \qquad \text{Equation 2.5}$$

Thus with a rapidly falling $N_d(E_F)$ with respect to energy we find Λ increasing rapidly with respect to energy which gives a negative contribution to thermo-e.m.f[12], hence the negative value of thermo-e.m.f. for platinum in Table 2.1.

A positive thermo-e.m.f. can arise from a decrease in Λ (e.g. a rapidly climbing density of d states with respect to energy at the Fermi energy) or a decrease in the Fermi surface area with increasing energy. The latter is the origin of the positive thermo-e.m.f in noble metals such as copper[5]. The Fermi surface of copper touches the Brillouin zone on the (111) faces of the first Brillouin zone (see Figure 2.2). As the Fermi surface expands with increasing electron energy, the effective Fermi surface area decreases as the Fermi surface area in contact with the Brillouin zone increases. This makes a positive contribution to the thermo-e.m.f[5].

2.1.2 Alloys

The addition of a large atomic percent of a second element to a metal generally changes the electronic structure of the host metal. Resistivity increases with alloying due to the scattering sites represented by the inclusion of the alloying element in the host metal lattice while the thermo-e.m.f. depends more subtly on the electronic structure. The resistivities and thermo-e.m.f.'s of gold, gold-palladium and palladium are presented in Table 2.2.

Table 2.2: Electrical properties of gold-palladium and its constituents at 20°C

Metal	Resistivity ($\mu\Omega$.cm)	Thermo-e.m.f (μV/K)
Palladium	10.8[4]	-10[6]
Gold	2.35[4]	+1.9[6]
$Au_{50}Pd_{50}$(at%)	23.53[13]	-35 (0°C)[14]

In reviewing the electrical properties of gold-palladium [7,13,14,16,17] it was hoped to find a variation of the density of states with energy curve on which to base any subsequent discussion. Rowland et al[16] make extensive reference to the electronic structure of pure palladium and deductions made by Dugdale and Guenault[15] and use equations formulated in studies on silver palladium by Dugdale and Guenault to explain the dependence of the electrical properties on composition in gold-palladium. Their theoretical discussion is based on what they regard as widely used assumptions about the density of states in transition metals. In short it appears that the electronic structure of gold-palladium is assumed by Rowland et al[16] to be similar enough to that of silver-palladium for there to be no need to calculate it and refer to it specifically.

In this review a similar approach will be followed. The conclusions reached by Dugdale and Guenault about the applicability of the rigid band model will be reviewed. The review will then cover calculations by Rossiter[7] of the dependence of the resistivity on composition in gold-palladium, which agree well with the measurements made by Kim and Flanagan[17] in their studies on the effect of deformation on the

resistivity of gold-palladium alloys, and the explanation of the dependence of the thermo-e.m.f. of gold-palladium on composition made by Rowland et al[13].

2.1.2.1 Electronic structure of gold-palladium

Calculations done by Rossiter[4] on the electrical resistivity in the gold-palladium system show a composition at which there is an inflection point in the resistivity vs. composition curve corresponding to the filling of the d band and the consequent absence of s-d scattering after this composition. While these calculations were admittedly done after the rigid band model had been discarded, it is possible to attempt to explain such results in terms of the rigid band model and to attempt to apply the model to the gold-palladium system.

For a series of transition metal/simple metal alloys, such as occurs in the gold-palladium system, the rigid band model assumes that electronic structure of the transition metal is preserved on alloying with the simple metal. The d band peaks in the variation of the palladium density of electron states with energy are expected to remain at the same position relative to the s band when the palladium is alloyed with gold. The only change in electronic structure on alloying is the increase in the Fermi energy as electron concentration increases with the addition of more gold.

The dependence of the electrical properties on composition in the gold-palladium system indicates a full d band at approximately 60 at. % gold. This corresponds to 0.6 s electrons per palladium atom at that concentration. According to the rigid band model the electronic structure is unchanged on alloying so this result holds for pure palladium as well. This assumption leads to an incorrect value for the number of s electrons per atom of 0.6 s electrons per atom compared to measured values for pure palladium of 0.36 s electrons per atom[12]. The electronic structure of palladium is not preserved on alloying and the s band moves relative to the palladium d band peaks to change the concentration of s electrons per atom[16].

2.1.2.2 Resistivity of gold-palladium

The dependence of resistivity on composition in gold-palladium alloys is shown in Figure 2.6 and Figure 2.7 respectively. The following set of equations[7] generate a theoretical curve which is close to the experimental curve in Figure 2.7.

$$\rho = \rho_{s-s} + \rho_{s-d} \qquad \text{Equation 2.6}$$

$$\rho_{s-s} = A \bullet C_{Au} C_{Pd} \qquad \text{Equation 2.7}$$

$$\rho_{s-d} = \left| B(C_0 - C_{Au}) C_{Au}^2 C_{Pd} \right| \qquad \text{Equation 2.8}$$

for $C_{Au} \leq C_0$ where $C_0 = 0.55$

The s-s scattering term thus has a parabolic dependence on composition and once the d states are filled near 60 at. % gold this dependence is seen in Figure 2.7. The s-d scattering term increases the resistivity substantially in palladium-rich compositions. The density of d states decreases with increasing gold concentration causing the resistivity to decrease. The inflection point near 60 at. % gold reflects the change in resistivity behaviour from s-d to s-s scattering upon the d band being filled.

The dependence of resistivity on temperature decreases with increasing gold content as shown in Figure 2.8. Pure palladium has a dependence of resistivity on temperature similar to that of platinum.

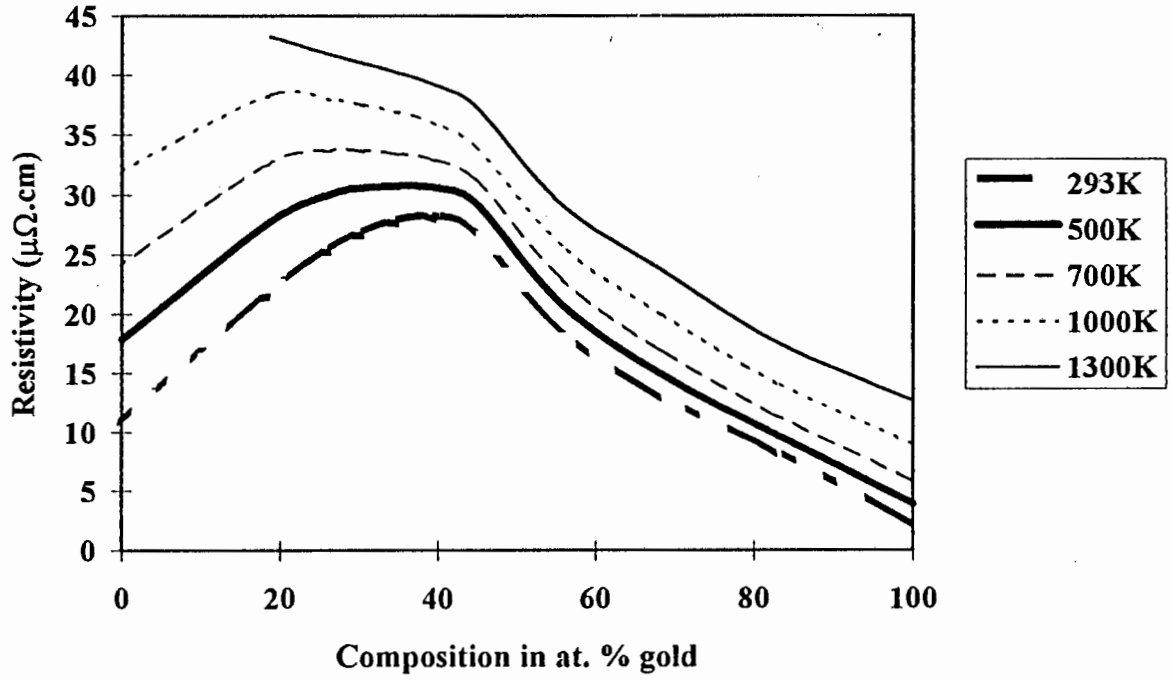

Figure 2.6: Resistivity versus composition for gold-palladium at elevated temperatures (after Ho et al[13]).

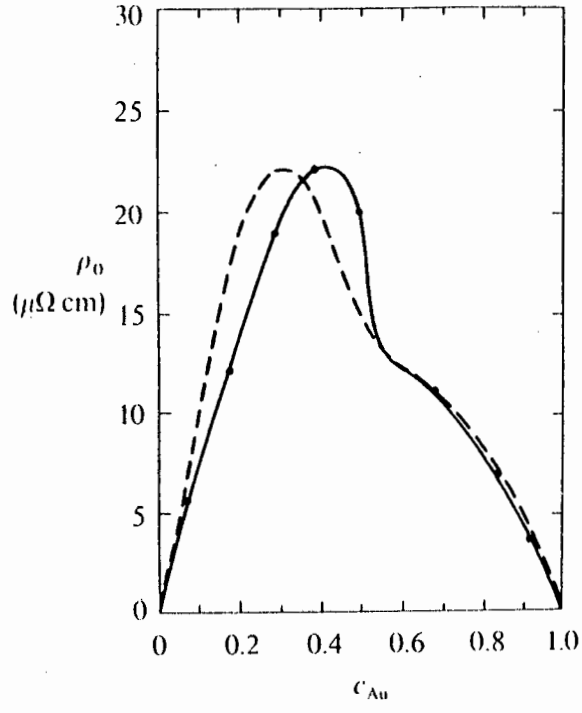

Figure 2.7: Residual resisitivity vs. composition for gold-palladium (after Rossiter[7] and Kim and Flanagan[17]). The dashed line is the calculated resistivity.

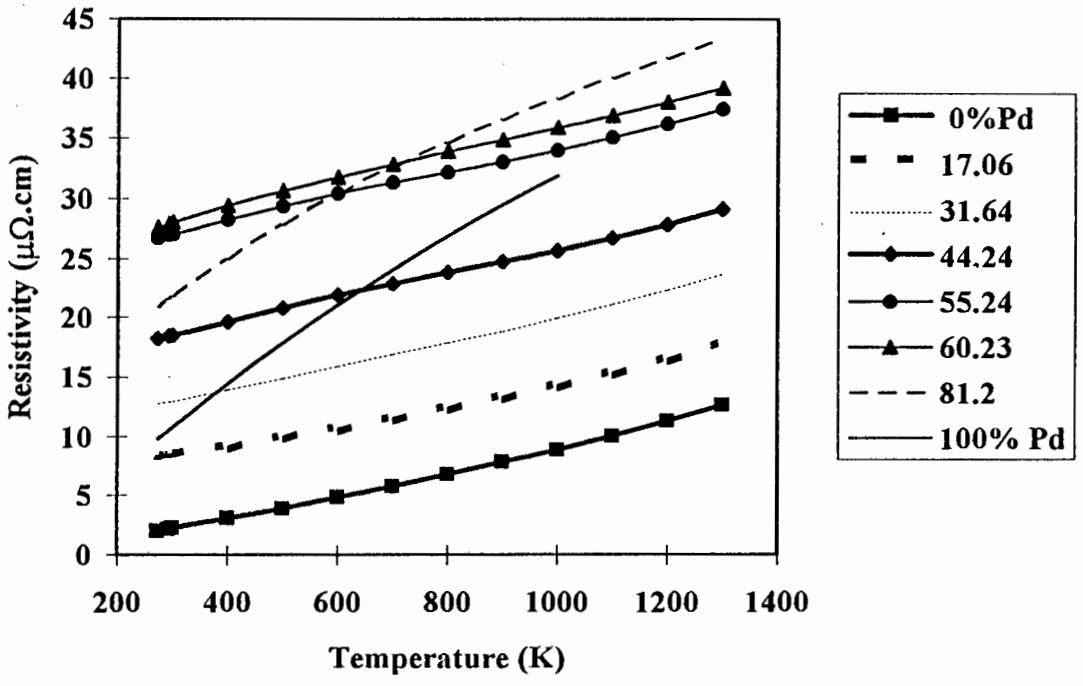

Figure 2.8: Resistivity versus temperature for various gold-palladium compositions (0% palladium = gold) (after Ho et al[13]).

2.1.2.3 Thermo-e.m.f. of gold-palladium

The thermoelectrical behaviour of gold-palladium is well established and a recent paper[14] contained the results shown below.

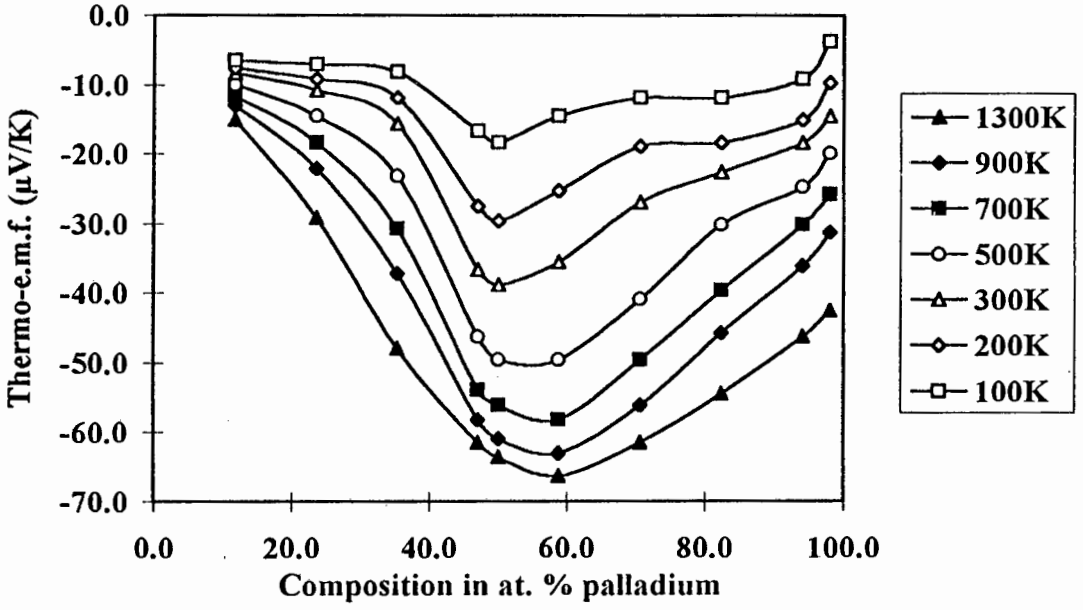

Figure 2.9: Variation of thermo-e.m.f. with composition of gold-palladium at various temperatures (after Ho et al[14]).

The Mott relation (equation 2.3) for thermo-e.m.f. can be applied to the gold-palladium system. The strong dependence on composition of thermo-e.m.f. is accounted for by the position of the Fermi energy relative to the palladium d band. If the Fermi energy corresponds to a region where the density of d states is decreasing rapidly with energy[16] the result will be a large negative contribution to the thermo-e.m.f. This is assumed to be the case at compositions between 40 at. % palladium and 70 at. % palladium. Thermal broadening causes the variation of the density of d-states to be depend less strongly on energy and hence the minimum in thermo-e.m.f. is not as pronounced at higher temperatures. Higher gold concentrations correspond to an area in which the density of d states varies more smoothly with energy, resulting in a lower negative contribution to thermo-e.m.f.

2.1.3 Intermetallics

Intermetallics are ordered materials in which a particular stoichiometric ratio of the metallic constituents corresponds to maximum order. The bonding between the atoms has a higher covalent character than is usual in a metallic bonding. There is a large variety of intermetallics with varying electrical properties but a family of aluminides from the 3d transition metals, namely iron aluminide, cobalt aluminide and nickel aluminide[18,19] will be considered here.

2.1.3.1 Atomic and electronic structure of nickel aluminide, cobalt aluminide and iron aluminide

All of the above aluminides have the same ordered B2 (BCC) CsCl structure. This means that the atomic structure conforms, to a lesser or greater degree depending on the intermetallic concerned, to the ideal of two interpenetrating simple cubic lattices as shown Figure 2.10.

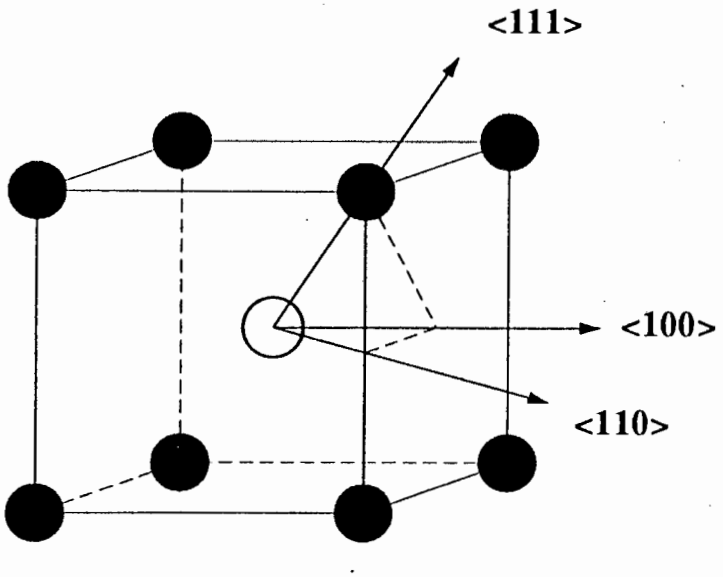

Figure 2.10: Idealised schematic diagram of the B2 (BCC) (CsCl) atomic structure (after Lin et al[2]).

The electronic configuration and properties of these intermetallics and their constituents are shown in Table 2.3.

Table 2.3: Electrical properties of aluminides and their constituents near room temperature (after Sellmyer et al[15] unless otherwise indicated)

Material	Electronic Configuration	Resistivity (μΩcm)	Thermo-e.m.f. (μV/K)
Aluminium	$(3s)^2(3p)^1$	2.61 [1]	-1.6 [2]
Cobalt	$(4s)^2(3d)^7$	5.2 [1]	not available
Nickel	$(4s)^2(3d)^8$	6.2 [1]	-16.8 [2]
Iron	$(4s)^2(3d)^6$	8.7	-51.3[20]
Nickel aluminide	$(3d)^{10}(s,p)^{1.5}$	9.8	-5
Cobalt aluminide	$(3d)^{9.2}(s,p)^{1.4}$	14	-20
Iron aluminide	$(3d)^{8.6}(s,p)^{1.2}$	56.7	+14.3

Calculated electronic structures are a useful aid to discussion but the electronic structure depends on the atomic structure which in turn is influenced by processing routes. An example of this is seen when Lin et al[2], in calculating the electronic structure of nickel aluminide, have to allow for anti-phase boundaries (APB) and their associated energies. An APB is a defect that occurs when two regions of ordered atomic structure are adjacent and mismatched such that atoms have like atoms as nearest neighbours. Order can also be disrupted or favoured by different processing routes and the presence of impurities. Thus deviations from properties predicted on the basis of calculated electronic structures can be expected.

The similarity in atomic structure of cobalt aluminide and nickel aluminide to brasses led Sellmyer et al to consider them as 3/2 electron compounds[15,16]. It is stated by Sellmyer et al that this is more applicable to nickel aluminide than cobalt aluminide and iron aluminide. It was observed that the packing in nickel aluminide and cobalt aluminide left vacancies for cobalt or nickel atoms in aluminium-rich compositions and

this was attributed to the stability of the 3/2 electron compound configuration. In iron aluminide, aluminium substitituted for iron in aluminium-rich compositions.

Nickel aluminide is classified by Sellmyer et al[18] as a nearly free electron metal, i.e. the energy gap across the first Brillouin zone is small enough to permit overlap and a nearly spherical Fermi surface[21]. The Fermi surface is found to be relatively simple and approximately spherical, similar to ordered CuZn and overlaps into the second Brillouin zone. Sellmyer et al[18] use the similarity of NiAl's Fermi surface to that proposed by the nearly free electron model, to classify nickel aluminide as a 3/2 electron compound although the proximity of the nickel d bands to the Fermi surface is recognised. Nickel aluminide, cobalt aluminide and iron aluminide are also all discussed by Sellmyer et al[18] in terms of the two band s-d model of transition metal electronic structure of Mott[12]. This model proposes a low density of mobile s electron states, which are primarily responsible for the conduction, and a high density of relatively immobile d electron states at the Fermi energy, into which s electrons are scattered causing the major contribution to resistivity in transition metals.

The variation of the density of states with energy of nickel aluminide is shown in Figure 2.11 with the Fermi energies of iron aluminide and cobalt aluminide as shown. A more recently calculated partial variation of the density of states with energy shown in Figure 2.12 shows that the d electron state density at the Fermi energy is low in nickel aluminide as compared to that of iron aluminide and cobalt aluminide. The electronic configuration for nickel aluminide in Table 2.3 shows a full d band.

Assuming the rigid band approximation for cobalt aluminide and iron aluminide we see that their Fermi energies fall within the transition metal d peaks according to Figure 2.11, predicting non simple metal behaviour with the two-band s-d theory being applicable. Accordingly the Fermi surfaces of these two intermetallics are complicated.

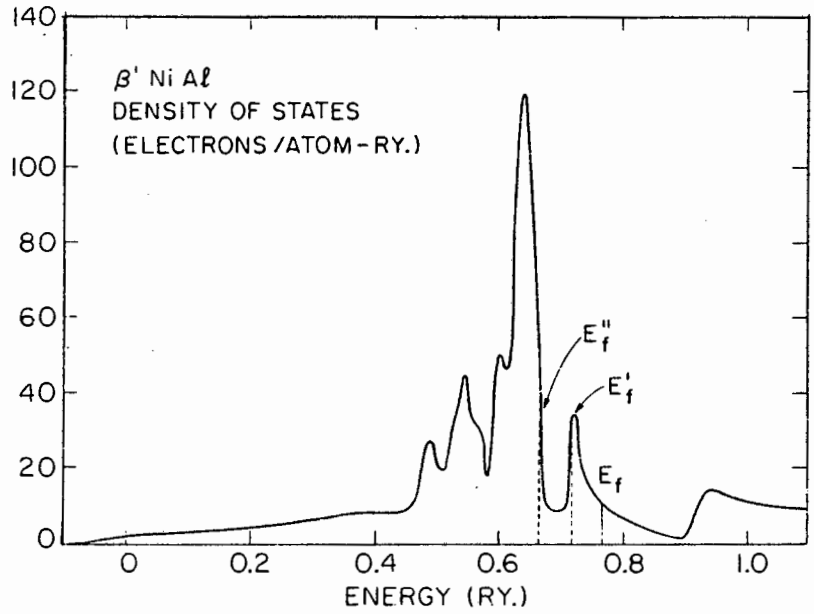

Figure 2.11: Variation of density of states with energy for nickel aluminide with $E_F^{''}$ and $E_F^{'}$ estimates of the E_F of cobalt aluminide and iron aluminide respectively (after Sellmyer et al[19]).

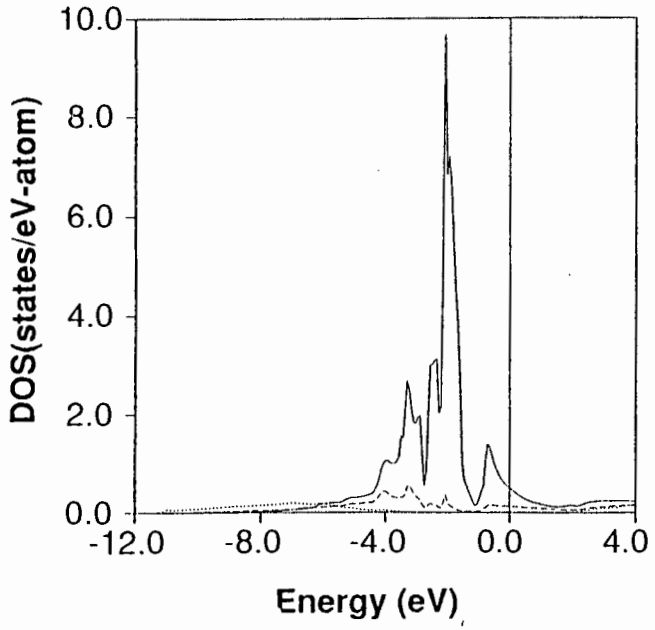

Figure 2.12: Partial variation of the density of states of nickel aluminide with energy. The solid line represents the nickel d electron density of states and the dotted and dashed lines the aluminium p and s electrons respectively (after Lin et al[2]).

2.1.3.2 Resistivity of nickel aluminide, cobalt aluminide and iron aluminide

The dependence of resistivity on composition is shown in Figure 2.13 for cobalt aluminide, in Figure 2.14 for nickel aluminide and in Figure 2.15 for iron aluminide. The high resistivity of some of the compositions further away from the stoichiometric point in the nickel-aluminium and cobalt-aluminium systems as compared to nickel, aluminium and cobalt is associated with alloying as is expressed in equations 2.7-2.9. The drop in resistivity is due to ordering which results in a more periodic lattice with fewer sites for scattering of conduction electrons. The lower degree of order in iron aluminide results in no local minimum at the stoichiometric point. The resistivity of nickel aluminide is low due to the simple metal character near the stoichiometric point and the small s-d contribution to the resistivity. Both cobalt aluminide and iron aluminide are subject to s-d scattering and consequently their resistivities are higher. Iron aluminide has a less-filled d band than cobalt aluminide, resulting in a greater resistivity owing to the greater probability of the scattering of s electrons into the higher density of unfilled d states.

The resistivity vs. composition curves exhibit different slopes on aluminium-poor and -rich sides of the stoichiometric point minima. This is related by Sellmyer et al[19] to the formation of different types of defects on either side of the stoichiometric point as is mentioned in the previous section. The different types of defects will have different scattering strengths resulting in different dependences of resistivity on composition.

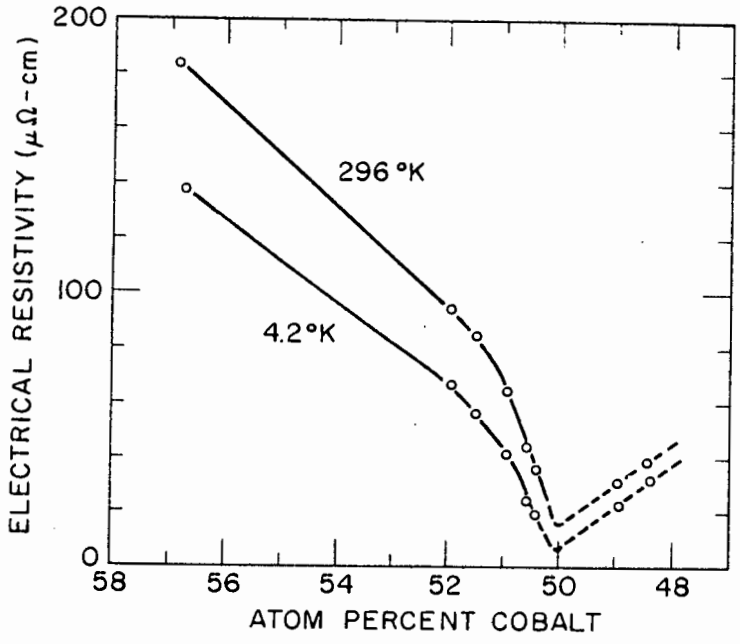

Figure 2.13: Resistivity vs. composition for cobalt aluminide near the stoichiometric point (after Sellmyer et al[19]).

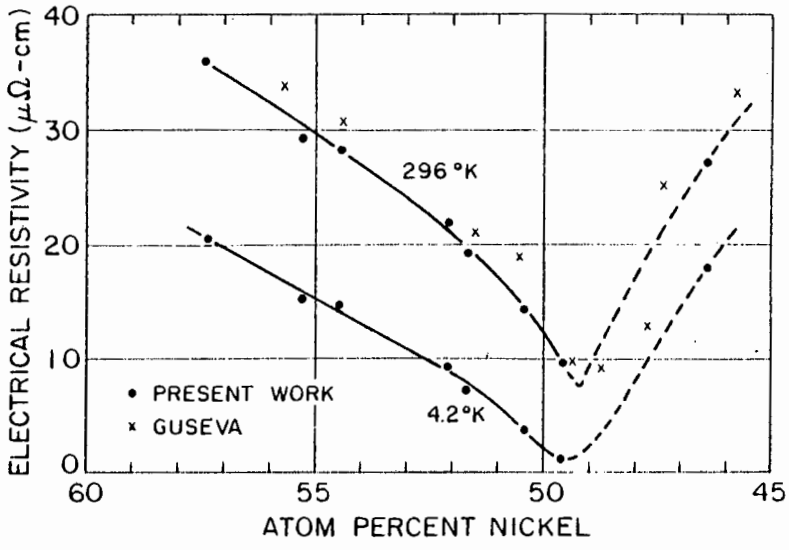

Figure 2.14: Resistivity vs. composition for nickel aluminide near the stoichiometric point (after Sellmyer et al[18]).

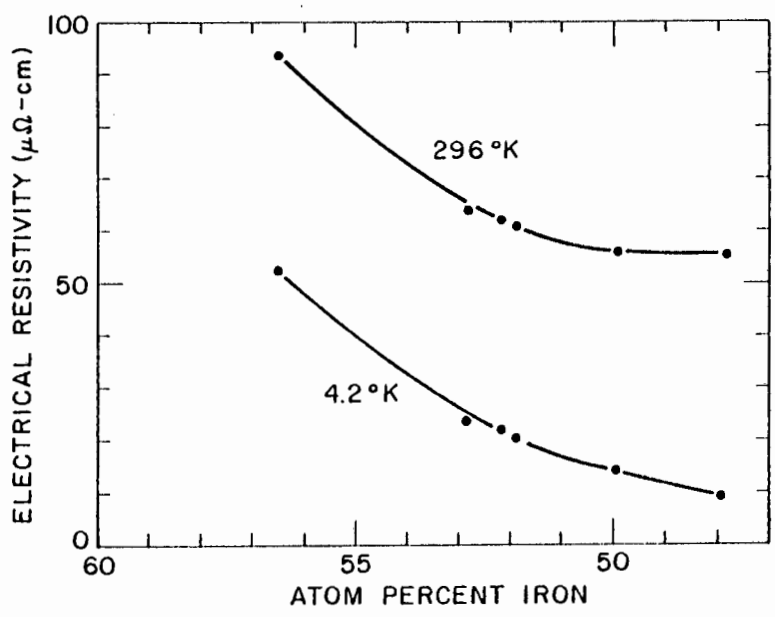

Figure 2.15: Resistivity vs. composition for iron aluminide near the stoichiometric point (after Sellmyer et al[18]).

2.1.3.3 Thermo-e.m.f. of nickel aluminide, cobalt aluminide and iron aluminide

Thermo-e.m.f. measurements show wide ranges of behaviour and in applying the Mott two-band s-d model Sellmyer et al[18] make a few assumptions. For nickel aluminide it is assumed that the mean free path varies with the square of the electron energy as is expected with a nearly free electron compound. It is also assumed that as the Fermi surface overlaps into the second Brillouin zone the Fermi surface area not in contact with the Brillouin zone is increasing with energy. This corresponds to two negative contributions according to the Mott relation (Equation 2.3).

To rationalise the thermo-e.m.f of iron aluminide and cobalt aluminide, Sellmyer et al made assumptions about the electronic structure of the aluminides. Conclusions drawn from the variation of density of states with energy in Figure 2.11 are not accurate in that the d band peaks may not be in identical positions for Ni, Co and Fe. Thus the magnitude and dependence on electron energy of the density of d states is not known

accurately. The variation of density of states with energy in Figure 2.11 shows that the density of d states could be falling rapidly with energy at the Fermi energy for iron aluminide which predicts a large negative thermo-e.m.f. based on the dependence of Λ on the density of d states. This is in contrast to the experimental results obtained and the discrepancy is rationalised by Sellmyer et al[15] by assuming that for the actual variation of the density of states with energy of iron aluminide, the sharp variations in the density of states due to the iron d bands might result in an increasing density of d states at the Fermi energy of iron aluminide. A peak in the thermo-e.m.f. of iron-aluminium is observed near 50 at. % aluminium as shown in Figure 2.17. Similarly the variation of density of states with energy for cobalt aluminide could be decreasing rapidly at the Fermi energy of cobalt aluminide explaining the large negative thermo-e.m.f.

The influence of the second term in the Mott relation (equation 2.3) cannot be estimated due to a lack of information about the Fermi surface which is expected to be complex. More accurate information on the electronic structure of iron aluminide and cobalt aluminide is required to rationalise the results for thermo-e.m.f.

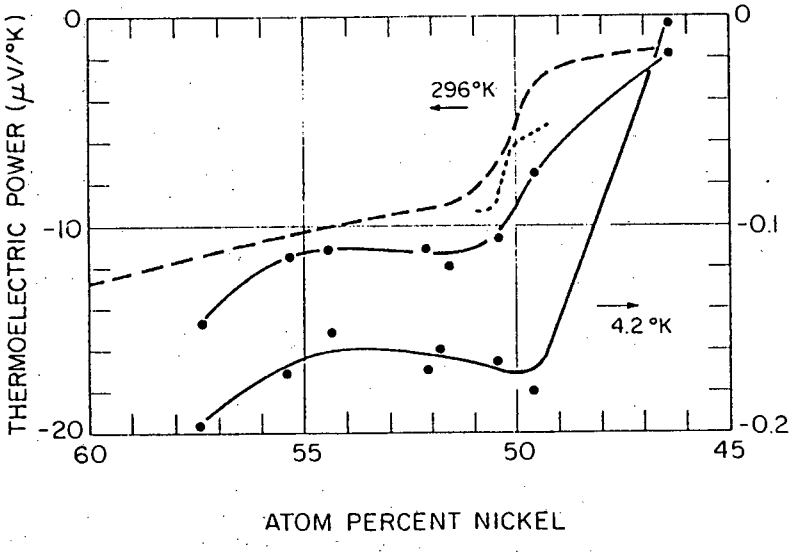

Figure 2.16: Thermo-e.m.f. vs. composition for nickel aluminide near the stoichiometric point (after Sellmyer et al[15]).

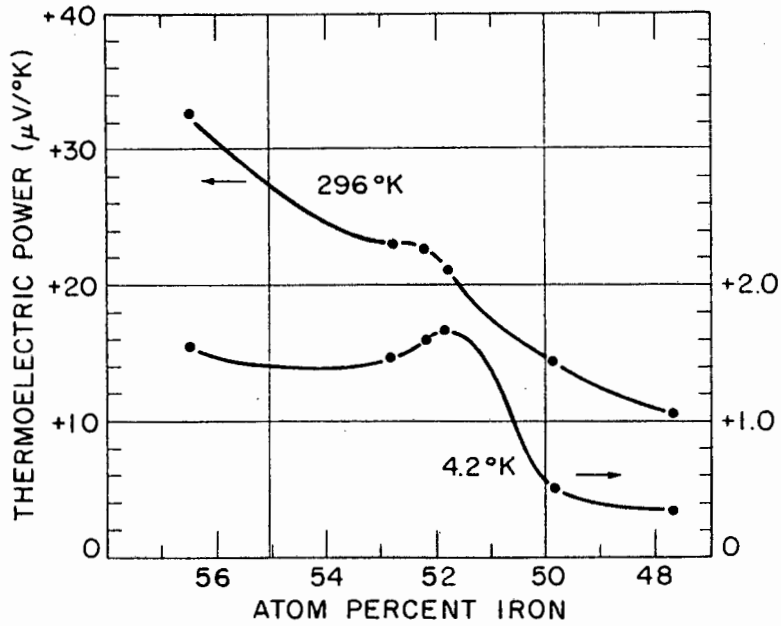

Figure 2.17: Thermo-e.m.f. vs. composition for iron aluminide near the stoichiometric point (after Sellmyer et al[18]).

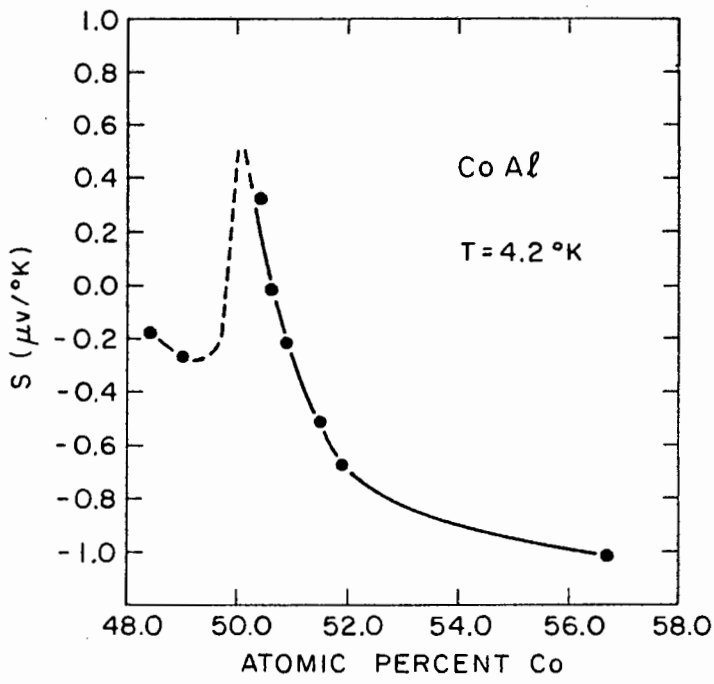

Figure 2.18: Thermo-e.m.f. vs. composition for cobalt aluminide at 4.2 °K near the stoichiometric point (after Sellmyer et al[18]).

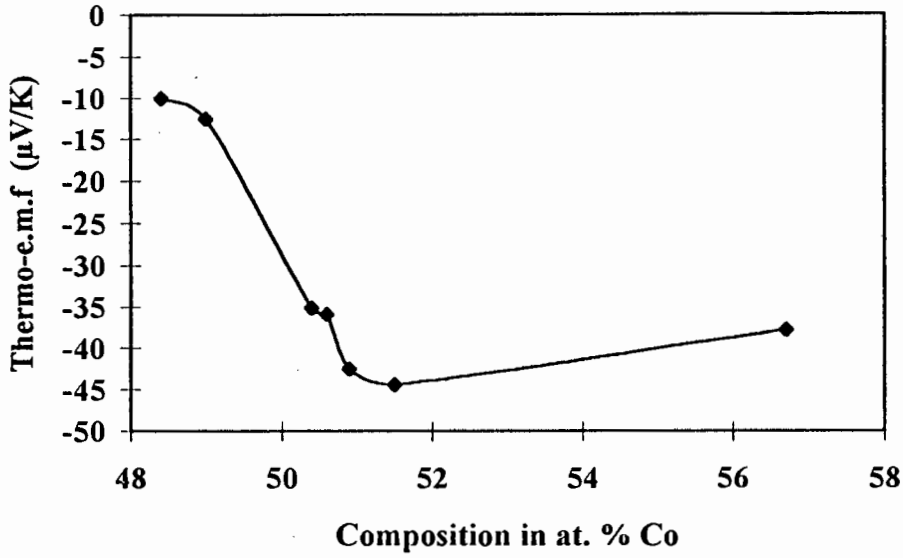

Figure 2.19: Thermo-e.m.f. vs. composition for cobalt aluminide at 300°K near the stoichiometric point (after Sellmyer et al[19]).

2.2 Ruthenium-aluminium

Ruthenium-aluminium alloys, which form an intermetallic phase near 50 at. % aluminium, initially attracted interested due to their unusual mechanical properties[1]. As a high melting point intermetallic (2060°C) ruthenium aluminide is able to undergo up to 16% true strain at room temperature. The electronic structure was studied to explain this ductility and the electronic structure of ruthenium-aluminide is pertinent to the later discussion of its electrical properties. Also reviewed in this section is a recent equilibrium phase diagram published for the ruthenium-aluminium system.

2.2.1 Phase equilibria

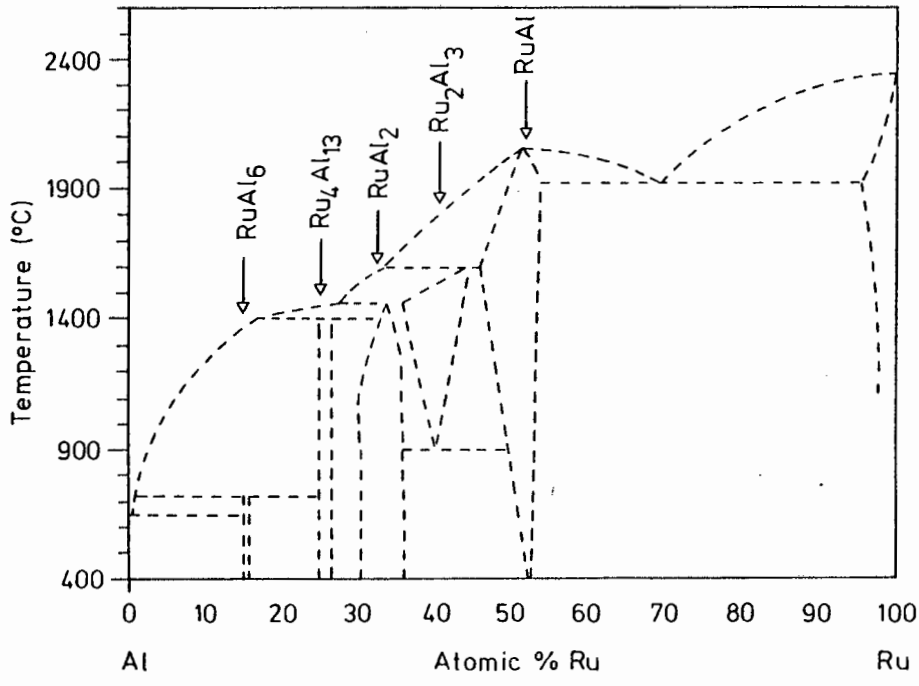

Figure 2.20: Equilibrium phase diagram for the ruthenium-aluminium system (after Boniface and Cornish[22]).

An equilibrium phase diagram for the ruthenium-aluminium system from a recent study by Boniface and Cornish[22] is shown in Figure 2.20. Ruthenium-rich off-stoichiometry compositions are expected to form a grain boundary phase consisting of the hexagonally close packed ruthenium-rich α phase (<5 at.% aluminium) with a eutectic phase of composition approximately 30 at% aluminium. For aluminium-rich off-stoichiometry compositions a succession of intermetallics can form, most notably Ru_2Al_3 or $RuAl_2$. This has a deleterious effect on properties. Annealed stoichiometric and ruthenium-rich samples[1] both show a bulk B2 phase with acicular ruthenium-α precipitates in the bulk phase.

2.2.2 Atomic and electronic structure

Ruthenium aluminide has the B2(CsCl) structure shown in Figure 2.21 which consists of two interpenetrating simple cubic lattices. The lattice parameter of ruthenium aluminide is .29916nm as determined by Fleischer[3] which is not in agreement with the value of .303nm given by Lin et al[2].

Calculations of the electronic structure always require simplifying assumptions. In addition to assumptions about the atomic potentials two basic assumptions required are the composition and structure of the metal concerned. In calculating the variation of the density of states with energy of ruthenium aluminide Lin et al[2] assume exact stoichiometry and a B2 structure. Anti-phase boundaries do effect the electronic structure by creating different types of ruthenium sites which influence the contribution of ruthenium atoms to the variation of the ruthenium aluminide density of states with energy. To calculate the APB energy of ruthenium aluminide two supercells are constructed: one with APB, as shown in Figure 2.22 and one without, as shown in Figure 2.23. With APB it is found that there are two different types of ruthenium sites within a supercell with APB: one has eight aluminium atoms as nearest neighbours (Ru-1) and the other has 6 aluminium and 2 ruthenium atoms for nearest neighbours (Ru-2). These three differences generate the three different partial variations of density of states with energy shown in Figures 2.26-2.28.

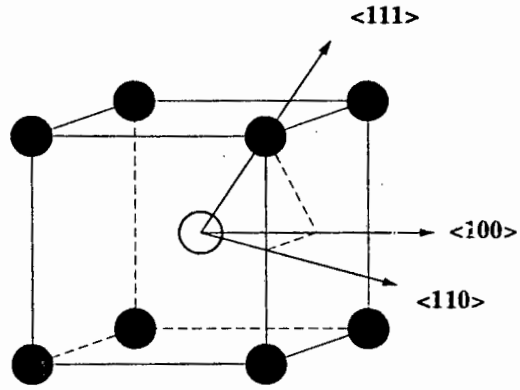

Figure 2.21: B2 structure of ruthenium aluminide (• -Ru) (after Lin et al[2])

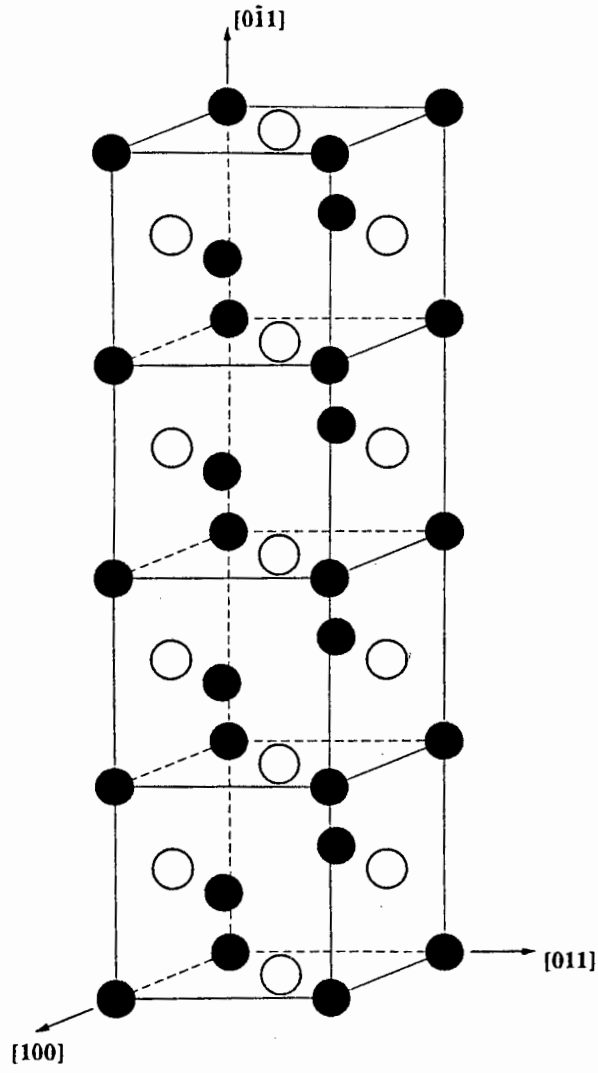

Figure 2.22: Eight layered B2 supercell without APB (• - Ru) (after Lin et al[2]).

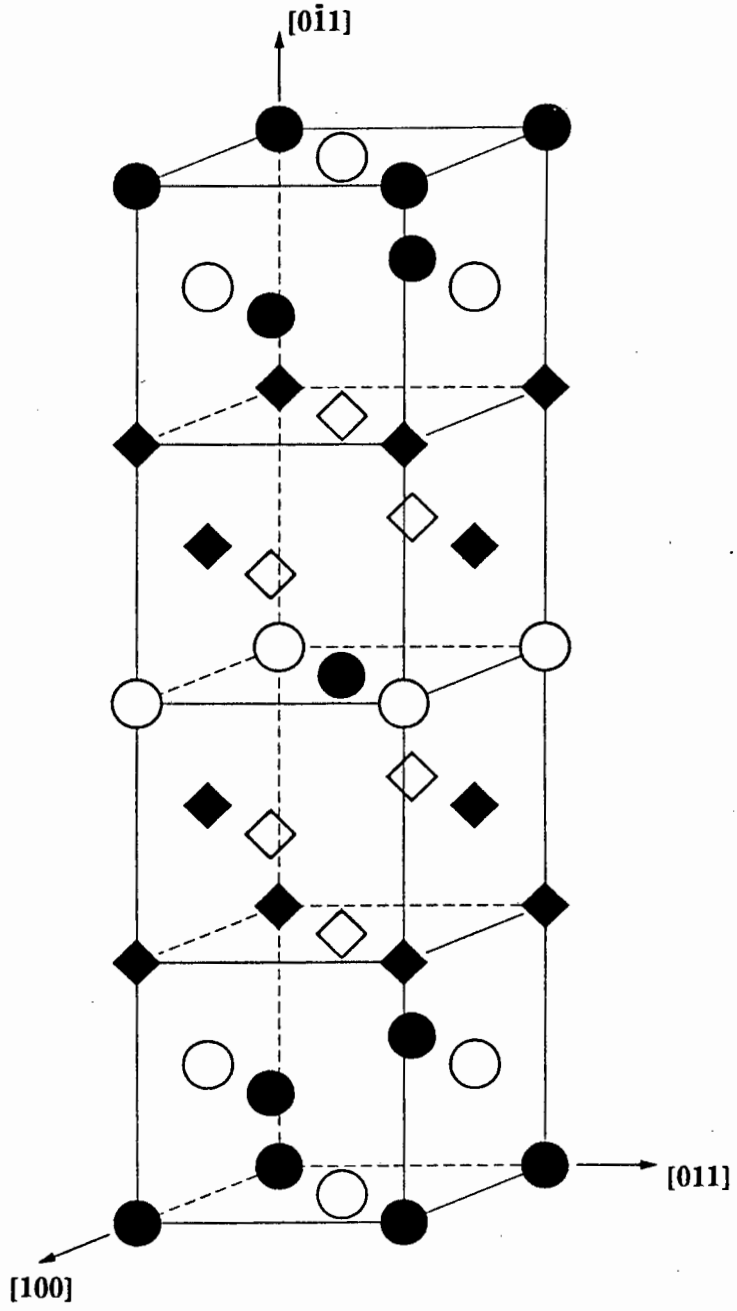

Figure 2.23: Eight layered B2 supercell with APB (• - Ru-1, ◆ - Ru-2) (after Lin et al[2]).

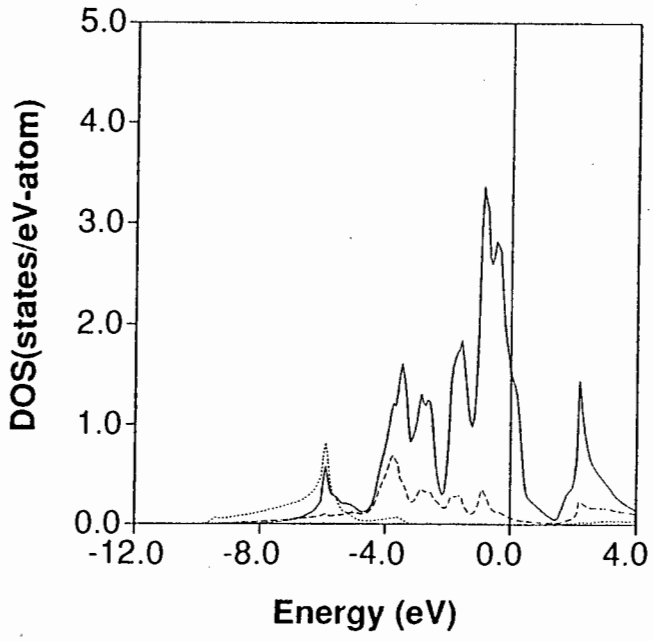

Figure 2.24: Partial variation of density of states with energy for ruthenium aluminide without APB (solid line denotes Ru-d electron density of states) (after Lin et al[2]).

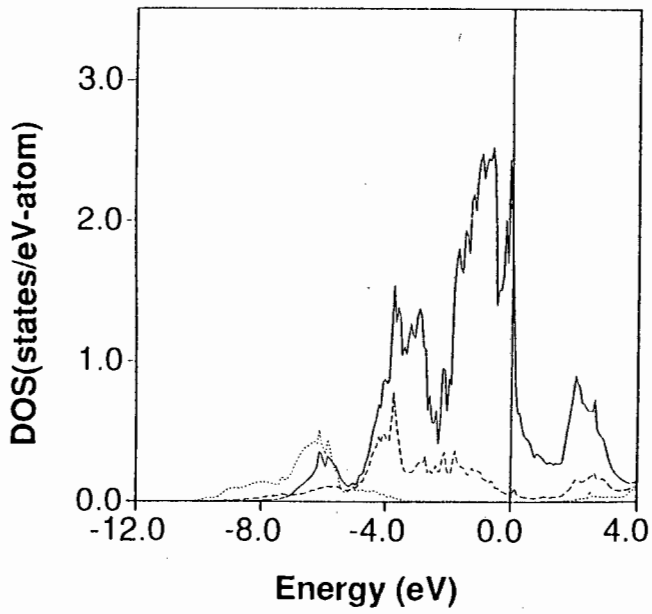

Figure 2.25: Partial variation of density of states with energy with APB for ruthenium aluminide for Ru-1 (solid line denoted Ru-d electron density of states) (after Lin et al[2]).

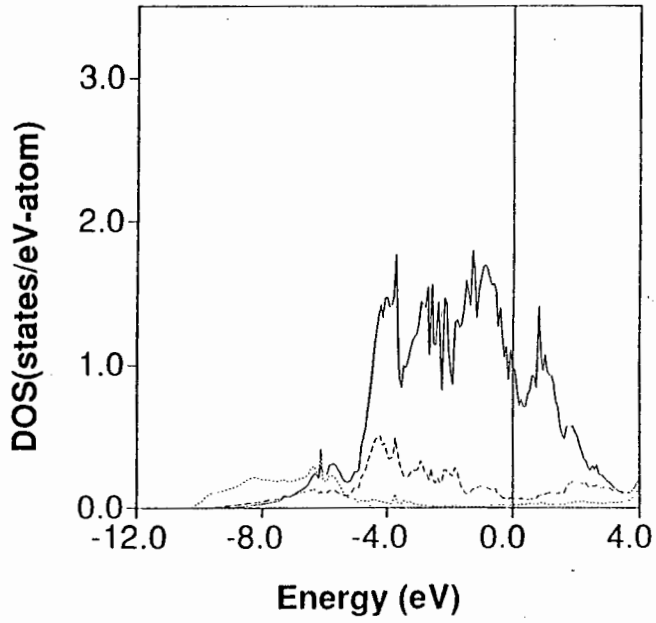

Figure 2.26: Partial variation of density of states with energy for ruthenium aluminide with APB for Ru-2 (solid line denotes Ru-d electron density of states) (after Lin et al[2]).

2.2.3 Oxidation resistance

As ruthenium aluminide and its alloys showed mechanical promise their oxidation resistance was investigated[23,24]. Ruthenium-aluminium alloys have an approximately parabolic oxidation kinetic up to 1200°C but above this temperature linear behaviour dominates as shown in Figure 2.27. Doping with chromium lowers the weight change very effectively as shown in Figure 2.28 but high concentrations of chromium embrittle the alloy[25]. It has been shown by experimental data[23] that it is necessary to balance the mechanical properties against the required oxidation resistance as shown in Figure 2.29.

The chisel toughness scale mentioned in Figure 2.29 is a scale devised by Fleischer[1] that is a rough measure of the ductility of an intermetallic. The higher the rating on the scale the tougher the intermetallic.

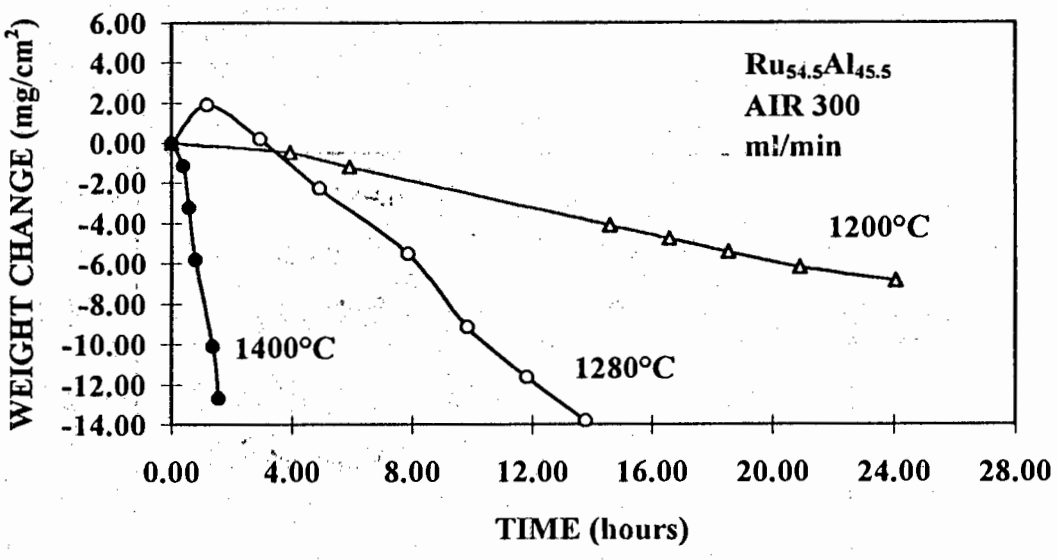

Figure 2.27: Weight changes versus time for $Ru_{54.5}Al_{45.5}$ heated in flowing air at various temperatures (after Mckee and Fleischer[23]).

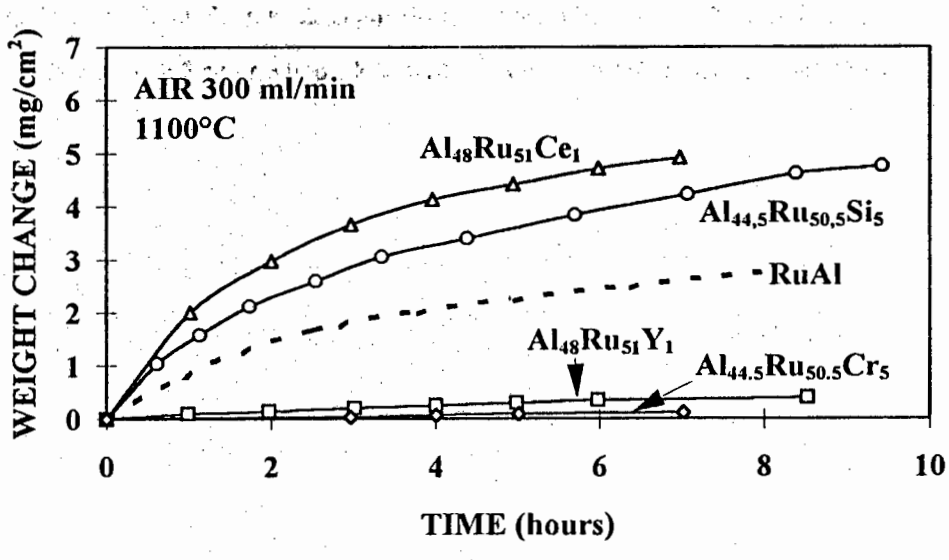

Figure 2.28: Weight changes versus time for various alloys based on Ru_XAl_Y on heating in flowing air at 1100°C (after McKee and Fleischer[23]).

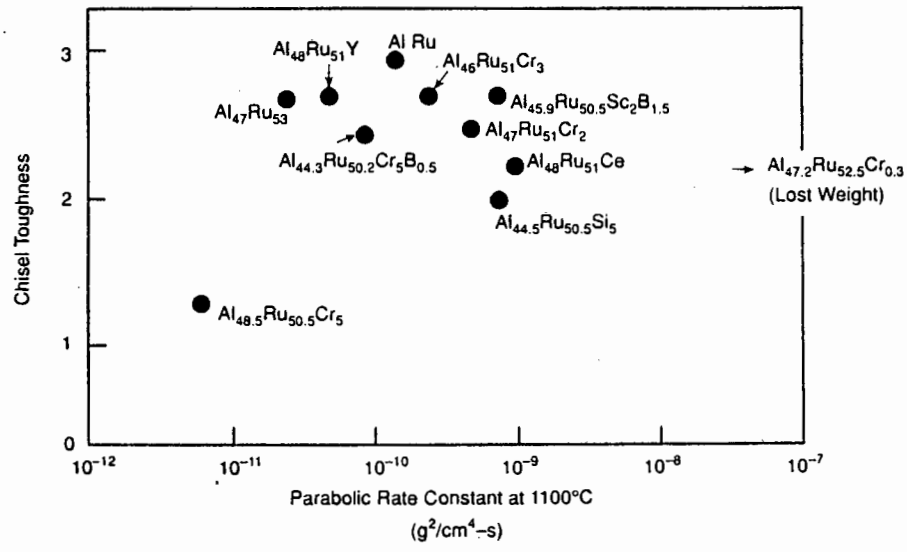

Figure 2.29: Parabolic rate constants (k) of various alloys versus the chisel toughness (CT). Desirable CT is > 2 and desirable k is < 10^{-10} gm^2cm^4/s (after Fleischer and Mckee[23]).

2.3 Measurement of electrical properties

2.3.1 Resistivity measurement

In 1958 Van der Pauw[26] proposed a method of measuring the resistivity of arbitrarily shaped discs.

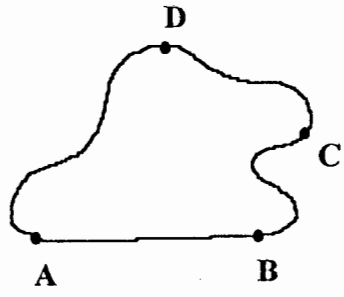

Figure 2.30: Arbitrary shaped sample with four small contacts at arbitrary places along circumference which can be used to measure resisitivity (after Van der Pauw[26]).

In his paper he proved the following theorem:

For a specimen of arbitrary shape with successive contacts A, B, C, D at arbitrary points along the perimeter of the specimen as shown in Figure 2.30 with the resistance $R_{AB,CD}$ defined as the potential difference V_D - V_C per unit current entering the sample at contact A and leaving at contact B (a similar definition holds for $R_{BC,DA}$) the following relation holds:

$$\exp\left(\frac{-\pi d R_{AB,CD}}{\rho}\right) + \exp\left(\frac{-\pi d R_{BC,DA}}{\rho}\right) = 1 \qquad \text{Equation 2.9}$$

where d is the thickness of the disc and ρ the resistivity.

A solution for the above equation is :

$$\rho = \left[\frac{\pi d}{\ln 2}\left(\frac{R_{AB,CD} + R_{BC,DA}}{2}\right)\right] \bullet f\left(\frac{R_{AB,CD}}{R_{BC,DA}}\right) \qquad \text{Equation 2.10}$$

where $f\left(\frac{R_{AB,CD}}{R_{BC,DA}}\right) \approx 1$ for $\frac{R_{AB,CD}}{R_{BC,DA}} \leq 2.$

Using equation 2.10 it is possible to find the resistivity provided the following conditions are met:

a) the contacts are at the circumference of the sample.

b) the contacts are sufficiently small.

c) the sample is homogenous in thickness.

d) there are no isolated pores within the material i.e. the surface should be singly connected.

This method is widely used[27,28,29,30] and operates as shown in Figure 2.31. With $R_{AB,CD}$ and $R_{BC,DA}$ defined as before, two measurements are carried out to determine V_{CD} and V_{DA} which are divided by I_{AB} and I_{BC} respectively.

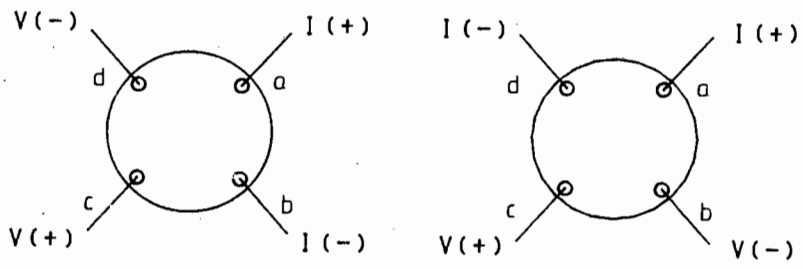

Figure 2.31: Schematic diagram of samples with four-point electrodes. Two measurements are carried out to determine V_{CD} and V_{DA} (after Futamata[30]).

Sun[31,32] has recently studied the application to square samples and has calculated the areas at the edge of the square sample suitable to the Van der Pauw method (Figure 2.32). A symmetrical square placement of probes testing a square area would allow

$$V_{CD} = V_{DA} = V \qquad \text{Equation 2.11}$$

This yields sheet resistance :

$$R_S = CV/I \qquad \text{Equation 2.12}$$

$$\text{where } \rho = dR_S \qquad \text{Equation 2.13}$$

Provided probes are located in this area, the correction factor $C \approx 4.53$.

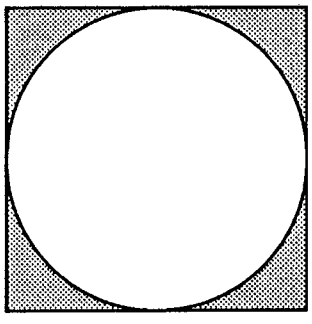

Figure 2.32: A diagram of a resistivity specimen with the shaded regions showing the area suitable for the placement of probes for the Van der Pauw method (after Sun[31]).

2.3.2 Thermo-e.m.f. measurement

The design requirements for thermo-e.m.f. measurement of brittle conductive specimens of irregular shape, as is the case in ruthenium-aluminium alloys, are to be found by considering measurement of thermo-e.m.f. in conductive ceramic materials[33]. A simple technique for measuring the thermoelectric response of a sample to heat pulses by analogue subtraction has been published[34]. This method is explained with the aid of Figure 2.33. An electrical wire heater pulses heat through the sample (C). A thermal gradient is thus created along the sample length. Two thermocouples, each consisting of materials A and B, are attached at opposite ends of the sample. They determine the sample temperature and are used by the analogue subtraction circuit to feed the thermoelectric voltages into two amplifiers (1000 x gain), A_1 and A_2. The difference between the two signals is amplified by a factor of 10 by a third amplifier, A_3. The signal from A_2 (X-Axis) is plotted versus the signal from A_3 (Y-Axis) on an XY plotter. The slope of the graph is proportional to the difference between the sample's thermo-e.m.f. (S_C) and the thermo-e.m.f. of one of the thermocouple materials (S_B):

$$S_{CB} = 10 S_{AB}\left(\frac{\Delta Y}{\Delta X}\right) \qquad \text{Equation 2.14}$$

where $S_{CB} = S_C - S_B$ and $S_{AB} = S_A - S_B$. S_{AB} can be found from the slope of voltage versus temperature for the thermocouple and the absolute thermo-e.m.f. of the sample, S_C, can be found by adding the absolute thermo-e.m.f. of one of the thermocouples, S_A, to S_{CB}.

There are several advantages to this technique: an accurate measurement of ΔT is not necessary and accurate measurements can be obtained from small temperature differences requiring short heat pulses which will not alter the material. The relatively cheap components required are also an attractive factor.

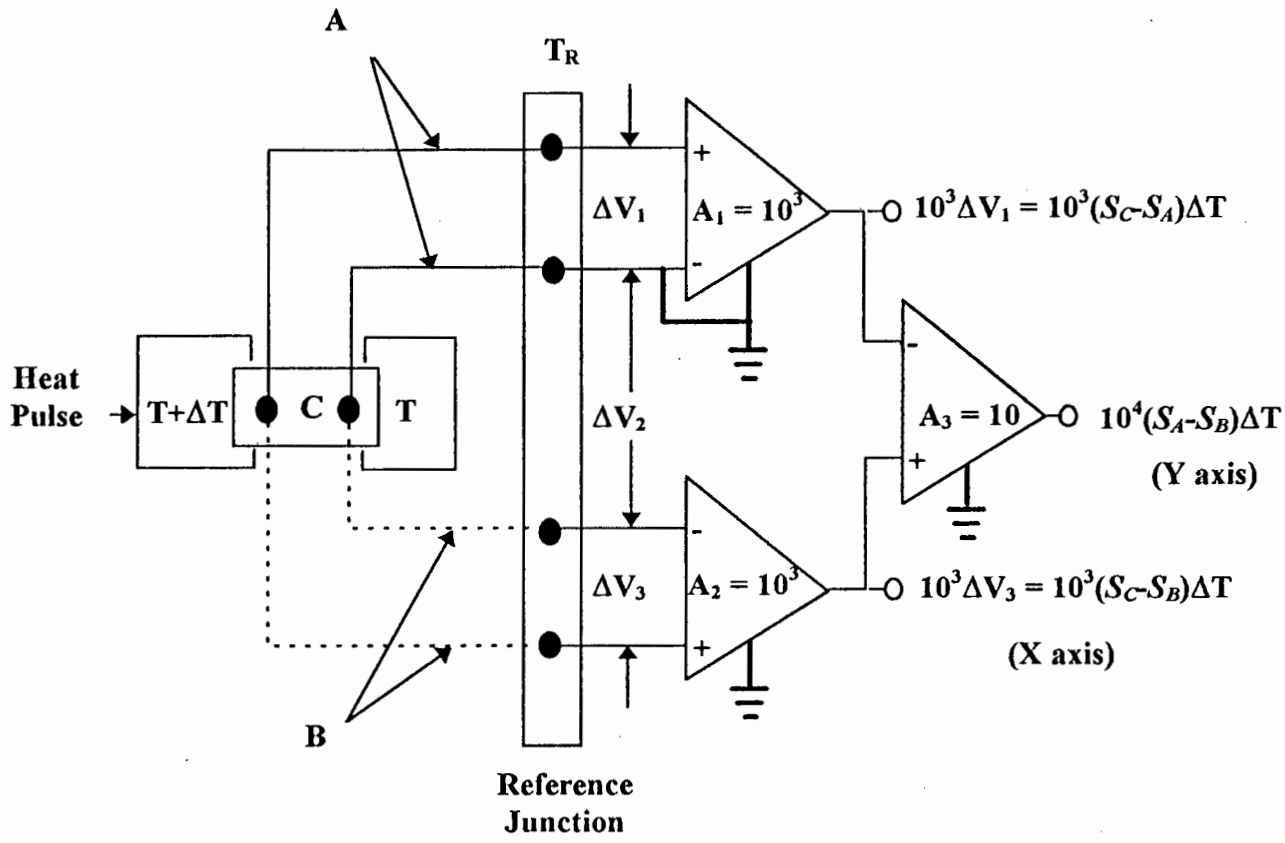

Figure 2.33: Schematic circuit diagram for thermoelectric power measurement by analogue subtraction (after Hodge[33]).

2.4 Summary of literature review

The electronic structure and some of the electrical properties of the relevant materials and the means of measuring the electrical properties have been reviewed.

Metals that have d electrons at the Fermi energy are classified as non simple metals and metals with only s electrons at the Fermi energy are classified as simple metals. In simple metals the only contribution to resistivity is s-s scattering and in non simple metals there is the extra contribution of s-d scattering. Thermo-e.m.f. depends on the change in conductivity with electron energy and the interaction of the Fermi surface with the first Brillouin zone. If alloying changes the electronic structure of a material in such a way as to completely fill the d band then only s-s scattering will occur and this will be reflected in the dependence of the electrical properties on composition.

Intermetallic materials' resistivity and thermo-e.m.f. can also be rationalised in terms of the above concepts. Simple and non simple metal behaviour is observed depending on the constituents.

The equilibrium phase diagram, atomic structure and electronic structure of ruthenium-aluminium alloys have been reviewed. The ruthenium-aluminium equilibrium phase diagram shows a narrow phase field associated with ruthenium aluminide formation and ruthenium aluminide's variation of density of states with energy shows d states at the Fermi energy.

Methods for measuring the electrical properties of resistivity and thermo-e.m.f. have been selected and reviewed; their modification to suit experimental constraints is introduced later in Chapter Four.

3. Experimental Methods

In this chapter the specimen preparation and compositional analyses performed are discussed. Metals such as platinum and gold-palladium are well documented and can be prepared and examined by standard techniques. Ruthenium aluminium alloys have only recently been studied in any detail. As a result problems encountered in the preparation of the alloys and the determination of their composition do not have documented solutions (although the problems are well documented).

3.1 Specimen preparation and history.

The electrical properties of a material are dependent on the atomic structure, the composition and the electronic structure which are in turn dependent on the processing route and method of preparation used.

3.1.1 Platinum and gold-palladium

Platinum and gold-palladium arc melted buttons of approximate mass 2g were cold rolled from 5mm to approximately 200μm and cut into 12mm× 12mm squares for resistivity measurements. Further gold-palladium was received in the form of 3mm thick plate which was cut and rolled to ≈1mm thickness for thermo-e.m.f specimens.

3.1.2 Ruthenium-aluminium

The initial processing route for ruthenium-aluminium was arc melting which produced unacceptably porous specimens. The samples prepared by hot isostatic pressing using a titanium can with a molybdenum diffusion barrier, which enclosed appropriate compositions of Ru powder and Al powder, were satisfactory. The nominally 50 at. % aluminium compositions were reacted at the same temperature but separately from other compositions, with a larger powder particle size (sub-106μm as opposed to sub-

53μm), and at 1600 bar and not 1500 bar. Samples were received in the form of ≈ 4mm disks cut from hot isostatically pressed samples. The disks were then spark eroded or diamond saw cut and ground into 1mm thick slices. Square 12mm×12mm resistivity specimens were then cut using a Dremel Moto tool with cut off wheel. Thermo-e.m.f. specimens were also prepared from the spark eroded disks as ≈1mm thick 12mm×8mm platelets or specimens approximating those dimensions.

The compositions studied are stable with respect to heat treatment and no structural or compositional changes accompany heat treatment at the temperatures used here (1000°C). The atmosphere for the resistivity measurements was air and an oxide scale formed on the specimens. Thermo-e.m.f specimens were exposed to lower temperatures (< 400°C) which produced no oxide.

3.2 Compositional analysis

Accurate compositional analysis is an important tool for analysing electrical measurements. The compositions of platinum and gold-palladium are easily measured by non-destructive and chemical means. Ruthenium-aluminium alloys, with their excellent chemical resistance, had not previously been successfully tested by chemical means. Common tools for evaluating metals non-destructively such as: energy dispersive spectroscopy (EDS), x-ray fluorescence (XRF) and x-ray microprobe analysis (XRM) have shortcomings when applied to ruthenium-aluminium alloys as detailed below.

3.2.1 Platinum and gold-palladium specimens

X-ray microprobe analysis showed the platinum to be pure relative to the standard employed and the gold-palladium resistivity specimens to have the composition indicated in Table 3.1. Thermo-e.m.f specimens had a nominal composition of 65 at. % (50 wt. %) gold.

Table 3.1: Composition of gold-palladium resistivity specimens.

Constituent	Wt.%	At%
Gold	56.06 ± 0.87	41.42 ± 0.76
Palladium	42.83 ± 0.76	58.58 ± 1.26

3.2.2 Ruthenium-aluminium

A number of tools for compositional analysis were considered for the present work. EDS proved unsatisfactory for absolute measurements due to the high absorbance that alumnium is subject to and readings were found to be dependent on the accelerating voltage and the coating employed. The calculation performed by the EDS software relies on a standardless analysis and this was considered unsatisfactory for *absolute* measurements. The EDS results confirmed the nominal compositions at low (30at%) aluminium concentrations but underread the higher (50at%) concentrations by as much as 5at%. Finally EDS is a surface technique and any variations through the specimen thickness might have gone undetected while still influencing the electrical properties. XRM analysis of ruthenium-aluminium alloys required a Ru standard which was unavailable. XRM could only analyse a small area of the specimen at a time unlike EDS which could scan the whole raster from the SEM giving a good average. XRF, which has been attempted by Fleischer[3] with unsatisfactory results, would be influenced by the lighter aluminium in a matrix with heavier ruthenium, the aluminium being excited by the ruthenium emissions to inflate the aluminium readings. XRF also requires a standard ruthenium-aluminium sample of which the composition is exactly known and with a relatively unstudied metal such as ruthenium-aluminium this is not possible. Of the non destructive techniques EDS, at an appropriate accelerating voltage of 15kV and with no conductive coating apart from a silver paint connection to the aluminium base of the specimen holder, proved satisfactory for determining *relative* compositions.

Compared to non-destructive methods chemical analysis would allow for inhomogeneities in the specimens and give absolute results but would not permit retesting of the specimens. Previous workers[3] have avoided chemical methods until

now because of the high chemical resistance of ruthenium-aluminium alloys. The route followed in this work was inductively coupled plasma spectroscopy (ICP). The solution used was sodium peroxide at ≈500°C. The reacted mass was rinsed with HCl to remove the sodium and a solution representative of the sample obtained by filtration. This sample was then diluted and analysed by ICP. This represents the first chemical analysis of ruthenium-aluminium alloys. The results for EDS and ICP are shown in Table 3.2 together with the nominal compositions.

Table 3.2: Comparitive compositional analysis for ruthenium aluminium alloys.

Compositions in at. % aluminium				
		Resistivity specimens		**Thermo-e.m.f. specimens**
Batch number	**Nominal**	**EDS**	**ICP**	**EDS**
R86b	30	30.2	≈50	none
R86c	30	29.7	none	none
R87ai	48	45.7	50.8	none
R88b	48	45.8	64.31	48.3
R88c	48	45.2	52.4	none
R89a	50	45	44.5	45.7
R89b	50	49	55.9	49.7
R87b	52	45.3	41.74	none
R87c	52	46.8	44.5	48.5

Some of the ICP results correlate badly with nominal compositions and even allowing for slightly inaccurate nominal compostions it is inconceivable that an alloy with 64 at. % aluminium be found in this series of compositions. Labelling errors or miscalibration are the only way to explain how a nominal eutectic composition near 30 at. % aluminium could actually have a composition nearer 50 at. % aluminium, especially when the nominal composition has been confirmed by EDS. These two results cast doubt on the whole ICP process. The solutions were also noted to change

colour within a day of being made which corresponds to chemical changes with possible complexing of the aluminium and ruthenium. While ICP is undoubtedly a better method than EDS for obtaining absolute compositions this is the first attempt to use it on alloys from the ruthenium-aluminium system and the technique will need to be refined and correlated with microstructural studies and processing routes to find the optimum operating conditions.

The EDS results correlate more strongly with the electrical properties measured than do the nominal compositions. In Chapter Five it will be seen that the resistivities of the two samples with nominal compositions of 50 at. % aluminium were the largest among the compositions near 50 at. % aluminium which is not at all what is expected for this type of system. Fleischer[3] recently assumed the ruthenium-aluminium alloys nominal compositions as exact to ± 0.4% on the basis that the processing route that was used (arc melted disk shaped ingots) had produced such a variance for other intermetallics. In view of the lack of information about diffusion kinetics and solidification in this system it is preferred not to make such assumptions.

The uncertainty about the ICP method and the need to have some means of analysing the relative aluminium concentrations of the samples apart from the nominal compositions which the electrical properties suggest can be incorrect (a variety of individuals from different institutions, from the original producers to the spark eroding personnel, handled the specimens and the possibility does exist that labels were mixed up, leading to confusing nominal compositions), motivates for the EDS results to be used as a basis for subsequent discussion on the dependence of the electrical properties on composition. Thermo-e.m.f. measurements could only be taken when there was sufficient material and in one case a resistivity specimen had to be remachined for thermo-e.m.f. measurements and was then used for ICP. As a result the EDS results for resistivity specimens are more complete and are used in plotting both resistivity and thermo-e.m.f. graphs. As EDS only reflects relative amounts of aluminium present in each of the specimens and the order of specimens in increasing aluminium % is the same for both sets of EDS results, using the resistivity specimen EDS results do not misrepresent the relative dependence of electrical properties on composition.

4. Construction of Measurement Apparatus

Central to the success of this research was the design, construction and operation of measurement apparatus. The methods chosen required unique designs. These designs overcame the constraints presented by measuring the electrical properties of a relatively brittle material such as a ruthenium-aluminium alloy in an electrically noisy furnace environment. The designs were practical and efficient enabling specimens to be changed conveniently and tested over a wide range of temperatures with accurate temperature measurement. Most importantly calibration with platinum and gold-palladium showed the apparatus to be accurate.

4.1 Introduction

The need for measurement of electrical properties of metals has led to the use of a wide variety of methods and apparatus. Ruthenium aluminide, of the three materials studied, is an intermetallic with electrical properties similar to that of platinum and gold-palladium but with very different mechanical properties and processing requirements. Methods assuming that the test material can easily be formed into plate or wire were not appropriate. The processing route of ruthenium-aluminium alloys, that of hot isostatic pressing, also limited the size of specimen available. The choice of method and design of apparatus had to primarily accommodate ruthenium-aluminium alloys specimens.

A further influence on the design of the apparatus was the high temperature (up to 1000°C) at which measurements had to be taken. Alumina was the most suitable material for the electrical insulation of probes and thermocouples and for the specimen stage. A design was therefore required that accommodated alumina's brittleness. The design also had to allow for the electrical shielding of probes in the electrically noisy furnace environment. The specimen stage had to be spring loaded to ensure good contact and allow for expansion during heating.

The furnaces available were laboratory bench furnaces with horizontal work tubes of diameters 40mm and 20mm. The designs had to be accommodated within this diameter. The specimen stage had to be in firm contact with support bars of the furnace spring loading mechanism in such a design and yet not deform wires leaving the specimen stage. The support bars could not obstruct the limited diameter of the work tube and had to leave space for wiring and insulation to make electrical connections outside the work tube.

Ruthenium-aluminium alloys' properties and processing, the construction materials appropriate to the measurement temperature and the limited furnace work space all posed problems for the design and construction of the apparatus. The solutions found are detailed in the following sections.

4.2 Resistivity measurement

The method selected is the Van der Pauw method detailed in Chapter Two. This method's requirements can be satisfied by ruthenium-aluminium specimens. Resistivity apparatus was built in two stages: room temperature and high temperature assemblies.

4.2.1 The Van der Pauw method

The Van der Pauw method was chosen owing to its ability to measure the resistivity of arbitrarily shaped discs. The specimen configuration and probe placement is shown in Figure 4.1. The shaded areas indicate the areas where the contacts may be placed and still satisfy the requirements of the Van der Pauw method.

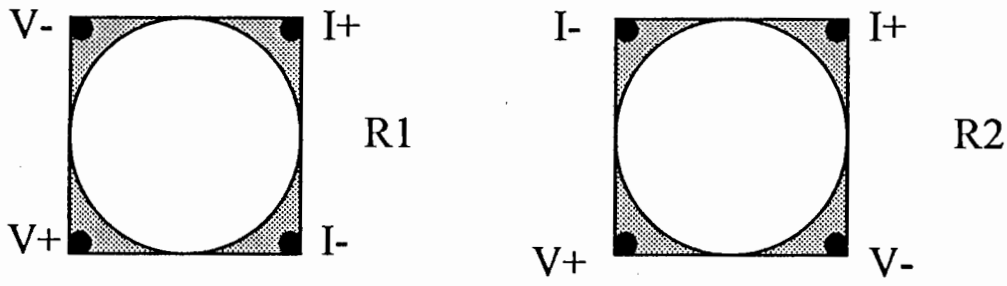

Figure 4.1: Probe placement to measure the two sheet resistances R1 and R2 for the Van der Pauw method.

$$\rho = \frac{\pi d}{2\ln 2}\left(\frac{\Delta V_1}{I_1} + \frac{\Delta V_2}{I_2}\right) = \frac{\pi d}{\ln 2}\left(\frac{R1 + R2}{2}\right) \qquad \text{Equation 4.1}$$

The voltages obtained from the two probe configurations shown in Figure 4.1 are used to calculate the resistivity as shown in equation 4.1.

Sun[31] showed that square specimens allowed probes to be situated on the corners, as opposed to point contacts at the edges. It is important for these probes to be in square array so as to obtain similar sheet resistances for the two measurements required (R1 and R2). An error in probe placement causes greater inaccuracy in small specimens of for example 5mm×5mm than in the larger 12mm×12mm specimens used in this study as the probe is more likely to stray out of the shaded areas.

Optimisation of probes and circuitry resulted in accurate room temperature measurements. Initially the probe configuration shown in Figure 4.2a was chosen. Platinum rods were machined to have conical tips protruding through a specially moulded and machined alumina disc. Loading the assembly as shown in Figure 4.2a to ensure good contact caused uneven deformation of the tips when loading was not perfectly normal to the specimen. The resulting lack of symmetry of contact area failed the requirement for a square array of probes.

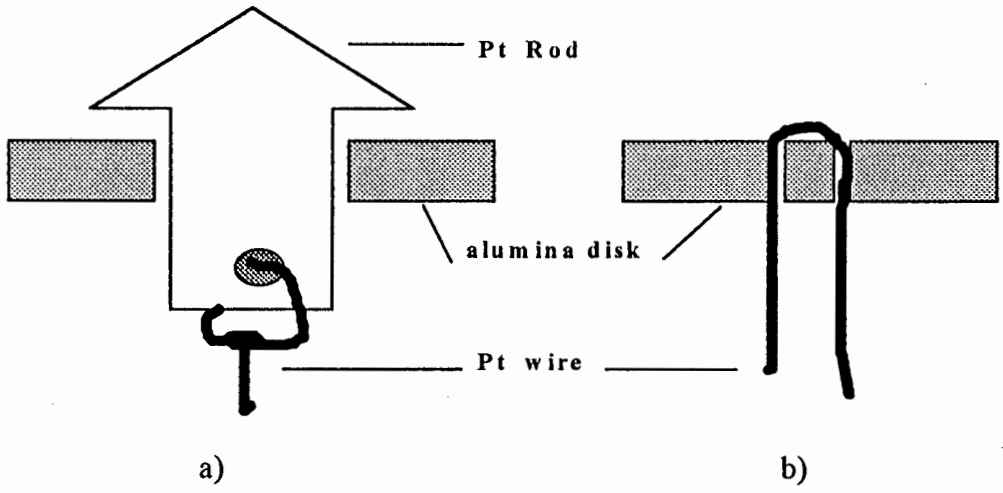

Figure 4.2a): Platinum Rod with conical tip and shoulder

b): Platinum wire twisted through closely spaced holes.

As Plomp[35] indicated an error of less than 5% associated with line contacts it was decide to twist platinum wire through closely spaced holes presenting a short line contact to the specimen, approximating a point contact as shown in Figure 4.2b. A square array of probes can be ensured by careful placements of the pairs of holes.

4.2.2 Circuitry and electronic apparatus

A simple circuit is used for processing the signal from the specimen as shown in Figure 4.3. The ammeter is a Voltcraft Multimeter and an Iwatsu Digital Storage Oscilloscope is used to monitor the signal output. The benefit of this is that any spurious voltages generated by the operation of the furnace can be detected on the signal and allowed for.

4.2.3 Room temperature apparatus

Once satisfied of the accuracy of the circuitry the apparatus was tested with a range of metals and specimen dimensions. An anomalous dependence on thickness was noted. According to the Van der Pauw equation, thicker less resistive specimens yield smaller signals:

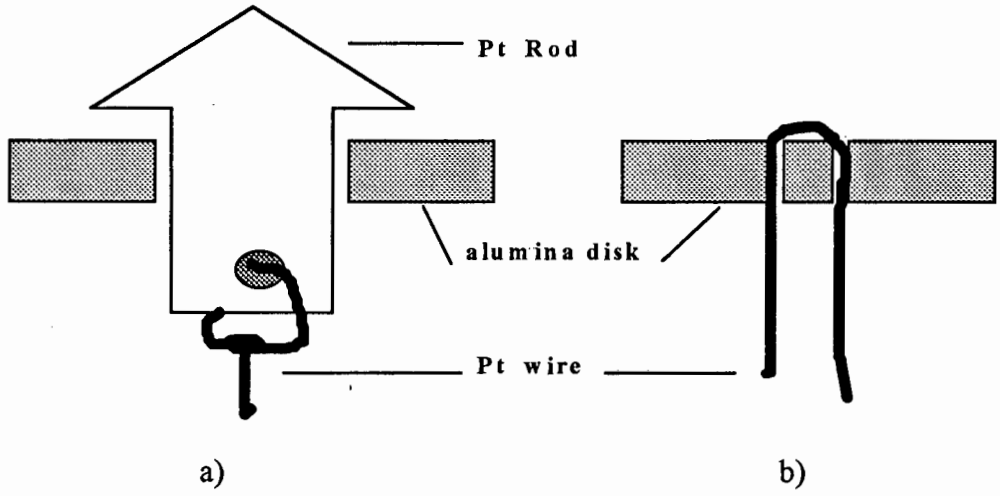

Figure 4.2a): Platinum Rod with conical tip and shoulder

b): Platinum wire twisted through closely spaced holes.

As Plomp[29] indicated an error of less than 5% associated with line contacts it was decide to twist platinum wire through closely spaced holes presenting a short line contact to the specimen, approximating a point contact as shown in Figure 4.2b. A square array of probes can be ensured by careful placements of the pairs of holes.

4.2.2 Circuitry and electronic apparatus

A simple circuit is used for processing the signal from the specimen as shown in Figure 4.3. The ammeter is a Voltcraft Multimeter and an Iwatsu Digital Storage Oscilloscope is used to monitor the signal output. The benefit of this is that any spurious voltages generated by the operation of the furnace can be detected on the signal and allowed for.

4.2.3 Room temperature apparatus

Once satisfied of the accuracy of the circuitry the apparatus was tested with a range of metals and specimen dimensions. An anomalous dependence on thickness was noted. According to the Van der Pauw equation, thicker less resistive specimens yield smaller signals:

$$V \propto \rho / d \qquad \text{Equation 4. 2}$$

Increasing the specimen signal by increasing the current failed to produce accurate results so it was deduced that the noise was proportional to the current.

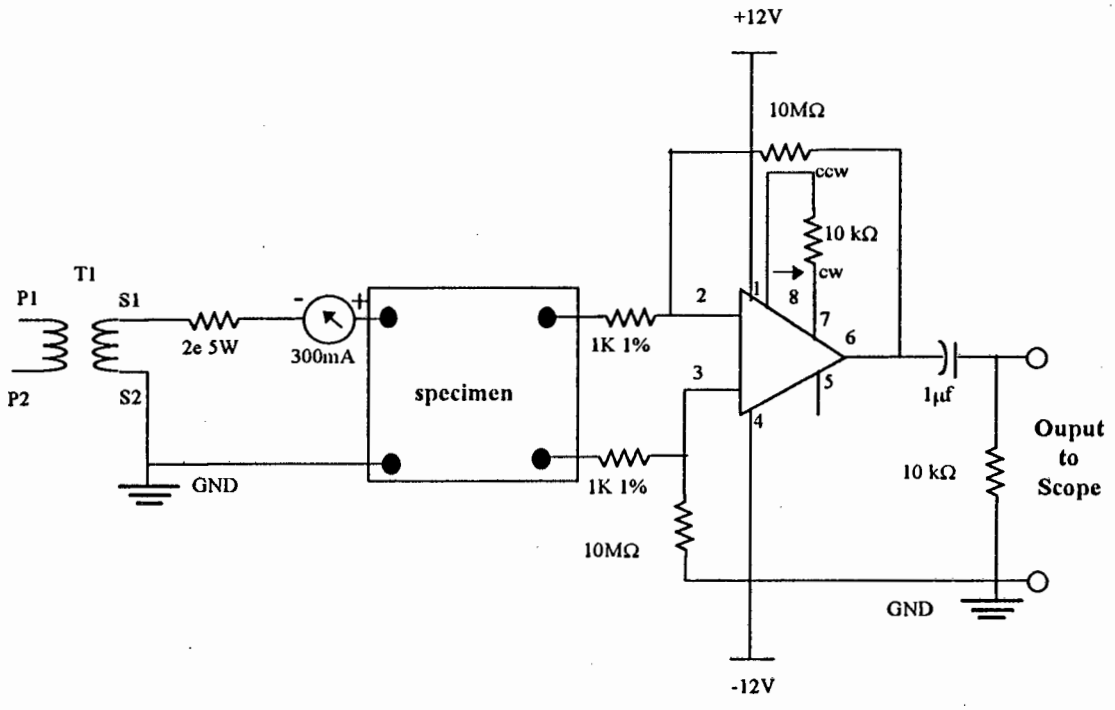

Figure 4.3: Circuit diagram for the signal amplifier.

Initially skin depth effects were considered but close analysis of our results eliminated this possibility. The origin of this noise was found to be inductive coupling. According to equation 4.3 a closed loop in a circuit can induct voltage onto itself and other conductors in the area if the current is changing, as was the case for the 300Hz AC current used.

$$V_{coupling} \propto A\left(\frac{\partial I}{\partial t}\right) \qquad \text{Equation 4.3}$$

where A is the enclosed area and t is time.

The specimen signal, according to the equation 4.1, is:

$$V_{specimen} = C\left(\frac{\rho}{d}\right) \bullet I \qquad \text{Equation 4.4}$$

and the coupling voltage can be written as follows:

$$V_{coupling} = K\left(\frac{\partial I}{\partial t}\right) \qquad \text{Equation 4.5}$$

where K and C are constant. Note that $\left(\frac{\partial I}{\partial t}\right)$ increases with I_{rms} due to the AC nature of the current (300Hz).

Increasing the RMS current increased the specimen signal but also the coupling voltage. If $C\left(\frac{\rho}{d}\right)$ >> K then the signal voltage is much larger than the coupling voltage and accurate readings can be obtained as observed for metal specimens. Thus it was necessary to minimise K. This was done by minimising current loop area and reducing the length of unshielded cable.

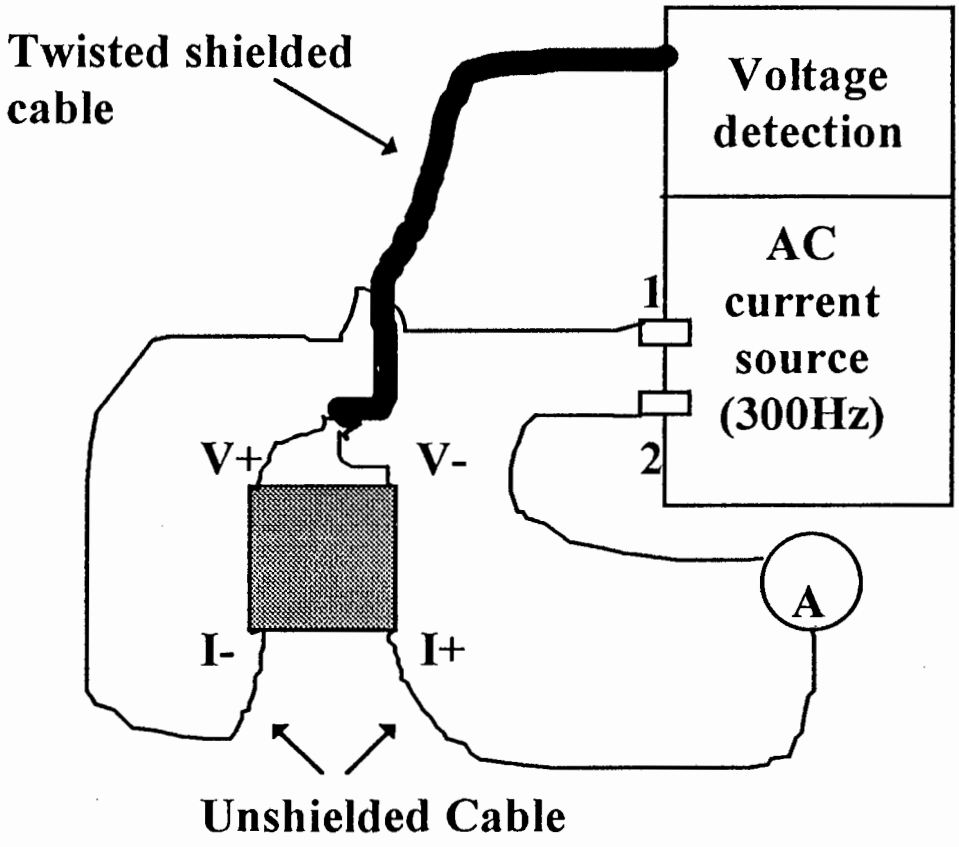

Figure 4.4: Original configuration for resistivity measurement showing large current loop and unshielded cable.

In the original configuration shown in Figure 4.4 the unshielded current cable had a high potential for inductive coupling with the coupling voltage being proportional to the area enclosed between the current leads beginning at 1 and 2. The configuration was changed as shown in Figure 4.5. The specimen stage was redesigned as shown in Figure 4.6 to aid the alignment of the conductors closely parallel to each other and the perspex specimen stage is shown in Figure 4.7. Using Cable 1 and 2 for the first R measurement and 3 and 4 for the second measurement no reconnection or movement of wires is required since the appropriate shielded pairs are unplugged from the voltage detection circuitry and the power source. By running the shielding up to the probes the length of bare wire was minimised, as is the current loop formed by the wires running up to the probe. The ammeter was also linked in series by running a length of cable into the power source box, making large loops of conductors to accommodate the ammeter unnecessary.

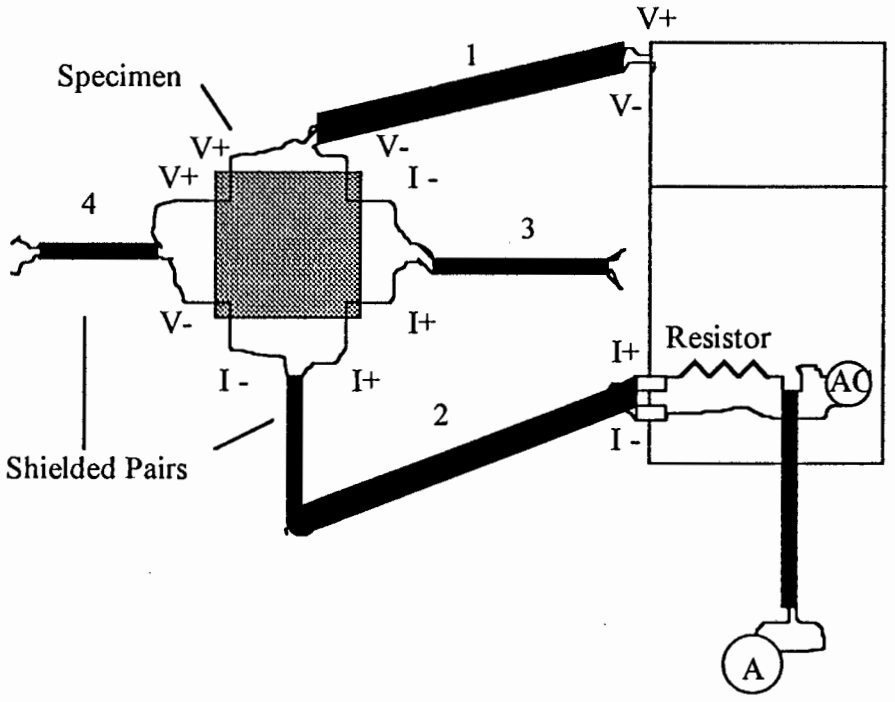

Figure 4.5: Present configuration showing shielded cables and probe arrangements.

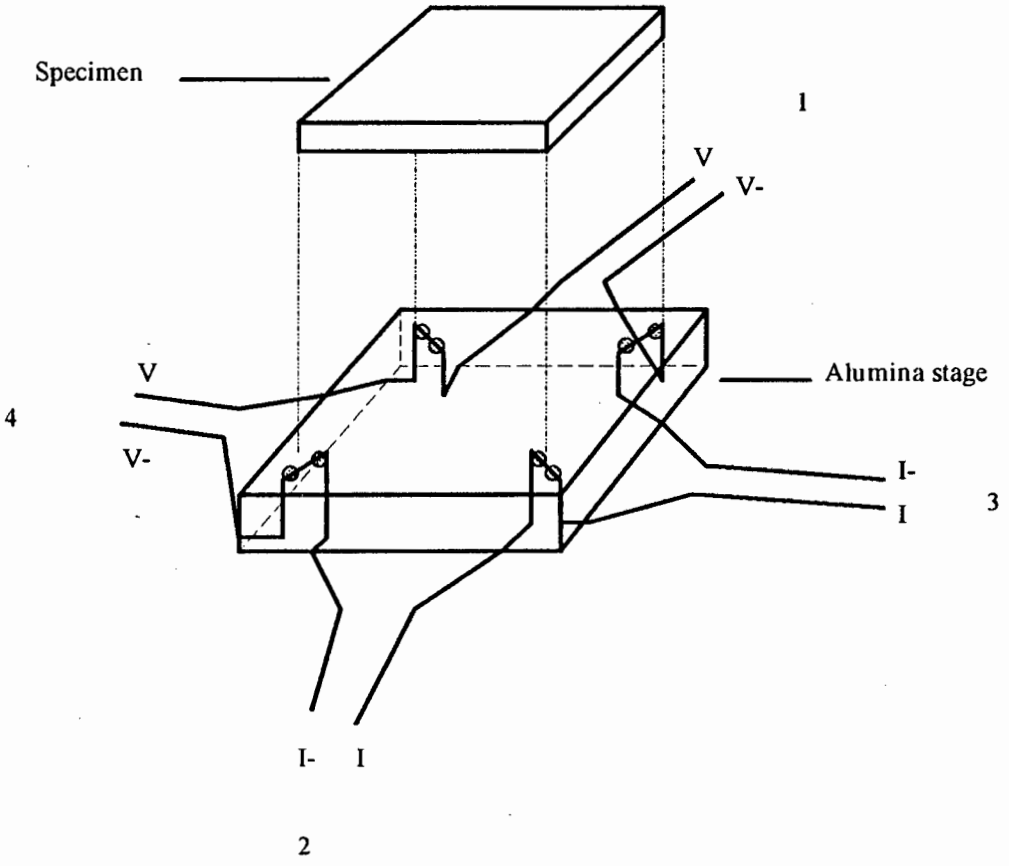

Figure 4.6: Resistivity specimen stage design which enables conductors to be arranged as shielded pairs.

The significance of this modification of the apparatus was that thicker and therefore less fragile specimens of ruthenium-aluminium could be used for accurate measurements.

Gold-palladium and platinum specimens of thickness ≈220μm yielded signals well in excess of a 50 mV 50Hz noise that was observed. Ruthenium-aluminium specimens however were thicker (1mm) and yielded signals of ≈ 600-800 mV. The noise was allowed for by subtracting the noise signal from the ruthenium-aluminium signal and calculating an uncertainty as follows:

$$\Delta\rho = \frac{\pi d}{4\sqrt{2}\ln 2}(50mV)\bullet\left(\frac{1}{I_1}+\frac{1}{I_2}\right) \qquad \text{Equation 4.6}$$

The consequence of this is that the error will increase slightly with temperature as the current drops.

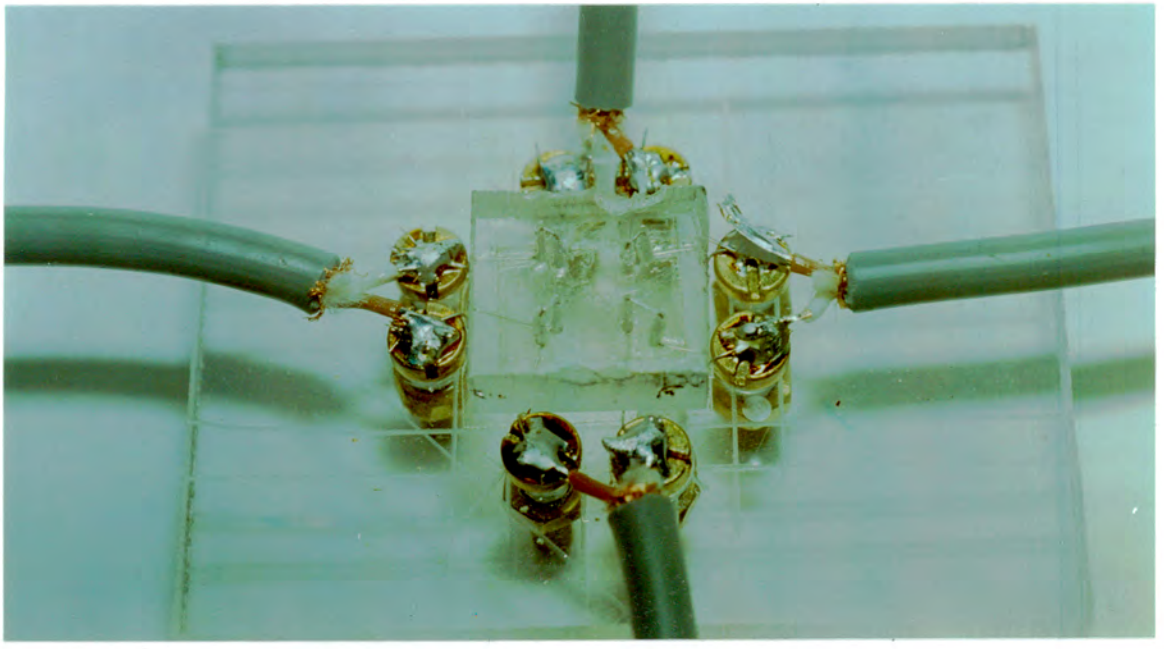

Figure 4.7 : Perspex Specimen Stage for room temperature measurements.

4.2.4 Design and construction of high temperature apparatus

To modify the room temperature apparatus for high temperature use it was necessary to use refractory materials as insulators and to spring load the specimen stage to ensure good electrical contact. The same multi bore alumina tubes to be used as insulators could also be load bearing; and to accommodate the new design of the specimen stage four pairs of insulated conductors were required to reach the specimen. The passage of these insulating tubes out of the furnace to the electrical connections must not be obstructed by the loading mechanism. Figure 4.8 shows the loading mechanism configuration and the location of the specimen stage between two spring loaded alumina support rods and within the tubular furnace wall.

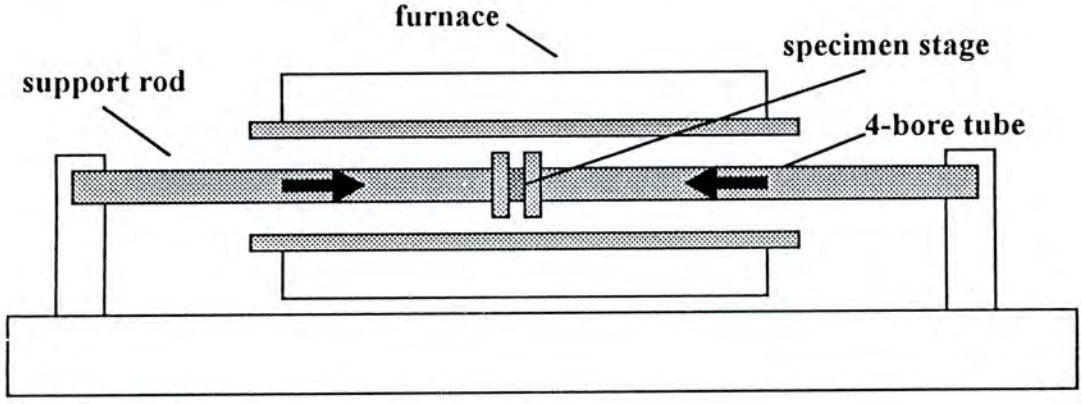

Figure 4.8: Furnace loading configuration

The four bore tube contained four two bore tubes (one for each pair of wires) and had a specially machined tip as shown in Figure 4.9 so as not to damage any of the wires moving into the stage when the tube was spring loaded. The tubes passed through the pre-drilled grub screw at the end of tube holder as shown in Figure 4.10.

Photographs of the actual apparatus are shown in Figures 4.11 - 4.22.

Figure 4.9: Specially machined tip of the four bore tube.

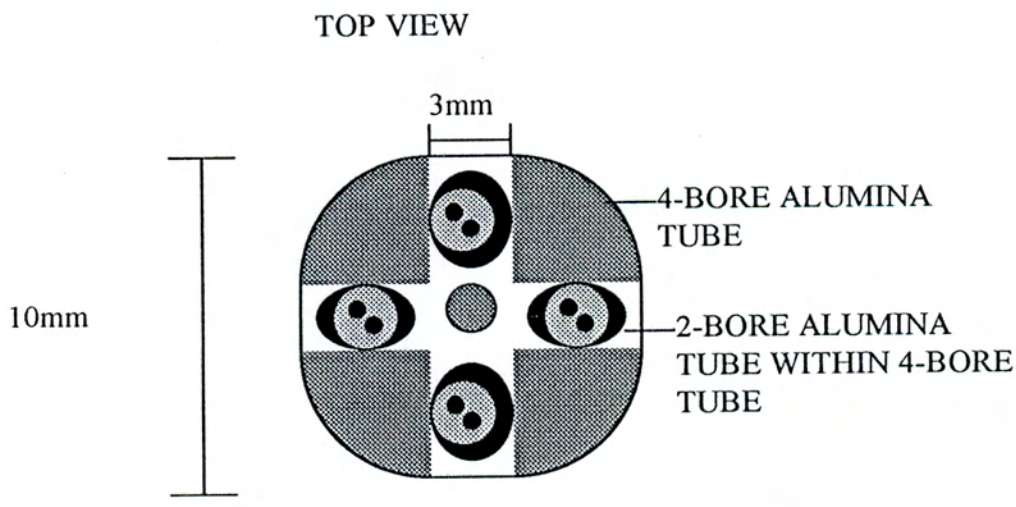

Figure 4.10: A diagram of the placement of the two bore insulator tubes in the four bore support tube. A cross shaped channel was cut into the tip of the four bore tube to allow conductor wires to leave the specimen stage and not be trapped between the tips of the four bore tube and the specimen stage. The pressure from the spring loading mechanism, which is applied through the four bore tube tips (dark quadrants), would deform the conductor wires.

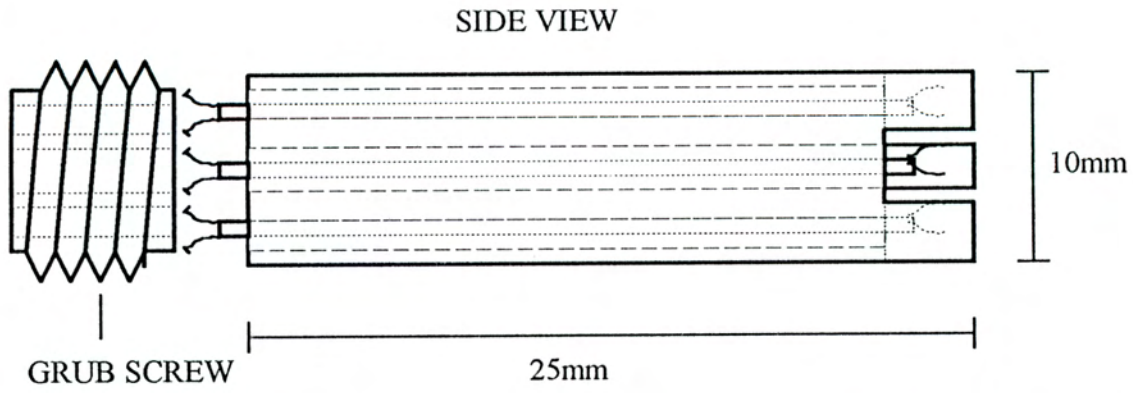

Figure 4.11: Side view of the four bore support tube assembly with the two bore insulators protruding from the end of the four bore support tube into the grub screw of loading mechanism.

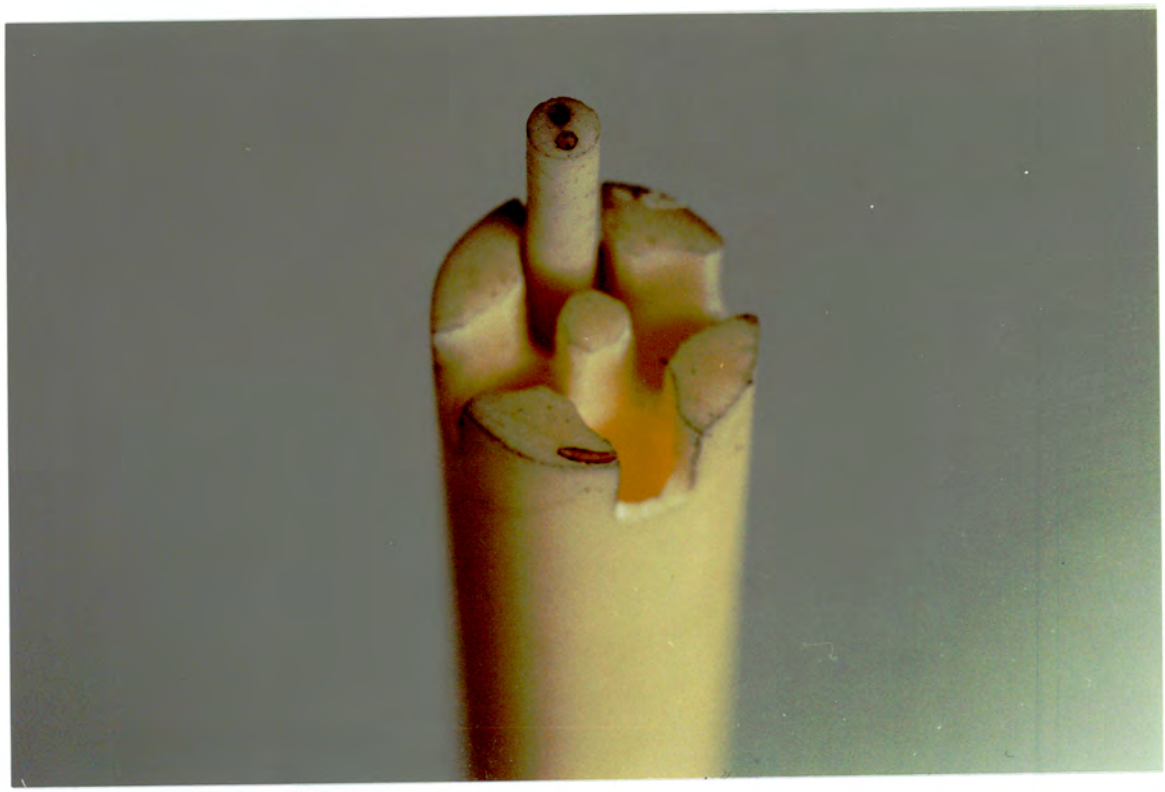

Figure 4.12: Four bore tube with two bore tube inserted.

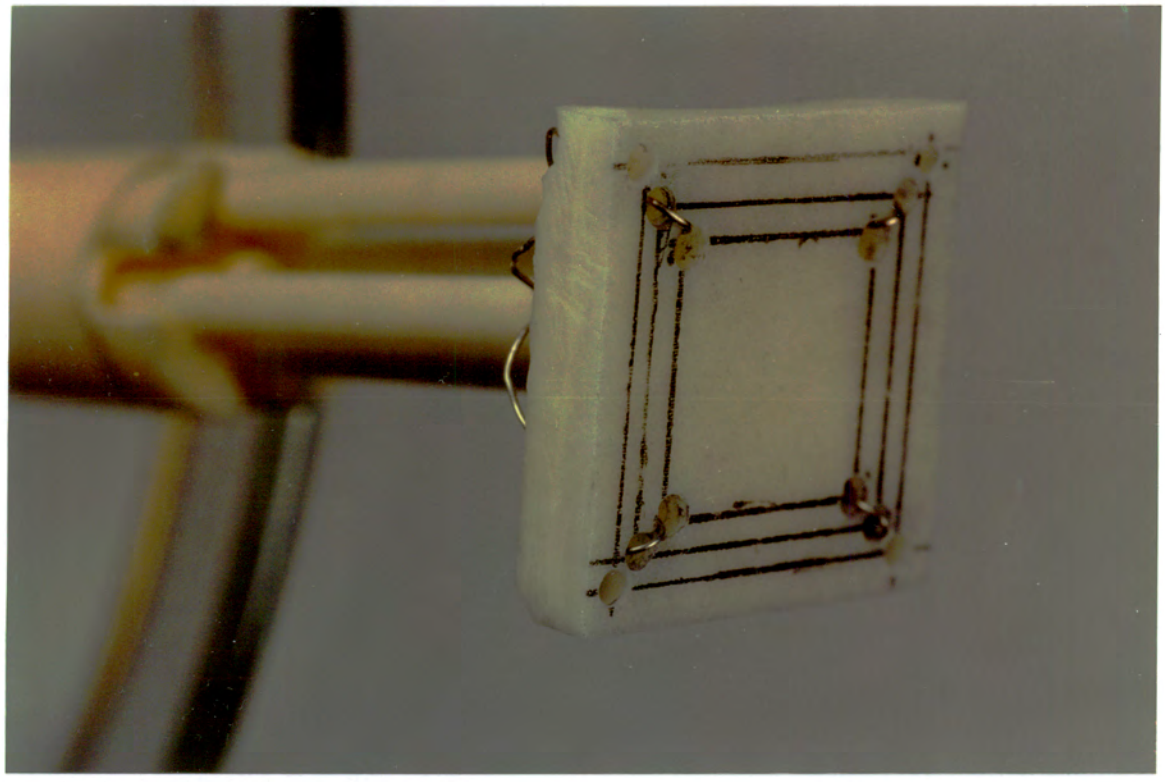

Figure 4.13: Oblique view of specimen stage.

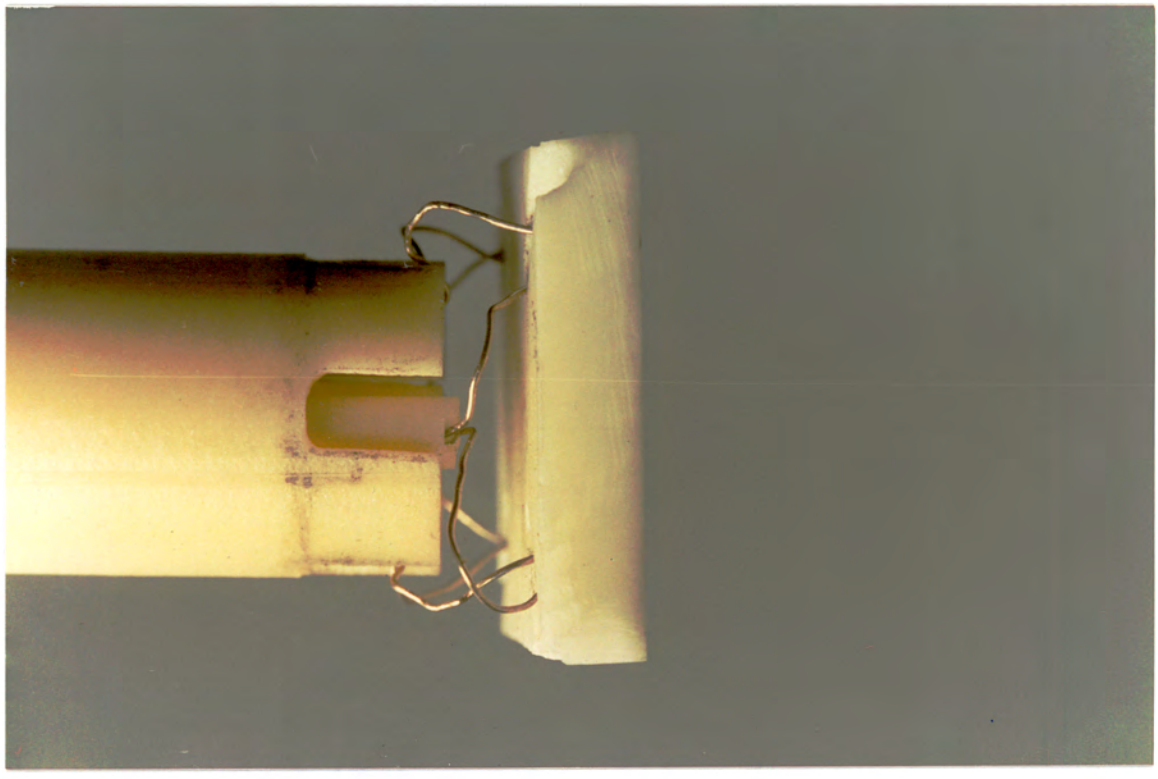

Figure 4.14: Side view of specimen stage.

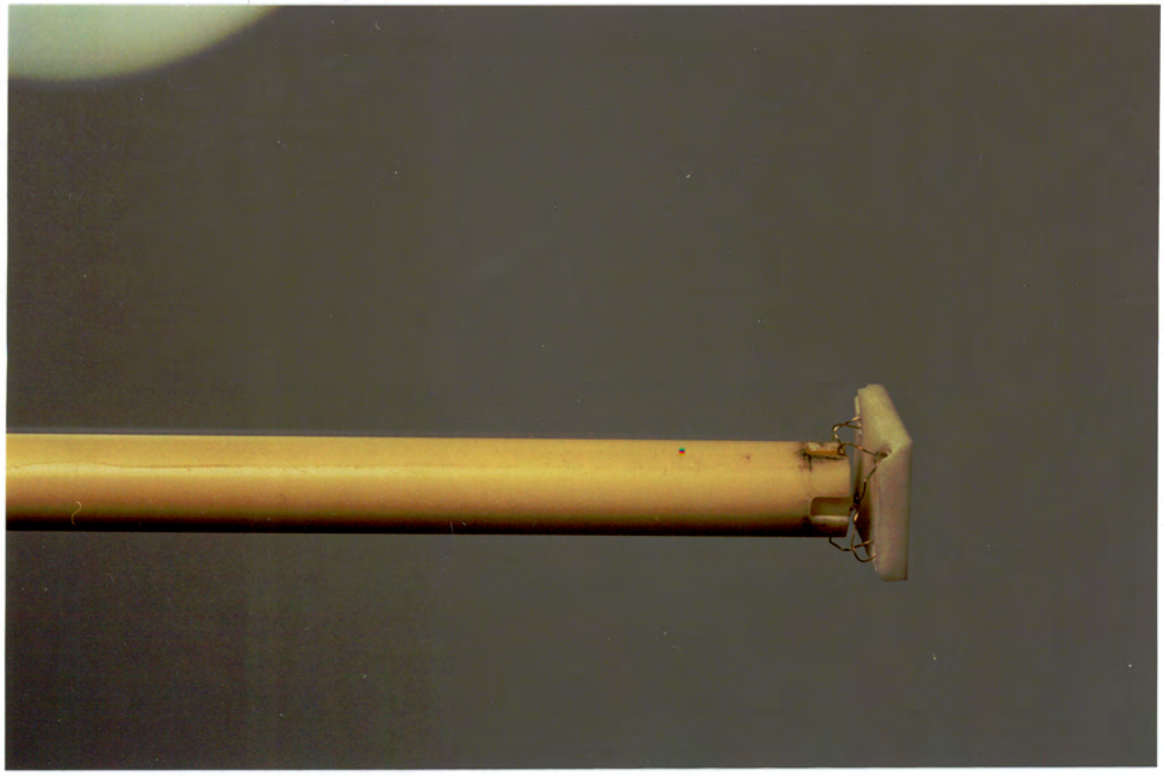

Figure 4.15: Four bore tube with stage.

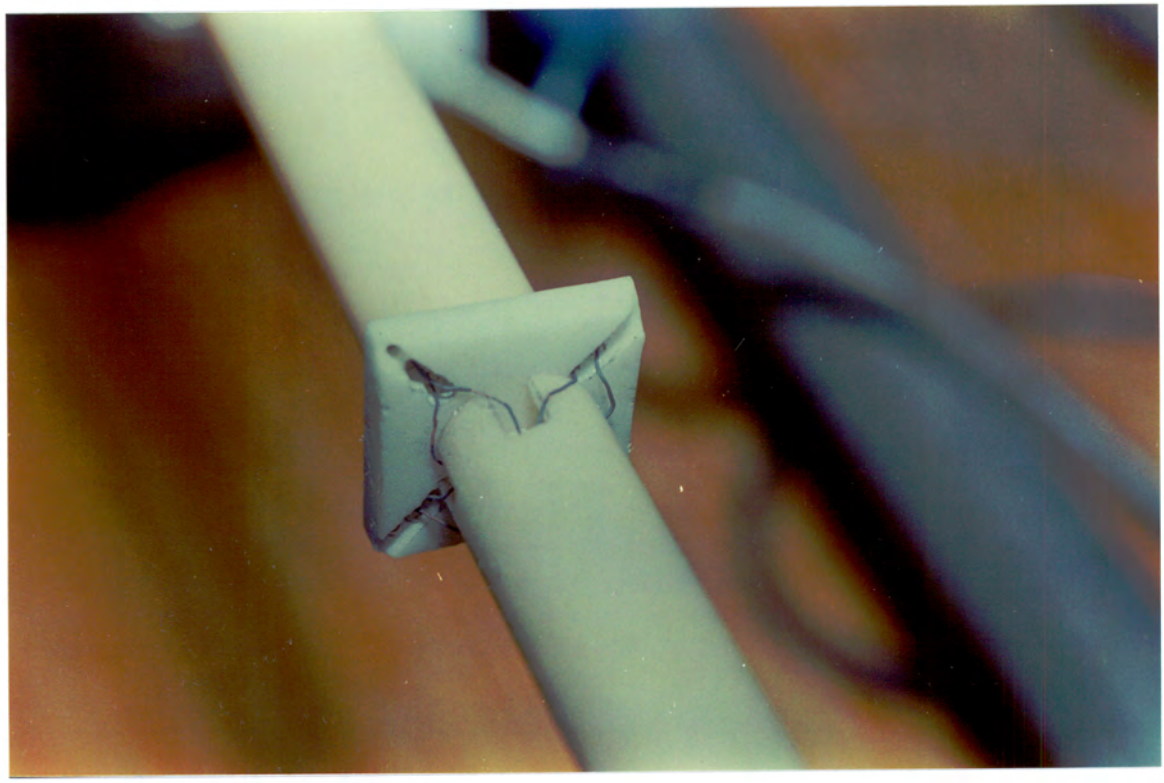

Figure 4.16: Rear view of loaded stage.

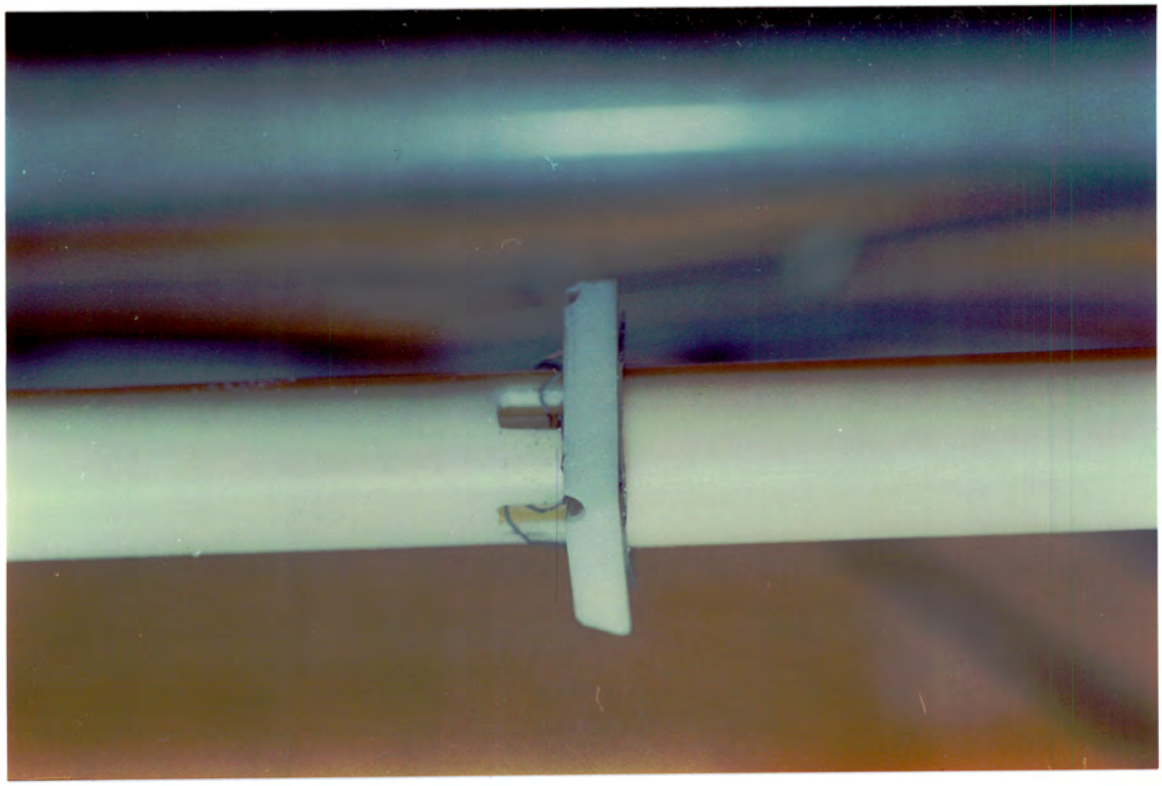

Figure 4.17: Side view of loaded stage.

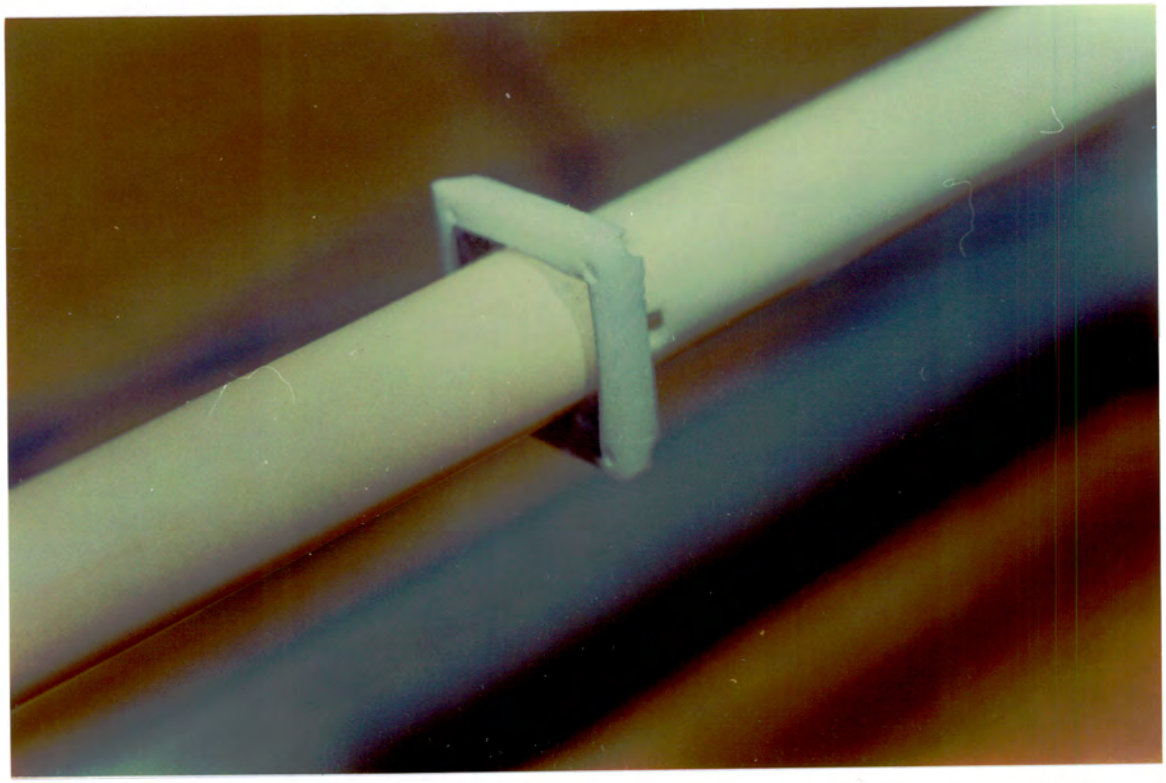

Figure 4.18: Frontal view of loaded stage with platinum specimen. This assembly had been to 800°C and the platinum shown here is oxide free. The oxidation of the copper wires can be seen in the two preceding photographs. The copper wires were subsequently replaced with platinum wires.

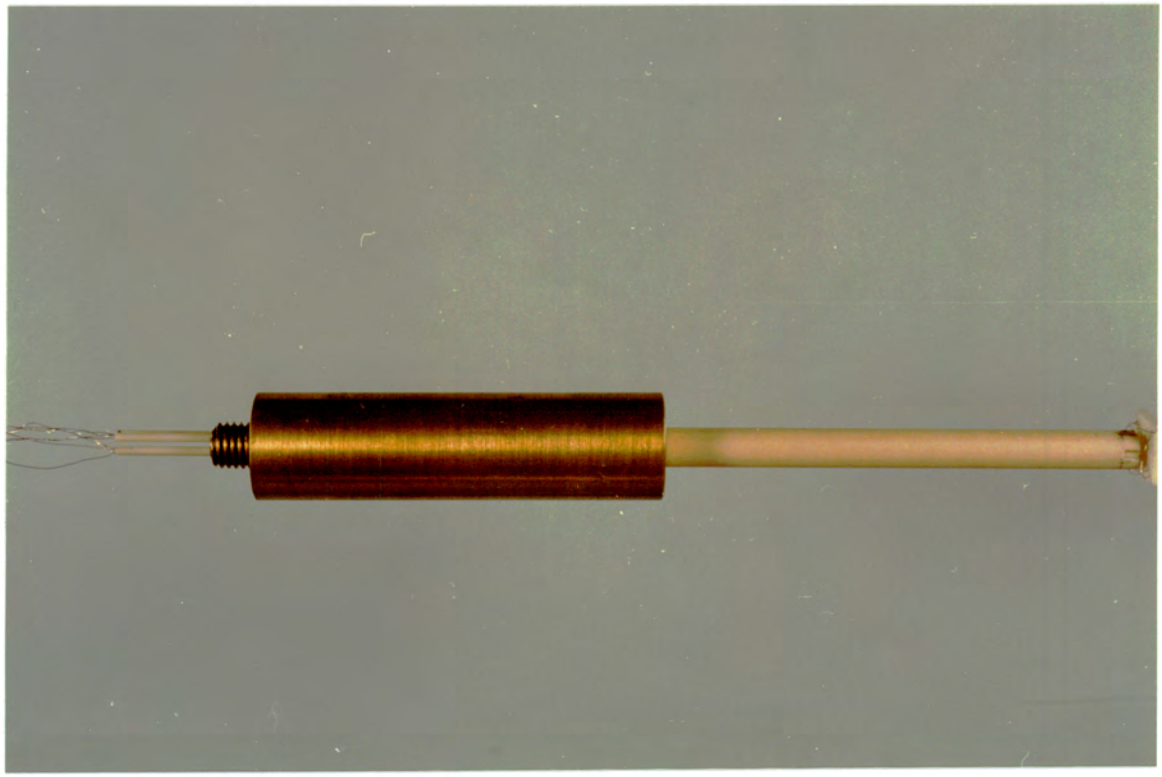

Figure 4.19: Four bore tube within brass holder with two bore insulators protruding from the grub screw at the back.

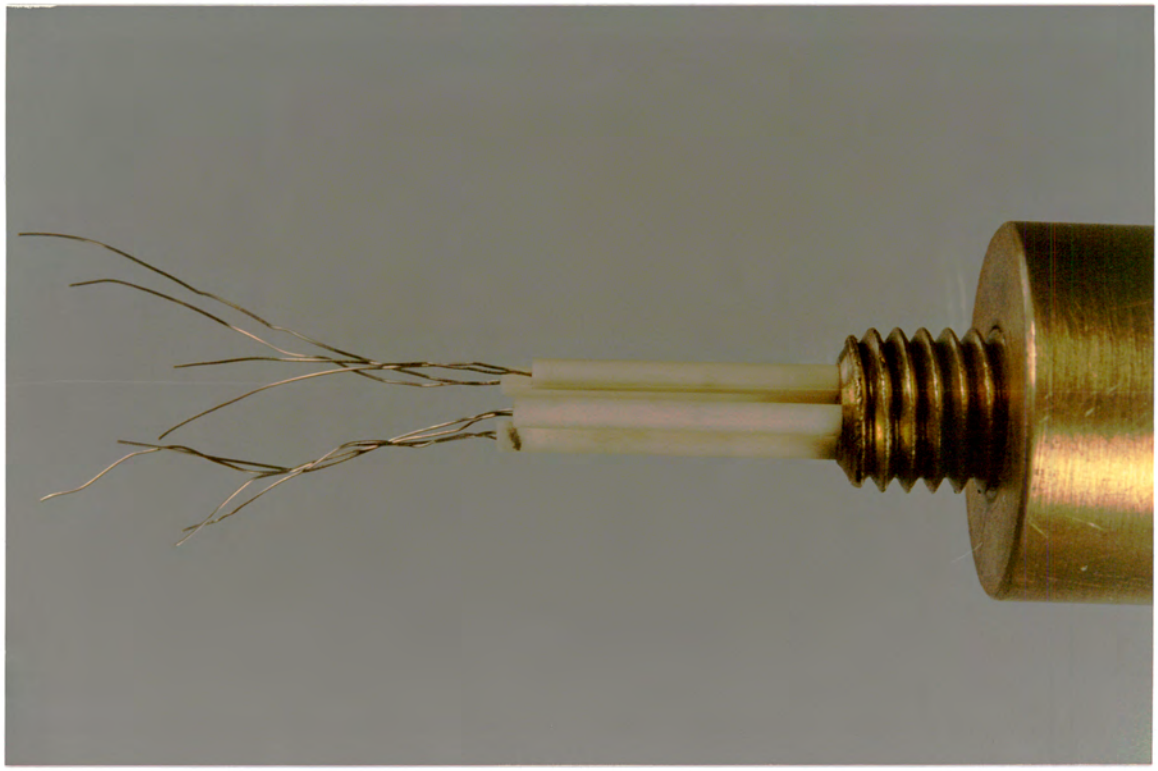

Figure 4.20: Close up of grub screw and insulators.

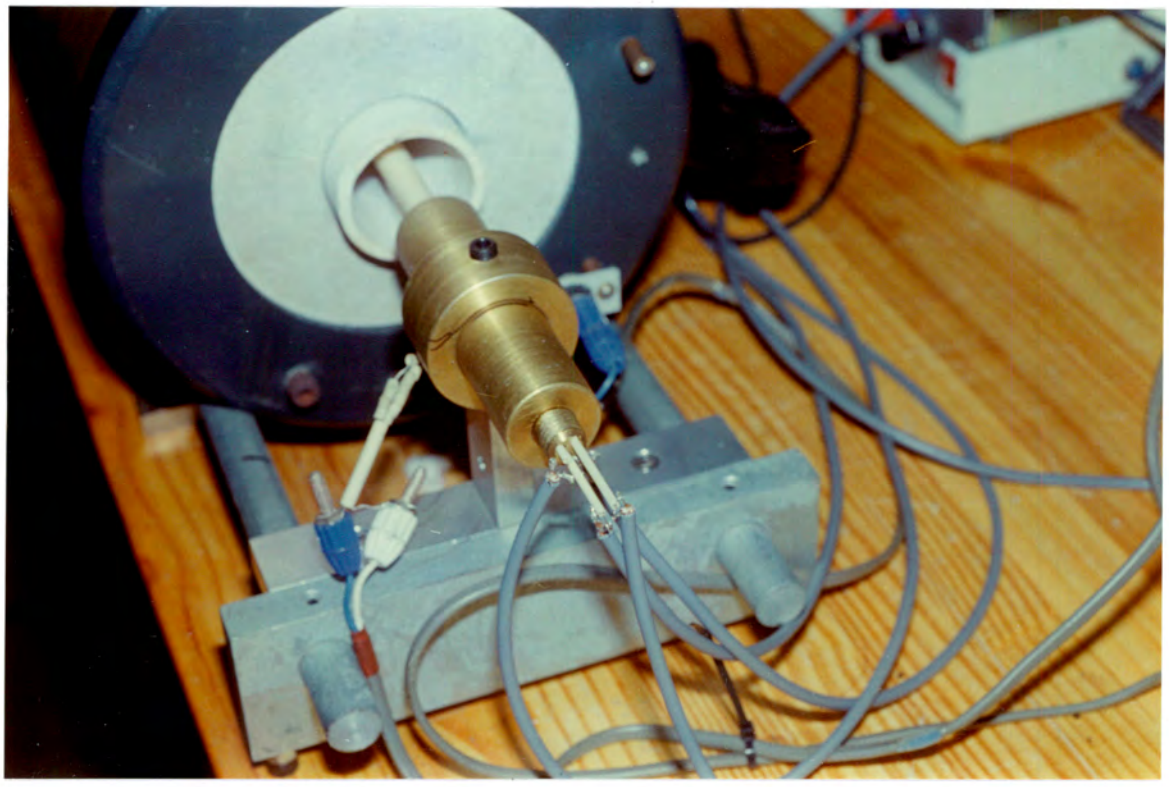

Figure 4.21: Close up of electrical connections to wires in the insulators.

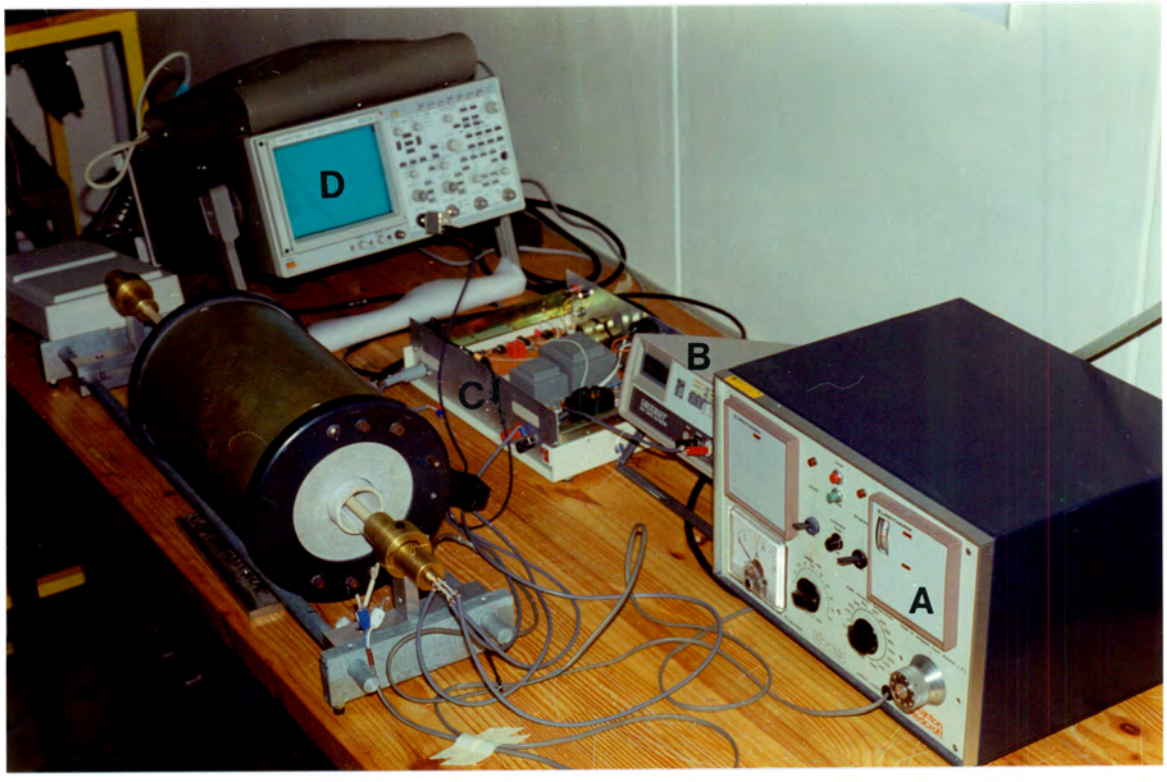

Figure 4.22: Furnace with controller (A), ammeter (B), power supply and signal amplifier circuitry (C) and digital storage oscilloscope (D).

4.3 Thermo-e.m.f. measurement

The construction of a thermo-e.m.f. measurement apparatus for the analogue subtraction method was not without difficulty. Initially the specimen was aligned perpendicular to the furnace worktube and type R thermocouples were used as well as a specially machined alumina casing for the platinum heater which rested on top of the specimen. Thermocouples were also run in grooves along the sides of the support bars resulting in a large inductive coupling effect. The specimen alignment required perfectly parallel support rods with squared faces to ensure good contact, which was difficult to obtain, and type R thermocouples proved inappropriate as will be explained below. The heater casing proved difficult to position to ensure good thermal contact with the specimen. The improved design described below provided accurate results and is easier to work with.

4.3.1 Design and construction of specimen holder

The specimen stage shown below in Figure 4.23 satisfies the requirements of the method. The thermocouple beads are in contact with the specimen at its ends and there is a platinum heater adjacent to one end such that a dynamic temperature gradient can be created across the specimen. The specimen must be in contact with the alumina disc near the heater to ensure a large enough temperature gradient. The thermocouple wires are encased in thin two bore tube insulators to minimise loop area and prevent inductive coupling.

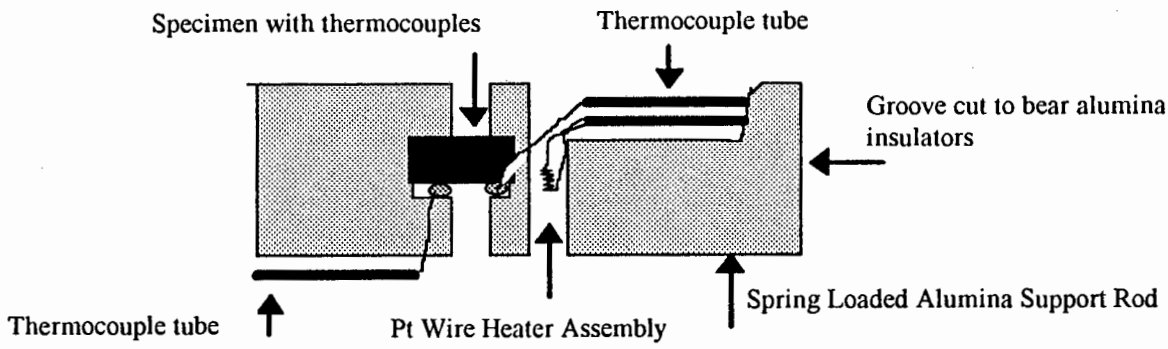

Figure 4.23: Diagram of side view of thermo-emf specimen stage.

4.3.2 Thermocouple choice and testing procedure

Platinum/platinum-rhodium (type R) and copper/constantan (type T) thermocouples were assessed. Gold-palladium's thermo-e.m.f. was measured successfully with both at room temperature but the small thermo-e.m.f. of ruthenium-aluminium alloys requires large thermocouple voltages in order to be measured accurately and attempts to measure the thermo-e.m.f. with type R thermocouples failed. The reason for this is that the platinum heater generates at most a 5°C temperature gradient across the sample. For gold-palladium and the ceramics that this method was designed for, this would generate a large thermo-electric voltage from the specimen. A combination of ruthenium-aluminium specimens and type R thermocouples produces a very small voltage which cannot be processed accurately. Type T thermocouples would also register an $\approx$ 0.2mV DC voltage for a similar temperature gradient as opposed to a 0.03mV maximum voltage for type R thermocouples. Type T thermocouples with the new specimen stage yielded reproducible results for ruthenium-aluminium alloys. An added advantage of using type T thermocouples is that platinum can be measured for calibration purposes as the analogue subtraction method will give results in terms of thermo-e.m.f. relative to copper and not platinum, which would be the case if type R thermocouples were used.

The limitation of using type T thermocouples is that the maximum operation temperature is $\approx$ 400°C. The very linear resistivity behaviour of ruthenium-aluminium alloys to 1000°C and the lack of phase changes suggests that the temperature dependence may be constant in the room temperature to 1000°C range and that studying the thermo-e.m.f. between 20°C and 400°C would be sufficient. Type T thermocouples were thus selected for the thermo-e.m.f. apparatus.

The alignment of the specimen (see Figure 4.23) was such that temperature gradients could exist along it but this poses no problem to the measurement of thermo-e.m.f. as it is the voltages generated by a changing temperature gradient that the circuitry uses to plot the straight line proportional to the sample thermo-e.m.f. The average specimen temperature can be measured using the two thermocouples that are in

contact with the specimen at its ends. The specimen was placed so that it was in the centre lengthwise of the furnace work tube. The thermocouples at both ends registered the same temperature to within a few degrees.

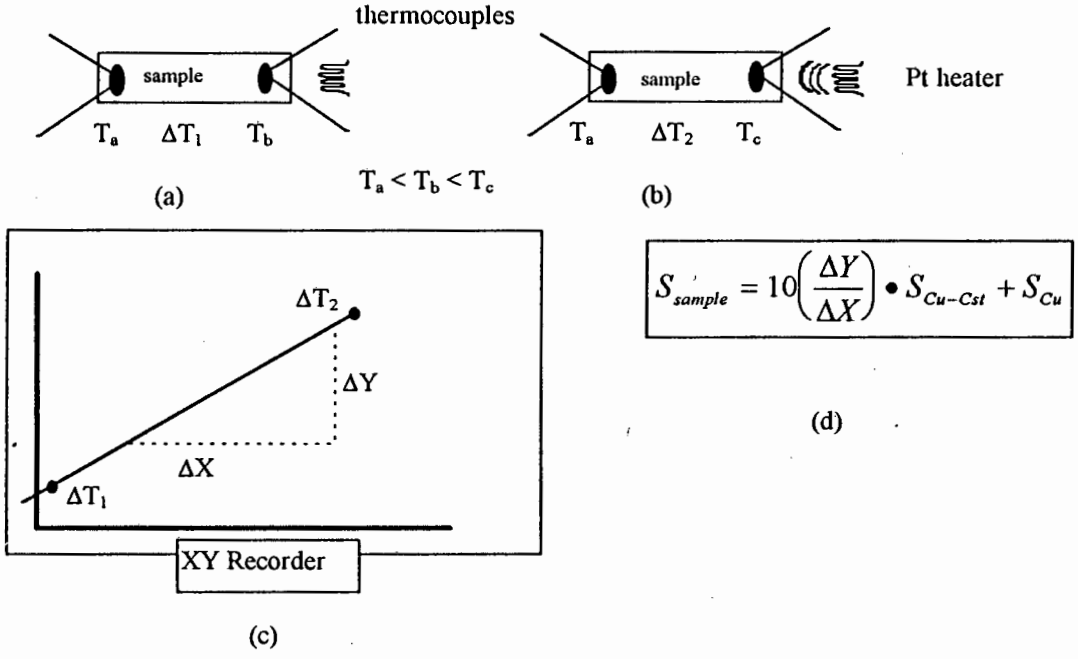

Figure 4.24: Idealised schematic diagram of operation of thermo-e.m.f. apparatus. A heater increases the temperature difference from (a) ΔT_1 to (b) ΔT_2. The analogue subtraction circuitry generates two signals from the thermocouples attatched at the sample ends. These signal are linearly related to each other by the absolute thermo-e.m.f. of the sample. The XY plot (c) of the two signals generates a straight line the slope of which is proportional to the absolute thermo-e.m.f. of the sample as expressed in the equation above (d).

The specimens were inserted into the specimen stage, tested and removed. This sequence was repeated to estimate any error due to changes in specimen-thermocouple contact. Thermocouple beads were not made but the copper and constantan strands were twisted together so that both were in contact with each other and with the specimen. Inserting the twisted wire into the grooves cut for the specimen and spring loading the assembly, heating it slowly, with prolonged dwells at intermediate

temperatures, to 400°C does lead to some degradation of the wire but results do not indicate a loss of accuracy of the equipment upon retesting of the same specimen.

The analogue subtraction method has no requirement for specific specimen shape and size. Specimens were generally 1mm thick and rectangular with a variety of aspect ratios.

4.3.3 Calculations and errors

Readings were taken by measuring the slope produced by the XY plotter by hand and using the equation in Figure 4.24. It was found that an error in measurement of 0.5mm corresponds to an error in the thermo-e.m.f. of 2.5 %. The calculations depend on the type T thermocouple coefficient which varies between 40μV/K at room temperature and 60μV/K at 400°C. The absolute thermo-e.m.f. of copper must also be known at the measuring temperature. The type T voltage-temperature table between 0 and 400°C was used to calculate the coefficient at 10°C temperature intervals by performing linear regression on the voltage-temperature data. The errors associated with these calculations was less than 0.1%. The main source of error is then in the measurement of the slope by hand.

5. Results

In this chapter the results obtained for the resistivity and thermo-e.m.f of platinum, gold-palladium and ruthenium-aluminium alloys are presented. The results obtained in this study for platinum and gold-palladium, which served as calibration materials, are compared with the published results for these materials. The dependence of the resistivity and thermo-e.m.f. on temperature of the ruthenium-aluminium alloys is reported. At the end of the resistivity and thermo-e.m.f. sections the results obtained for the two properties are tabulated for each composition over the measurement temperature range for ease of reference. Compositions referred to in this chapter are those obtained from EDS measurements.

The results obtained for platinum and gold-palladium compared well with the published values, as is detailed in the following sections, and therefore the equipment constructed is accurate and it may be assumed that the results obtained for the ruthenium-aluminium alloys are accurate. These results represent the first determination of the resistivity and thermo-e.m.f. in the ruthenium-aluminium system.

5.1 Resistivity vs. temperature

5.1.1 Platinum and gold-palladium

The concurrence between the results presented here and published results for platinum[4] and gold palladium[13] establishes the accuracy of the equipment that has been designed and constructed, as detailed in the previous chapter. The results for platinum were taken from a metal reference book which reported values at 20°C, 100°C, 500°C and 1000°C. These values were used to construct the published curve for platinum shown in Figure 5.1. The experimental results obtained in this study follow this curve closely. A published result for the resistivity of the gold-palladium composition used in this study could not be found. Ho et al[13] published a paper in 1983 which collated all the

available data on the electrical resistivity of the gold-palladium system. The data was used to generate curves for the dependence of the resistivity of gold-palladium on temperature and composition. For gold-palladium of composition $Au_{39.8}Pd_{60.2}$ Ho et al[13] report a value of 27.93μΩ.cm ± 2% at 20°C. In the present study a value of 27.7μΩ.cm at 20°C was obtained for gold-palladium of composition $Au_{41.4}Pd_{58.6}$. It is expected that the composition richer in gold should have a slightly lower resistivity and weaker temperature dependence. Taking this dependence of the resistivity and its temperature dependence on composition into account the slight mismatch observed in Figure 5.1 can be rationalized and the results obtained in this study for the resistivity of gold-palladium can be regarded as accurate. The resistivity of gold-palladium has a weaker dependence on temperature than platinum.

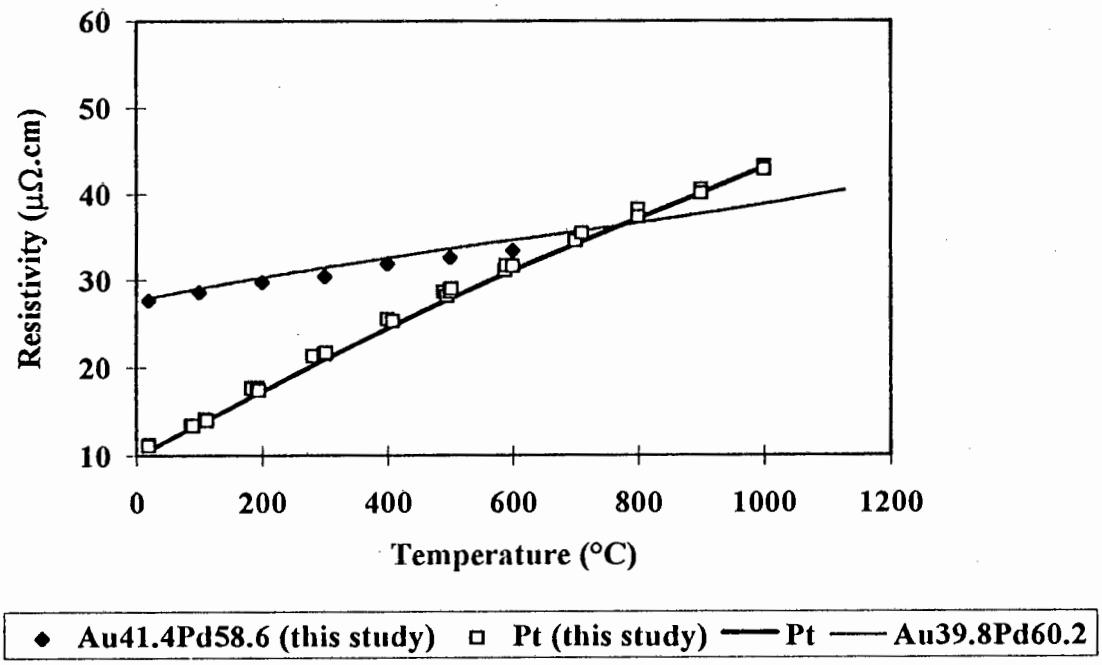

Figure 5.1: The dependence of resistivity on temperature for platinum and gold-palladium. The results from this study are indicated and the thick and thin solid curves are the published results for platinum[4] and gold-palladium[13] respectively.

5.1.2 Ruthenium-aluminium alloys

This section contains resistivity results for the ruthenium aluminium system and the following comments are applicable to all results. The error bars represent the electrical noise arising from circuitry and furnace which overshadows possible contributions from incorrect temperature measurement and statistical deviation of the mean resistivity value at each measurement temperature. Details of the error bar calculation are given in the chapter on the construction and design of the apparatus. Hysteresis was not observed when both heating and cooling curves were recorded as cooling curve data fell above and below the heating curve and within the experimental error. Most samples were exposed to temperatures near 1000°C in air for approximately 12 hours and this was not seen to effect the resistivity.

Two groups of data are presented. The first is for the eutectic compositions near 30 at. % aluminium. These are characterized by a high room temperature resistivity but a weaker dependence of resistivity on temperature than the compositions near the stoichiometric point at 50 at.% aluminium. The second group of data are measurements on samples from nominal compositions near the stoichiometric point. None of the samples show any change in the resistivity vs. temperature slope with increasing temperature and the curves have linear correlation coefficients of resistivity to temperature of 0.99 or better, reflecting their linearity. This enables isotherms to be constructed for the dependence of resistivity on composition which is shown in the discussion chapter. Each graph has a published platinum curve[4] included for reference.

The resistivity values for all the ruthenium-aluminium samples and the results obtained in this study for platinum are included in Table 5.1 at the end of this section. In Table 5.2 the slopes of the resistivity vs. temperature graphs for ruthenium-aluminium and platinum are recorded and the calculated temperature coefficients are shown. The slopes and temperature coefficients have been calculated over the range 20°C to 1000°C and

although this is not strictly appropriate to platinum, because of the downward curvature of the platinum resistivity vs. temperature curve, the values are included for comparison.

5.1.2.1 Eutectic compositions (near 30 at. % aluminium)

The 30.2 at. % aluminium alloy shows both a lower room temperature resistivity and shallower temperature dependence of resistivity on temperature than the 29.7 at. % aluminium composition. These differences are however within the experimental error and no inferences can be drawn from them.

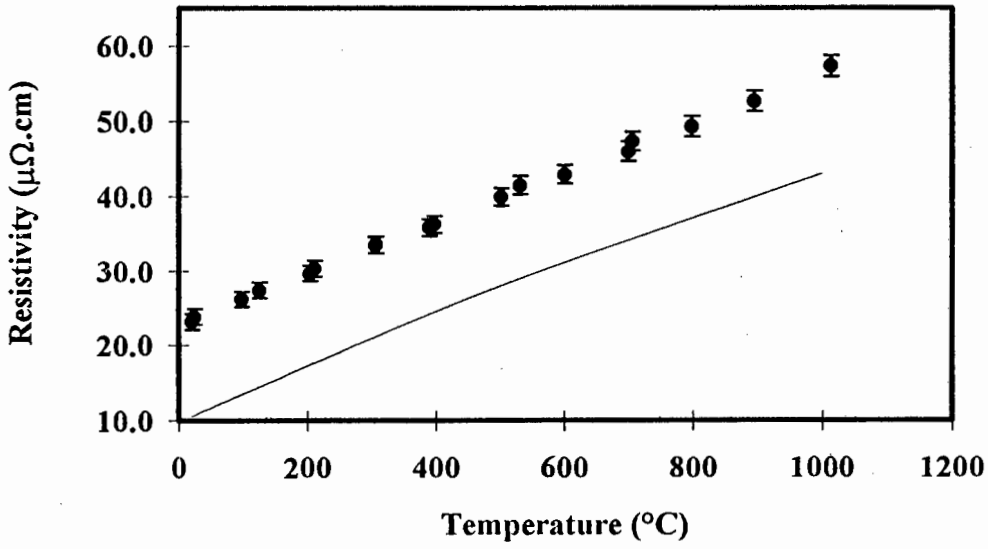

Figure 5.2: Variation of resistivity with temperature for the 30.2 at. % aluminium alloy. The solid line represents the published platinum curve referred to in section 5.1.1.

The linearity of the dependence of resistivity on temperature of the 30.2 at. % aluminium composition is seen in Figure 5.2. The 30.2 at. % aluminium alloy's resistivity curve parallels the platinum resistivity curve except for the slight downward curvature of the platinum curve near 1000°C.

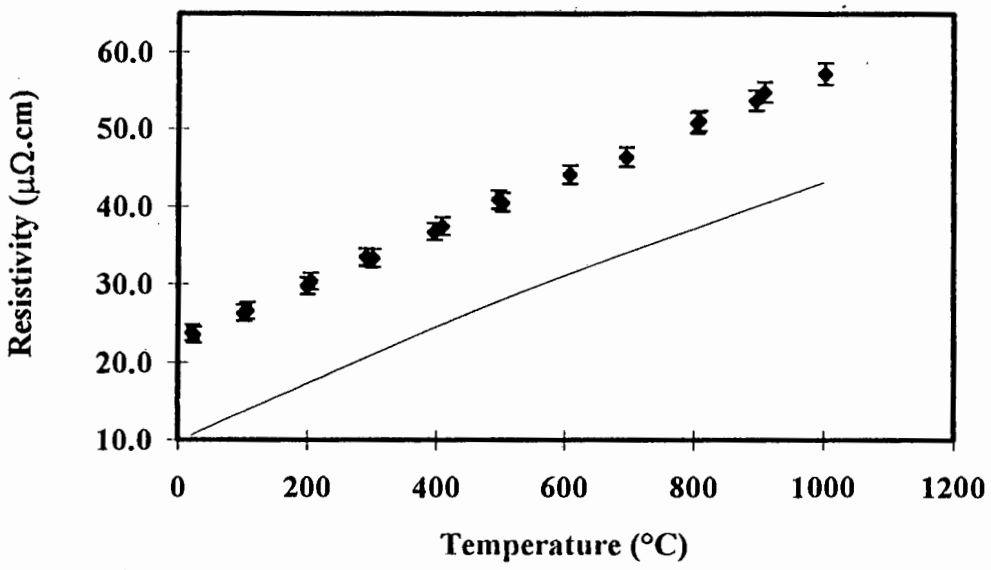

Figure 5.3: Variation with temperature of resistivity for the 29.7 at. % sample. The solid line represents the published platinum curve referred to in section 5.1.1.

In Figure 5.3 resistivity values at similar measurement temperatures show strong correspondence. The fact that these readings were taken during different temperature runs also illustrates the lack of influence of repeated cycling to high temperatures on the resistivity behaviour of the 29.7 at. % aluminium sample This can also be seen in the dependence of the 30.2 at. % aluminium sample where the resistivity shows the same lack of dependence on temperature cycling even to elevated temperatures such as a 1000°C.

The 29.7 at. % aluminium sample's resistivity vs. temperature curve is also seen to parallel the platinum resistivity vs. temperature behaviour.

5.1.2.2 Compositions near 50 at.% aluminium

All compositions near 50 at. % aluminium show resistivities lower than the eutectic compositions at 20°C. Their dependence of resistivity on temperature is greater, resulting in compositions near 50 at. % aluminium being only marginally lower in resistivity than eutectic compositions at 1000°C. Resistivity vs. temperature graphs are presented in order of increasing atomic % aluminium over a range of approximately 5 atomic % beginning at 45.0 atomic %. These compositions were measured using energy dispersive spectroscopy and are expected to represent the relative atomic percent aluminium in the samples accurately if not the absolute values on account of the analysis being standardless. The 45.0 at. % aluminium sample has one of the higher resistivities of the near stoichiometric compositions and the resistivity vs. temperature slope seen in Figure 5.4 only parallels platinum's resistivity vs. temperature behaviour up to 500°C, where the downward curvature of the platinum curve becomes evident. Resistivity values of the 45.0 at. % aluminium sample are seen to correlate closely with each other and deviations are all within the experimental error.

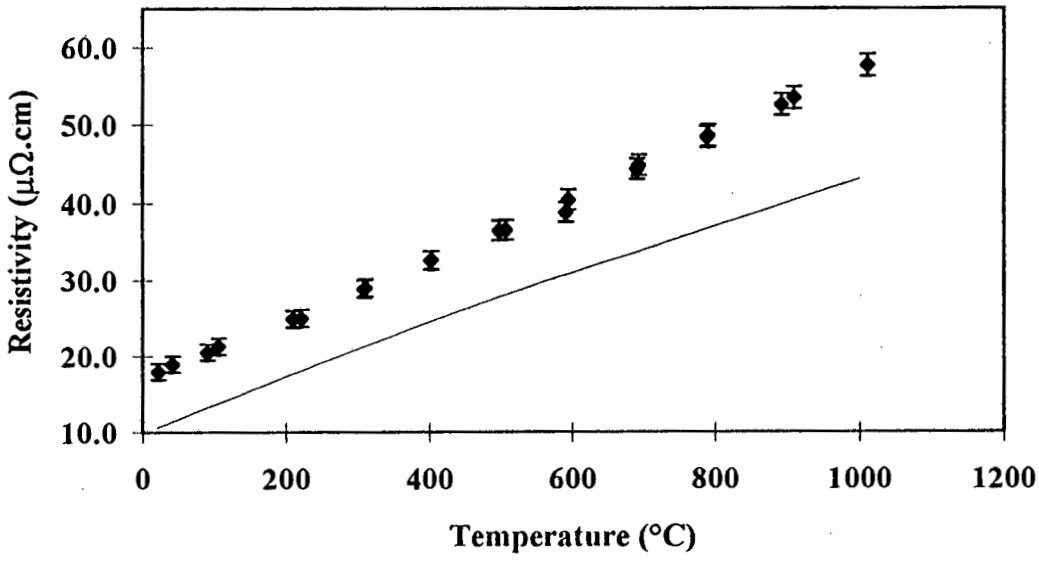

Figure 5.4: Variation with temperature of resistivity of the 45.0 at. % aluminium alloy. The solid line represents the published platinum curve referred to in section 5.1.1.

The 45.2 at. % aluminium sample has a slightly lower resistivity than the 45.0 at. % aluminium sample but shows a similar dependence of resistivity on temperature as shown in Figure 5.5. The departure of the resistivity curve of the 45.2 at. % aluminium sample from being parallel to the platinum curve also becomes evident near 500°C. The resistivity values are seen to correlate closely with each other except near 400°C. This deviation is within the experimental error. As with the 45.0 at. % aluminium sample no hysteresis is observed and the dependence of resistivity on temperature is approximately linear.

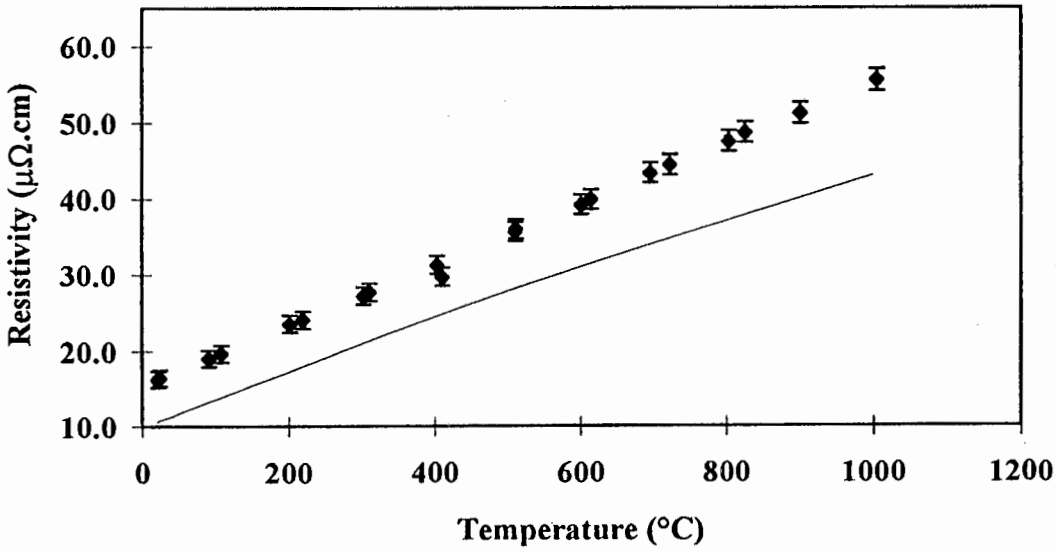

Figure 5.5: Variation with temperature of resistivity for the 45.2 at. % aluminium alloy. The solid line represents the published platinum curve referred to in section 5.1.1.

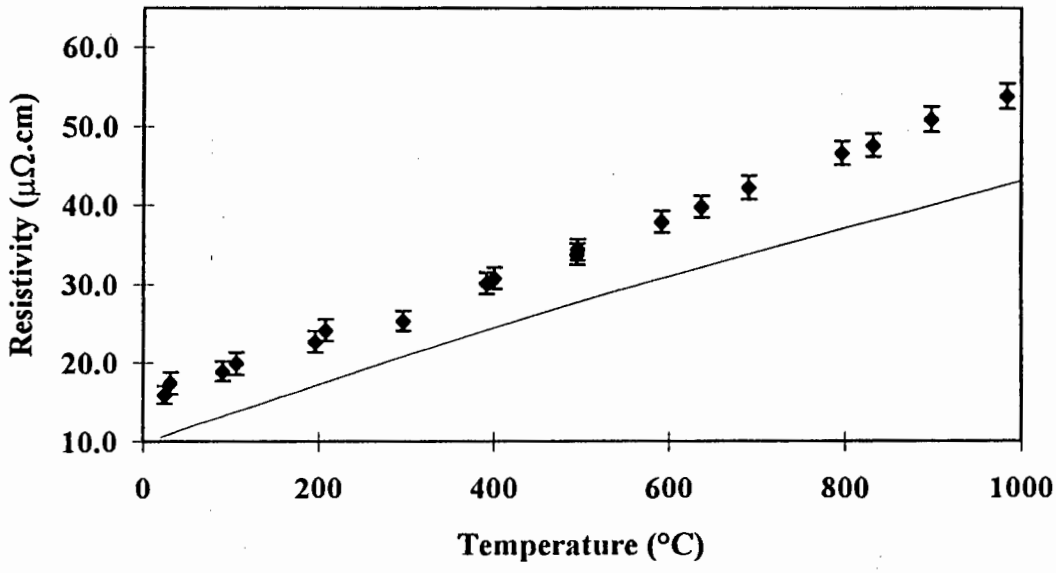

Figure 5.6: Variation with temperature of resistivity for the 45.3 at. % aluminium alloy. The solid line represents the published platinum curve referred to in section 5.1.1.

Measurements of resistivity on the two temperature ramps for the 45.3 at. % aluminium sample were not all made at the same temperature, particularly at higher temperatures, but linear behaviour is nevertheless evident in Figure 5.6. Resistivity values for the 45.3 at. % aluminium sample are markedly closer to platinum than the previous samples of 45.0 and 45.2 at. % aluminium composition. The temperature dependence of the 45.3 at. % aluminium sample is similar to both of the previous compositions considered in that it ceases to parallel that of platinum at higher temperatures.

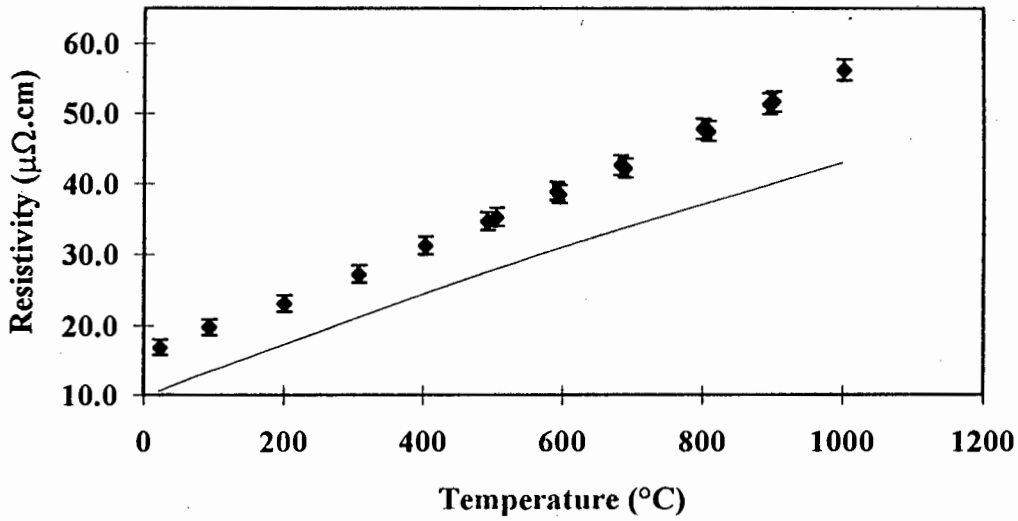

Figure 5.7: Variation with temperature of resistivity for the 45.7 at. % aluminium sample. The solid line represents the published platinum curve referred to in section 5.1.1.

The 45.7 at. % aluminium sample has similar behaviour to that of the 45.3 at. % aluminium sample and has a slightly higher resistivity than the 45.8 at. % aluminium sample, to be considered after this composition. The linearity of the resistivity vs. temperature curve is retained in this composition as is the departure from the platinum curve at higher temperatures.

This specimen was originally a longitudinal section of the hot isostatically pressed cylinder cut from one end of the cylinder and not a transverse section from the central section of the hot isostatically pressed cylinder as were all other specimens. The difference in resistivity behaviour is highlighted and discussed in the next chapter and related to this slight difference in specimen preparation.

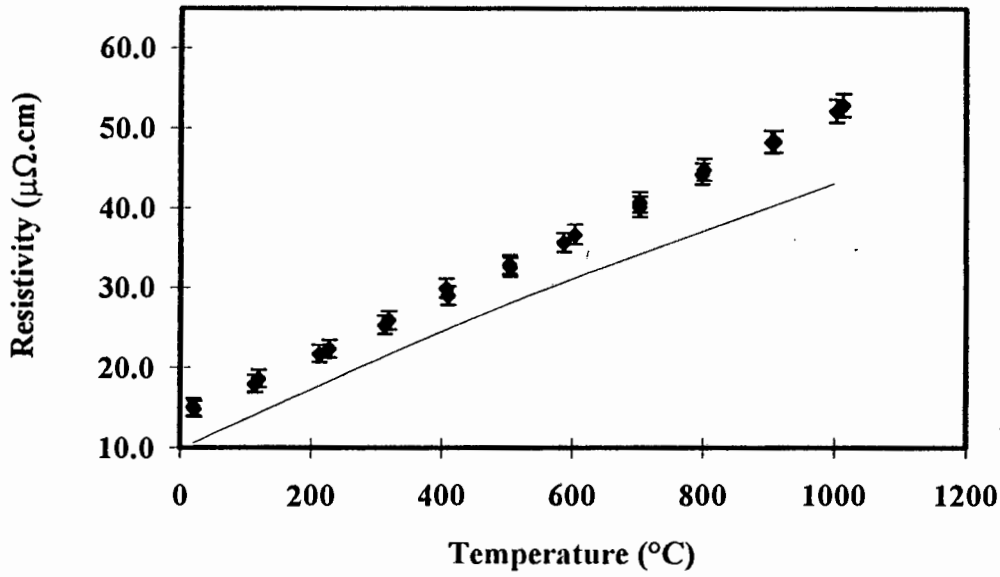

Figure 5.8: Variation with temperature of resistivity for the 45.8 at. % aluminium alloy. The solid line represents the published platinum curve referred to in section 5.1.1.

The 45.8 at. % aluminium sample parallels platinum's resistivity behaviour with temperature more closely than all the other ruthenium aluminium compositions as shown in Figure 5.8. The 45.7 at. % aluminium sample has a higher resistivity and a stronger temperature dependence than the 45.8 at. % aluminium sample. These differences cannot be accounted for in terms of the experimental error.

The 45.8 at. % aluminium sample shows the same linear dependence on temperature as the previous compositions and good correlation between readings from different runs to high temperature. All readings at similar temperatures fall within each other's experimental deviation.

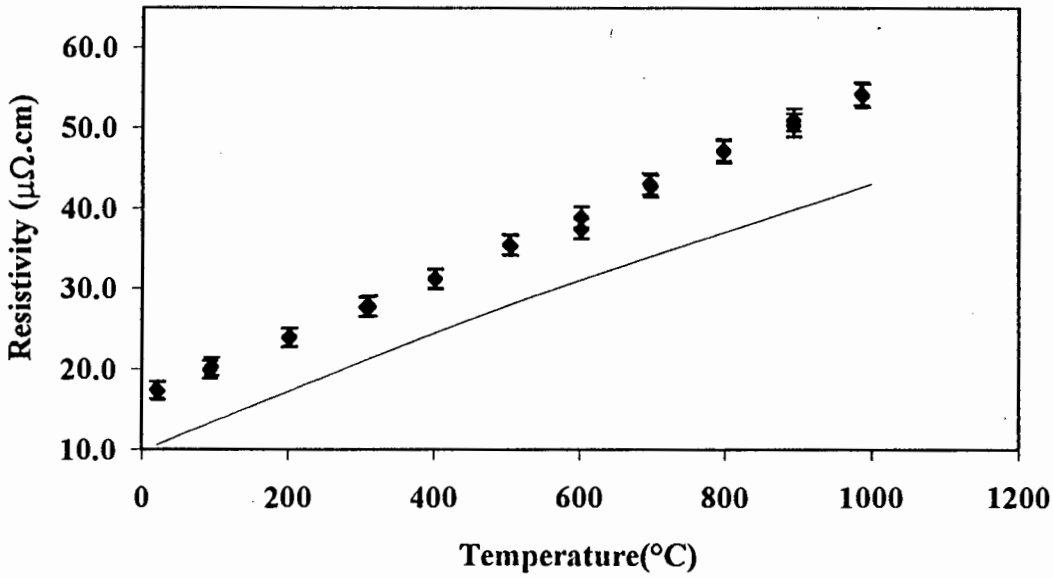

Figure 5.9: Variation with temperature of resistivity for the 46.7 at. % aluminium alloy. The solid line represents the published platinum curve referred to in section 5.1.1.

Comparing the 46.7 at. % aluminium sample's resistivity dependence on temperature in Figure 5.9 to that of the 45.8 at. % aluminium sample shows how the composition influences the resistivity and its dependence on temperature. The behaviour of the 46.7 at. % aluminium sample is similar to the previous compositions in its linear behaviour and deviation from platinum resistivity vs. temperature curve at higher temperatures, but its room temperature resistivity is closest to that of the 45.0 at. % aluminium sample. The correlation between resistivity measurements taken at similar temperatures is observed again, illustrating the same lack of dependence of resistivity on temperature cycling exhibited by all these compositions and the reproducibility of these results.

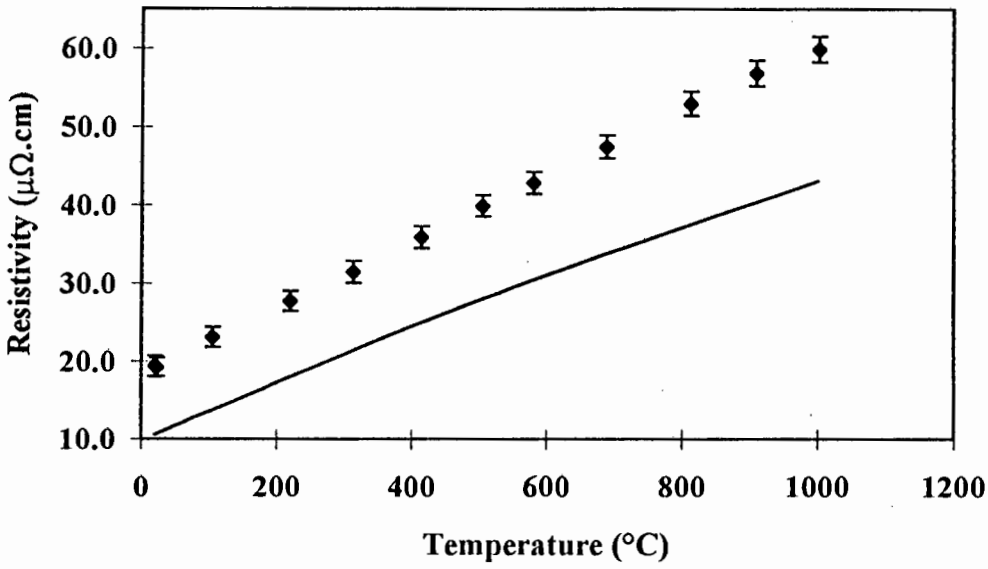

Figure 5.10: Variation with temperature of resistivity for the 49.0 at. % sample. The solid line represents the published platinum curve referred to in section 5.1.1.

The 49.0 at. % aluminium sample shows the greatest resistivity at room temperature of all the samples with compositions near 50 at.% aluminium. This was shown to be reproducible at room temperature and the same linear dependence on temperature was observed.

5.1.3 Summary

The dependence of resistivity on temperature in both eutectic and near-stoichiometric compositions is linear, and does not display any hysteresis on temperature cycling. Eutectic compositions have a greater room temperature resistivity but a weaker dependence of resistivity on temperature. There also exists a concentration at which the resistivity of ruthenium aluminium is close to that of platinum, and parallels the dependence of the resistivity of platinum on temperature closely.

Table 5.1: Resistivity results for platinum and ruthenium-aluminium from 20°C to 1000°C

Sample	**Pt**	**Ruthenium-aluminium (in at.% aluminium)**									
Composition	**Pure Pt**	29.7	30.2	45.0	45.2	45.3	45.7	45.8	46.8	49.0	
Temperature (°C)	**(resistivity in micro-ohm.centimeters)**										**uncertainty**
20	11.1	23.8	23.2	17.8	16.2	15.8	16.7	15.1	17.5	19.4	1
100	14	26.2	26.2	21.0	19.3	19.7	20.0	17.4	20.5	22.9	1.1
200	17.5	29.7	29.5	24.5	23.4	22.8	23.1	21.2	23.9	26.9	1.1
300	21.5	33.2	33.2	28.5	27.1	25.5	26.9	24.8	27.4	30.9	1.2
400	25.3	36.8	36.3	32.6	31.1	30.7	31.2	29.6	31.1	35.3	1.2
500	28.6	40.4	39.9	36.6	35.3	34.5	35.1	32.7	35.3	39.7	1.2
600	31.6	43.8	42.9	40.6	39.1	38.2	38.7	36.5	38.9	43.7	1.3
700	34.5	46.5	46.0	45.1	43.5	42.6	42.7	40.0	42.8	48.0	1.3
800	37.3	50.5	49.4	49.0	47.4	46.8	47.8	44.7	47.3	52.4	1.4
900	40.1	53.8	52.9	53.1	51.2	51.0	51.7	48.1	50.5	56.5	1.4
1000	43.1	57.1	56.0	57.2	55.4	54.5	56.1	52.0	54.5	59.8	1.5

Table 5.2: Slope of resistivity curves (dρ/dT) and temperature coefficients for platinum and ruthenium-aluminium

		Ruthenium-aluminium samples (composition in at. % aluminium)								
Sample	**Pure Pt**	**29.7**	**30.2**	**45.0**	**45.2**	**45.3**	**45.7**	**45.8**	**46.7**	**49.0**
dρ/dT (μΩ.cm/°C)	3.33E-02	3.44E-02	3.36E-02	4.02E-02	4.02E-02	3.89E-02	4.01E-02	3.81E-02	3.82E-02	4.20E-02
σ in dρ/dT (μΩ.cm/°C)	4.63E-04	2.44E-04	2.98E-04	3.44E-04	3.76E-04	4.71E-04	4.03E-04	2.38E-04	3.47E-04	2.48E-04
temp coefficient (1/°C)	3.00E-03	1.45E-03	1.45E-03	2.26E-03	2.48E-03	2.46E-03	2.39E-03	2.53E-03	2.19E-03	2.17E-03
σ temperature coefficient (1/°C)	2.74E-04	6.18E-05	6.38E-05	1.28E-04	1.55E-04	1.59E-04	1.45E-04	1.68E-04	1.26E-04	1.12E-04

5.2 Thermo-e.m.f.

5.2.1 Thermo-e.m.f. of platinum and gold-palladium

Tests were performed on platinum and gold-palladium to calibrate the thermo-e.m.f. apparatus. The results were obtained on single temperature ramps to 400°C. Results agree closely with published values for gold-palladium[14] from the same nominal composition (i.e. $Au_{50}Pd_{50}$ (wt.%)) and with values published for platinum[6], which gives confidence in the apparatus and the results obtained for ruthenium-aluminium. The results do not adhere strictly to the published curves but are spread narrowly over the expected trends. This reflects the measurement technique's inherent error of approximately 2.5% as is explained in section 4.1.3.3. Nevertheless the equipment's ability to accurately reflect the temperature dependence of thermo-e.m.f. for platinum and gold-palladium is shown. It was particularly important that accurate results be obtained for platinum as the small thermo-e.m.f of platinum would have generated small voltages similar to that of ruthenium-aluminium alloys. If the apparatus had failed to measure platinum accurately then accurate results for the ruthenium-aluminium system would not have been achieved.

5.2.2 Thermo-e.m.f of ruthenium-aluminium

The thermo-e.m.f. of ruthenium-aluminium is positive and increases linearly from 20°C to 400°C. The eutectic composition has a small positive thermo-e.m.f relative to compositions near 50 at. % aluminium. The compositions near 50 at. % aluminium have similar thermo-e.m.f's at room temperature but a variety of dependences of thermo-e.m.f on temperature. In order to construct isothermal composition curves, a linear regression was performed on each samples' thermo-e.m.f. vs temperature curve. Correlation coefficients for these curves were generally higher than 0.96. In order to make comparison easier the results are presented in groups. The two lowest aluminium concentrations are compared first and then second and third lowest and so on.

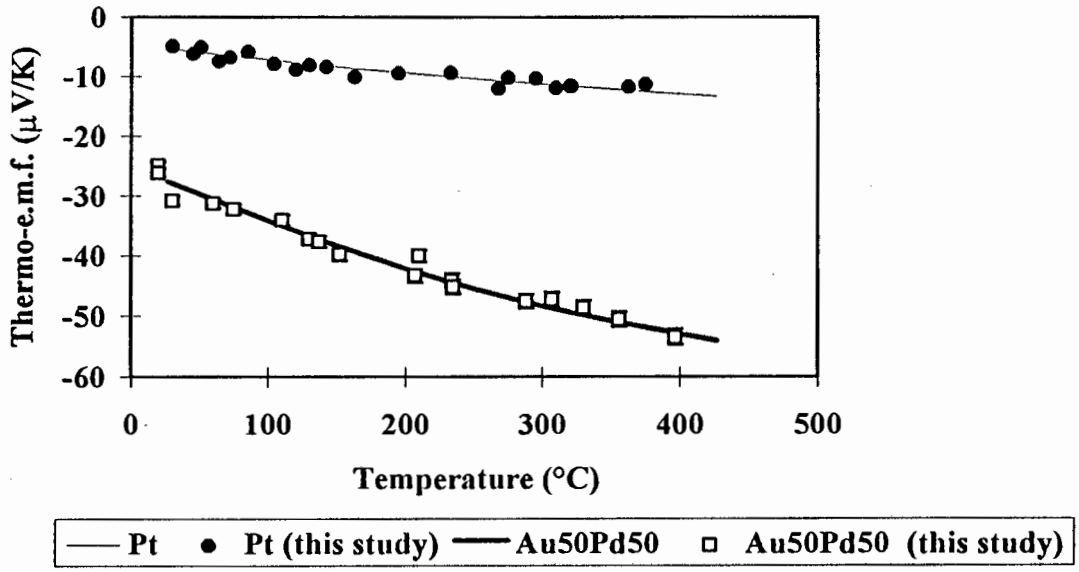

Figure 5.11: Thermo-e.m.f. vs temperature for Pt and AuPd. The results of this study are indicated and the published curves for platinum[6] and gold-palladium[14] are represented by the thin and thick solid lines respectively.

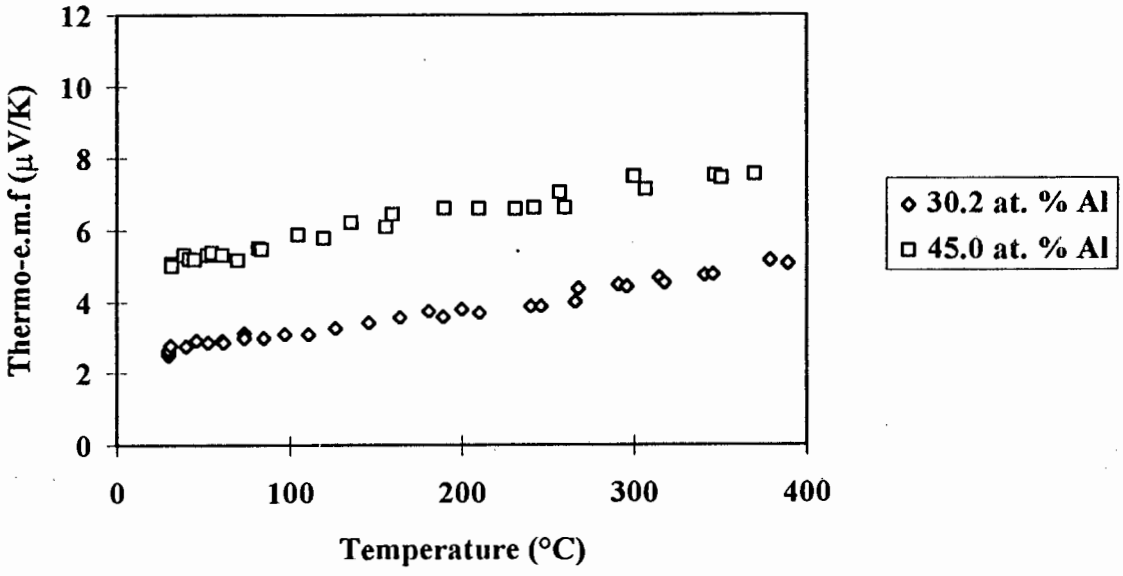

Figure 5.12: Variation of thermo-e.m.f. with temperature for the 30.2 and 45.0 at..% aluminium samples.

There is a marked difference in thermo-e.m.f. shown in Figure 5.12 between the 30.2 at. % aluminium alloy and the 45.0 at. % aluminium alloy. The thermo-e.m.f curves are approximately parallel and linear. The close grouping of the results of each sample shows reproducibility. It is not expected that the measurement temperatures will alter the samples in any way.

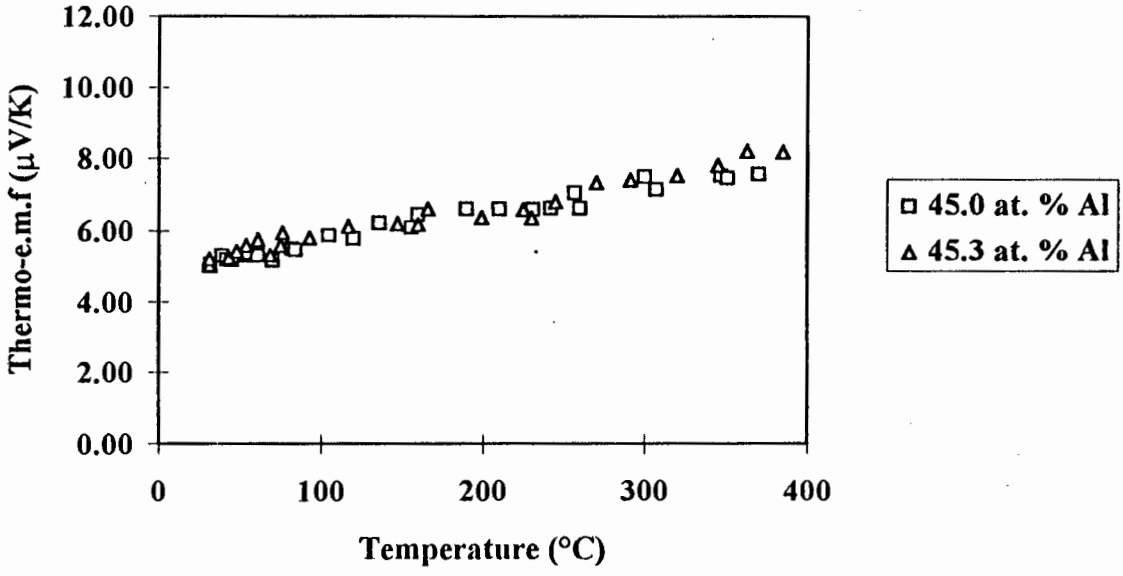

Figure 5.13: Variation of thermo-e.m.f. with temperature for the 45.3 at. % aluminium, and 45.0 at. % aluminium alloys.

The linear behaviour observed in Figure 5.12 for the 45.0 at. % aluminium alloy persists for the 45.3 at. % aluminium alloy shown in Figure 5.13 and there is a strong overlap in thermo-e.m.f. between the 45.0 at. % aluminium alloy and the 45.3 at.% aluminiuim alloy.

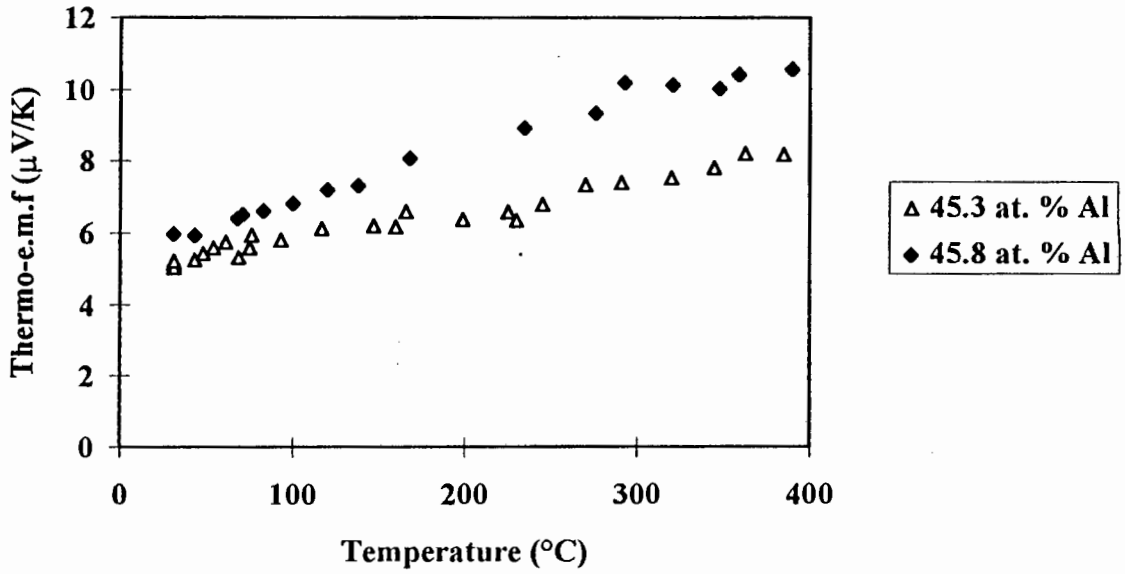

Figure 5.14: Variation of thermo-e.m.f. with temperature for the 45.3 at. % aluminium and 45.8 at. % aluminium alloys.

The measurements for the 45.3 at. % aluminium samples show in Figure 5.14 the linear trends observed for other compositions but the higher thermo-e.m.f. of the 45.8 at.% aluminium alloy and its stronger dependence of thermo-e.m.f on temperature mark this composition out as having very different electrical properties to the rest of the ruthenium-aluminium alloys.

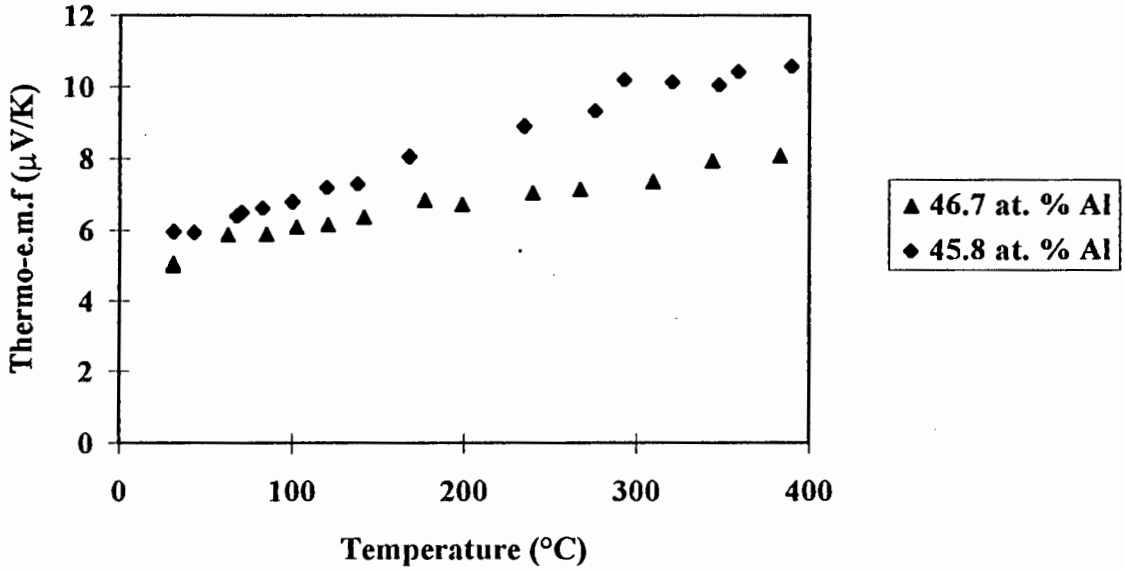

Figure 5.15: Variation of thermo-e.m.f. with temperature for the 45.8 at. % aluminium and 46.7 at. % aluminium samples.

In Figure 5.15 it can be seen that the increase in aluminium concentration from 45.8 to 46.7 at. % aluminium does not lead to a further increase in thermo-e.m.f. but rather a drop and a decrease in the dependence of thermo-e.m.f. on temperature. The linear dependence of thermo-e.m.f. on temperature is still present in both compositions, but the unique properties of the 45.8 at.% alloy compared to other alloys near its composition indicate that there is definite dependence of thermo-e.m.f. on composition.

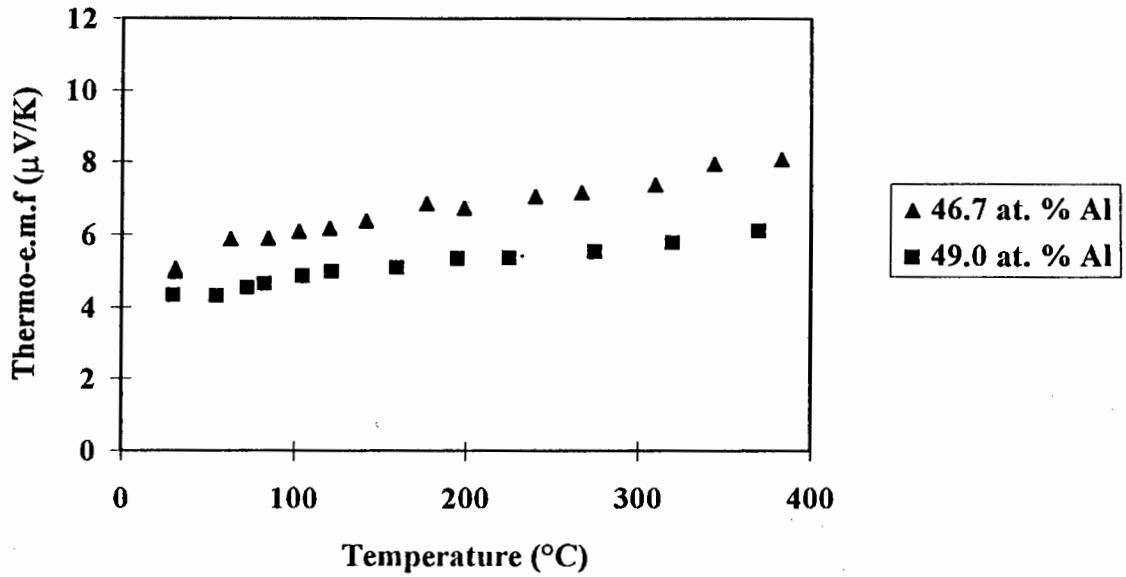

Figure 5.16: Variation of thermo-e.m.f. with temperature for the 46.7 at. % aluminium and 49.0 at. % aluminium alloys.

In Figure 5.16 the increase in aluminium concentration from 46.7 to 49.0 at. % aluminium is seen to decrease the thermo-e.m.f. and not to effect the linear dependence of thermo-e.m.f. on temperature. The 49.0 at. % alloy has the lowest thermo-e.m.f. of all the compositions near 50 at. % aluminium.

5.2.3 Summary

All the dependences of thermo-e.m.f on temperature. shown in Figures 5.12 - 5.16 are similar except for the 45.8 at. % aluminium sample which has a stronger temperature dependence. The two lowest thermo-e.m.f.'s are those exhibited by the eutectic composition (the 30.2 at. % aluminium sample) and the sample richest in aluminium (the 49.0 at. % aluminium sample).

The 45.8 at. % aluminium sample is the same sample which exhibited a minimum resistivity. Compositions that are both richer and poorer in aluminum than the 45.8 at. % aluminium sample have similar thermo-e.m.f.'s and dependences of thermo-e.m.f. on temperature.

Table 5.3: Thermo-e.m.f for ruthenium-aluminium alloys at various temperatures.

Temperature	**Composition in at. % aluminium**					
(°C)	30.2	45	45.3	45.8	46.7	49
	Thermo-e.m.f. in μV/K					
20	2.6	5.1	5.2	5.8	5.2	4.3
50	2.8	5.3	5.4	6.2	5.5	4.5
100	3.1	5.7	5.8	6.9	5.9	4.7
150	3.5	6.0	6.2	7.6	6.3	5.0
200	3.8	6.4	6.6	8.3	6.7	5.2
250	4.1	6.8	7.0	9.0	7.1	5.5
300	4.5	7.2	7.4	9.7	7.5	5.8
350	4.8	7.6	7.8	10.4	7.9	6.0
400	5.1	7.9	8.2	11.0	8.3	6.3

6. Discussion

This chapter will attempt to relate the measured electrical properties to composition and both electronic and atomic structure.

In Chapter Two the dependence of electrical properties on electronic structure in a number of materials was reviewed. A common approach was to explain this dependence on the basis of the variation of the density of states with electron energy and to refer to the Fermi surface (where this information was available). The electronic structure was also seen to depend on the atomic structure and composition. The atomic structure and composition are interdependent and dependent on the processing route employed. In Chapter Three, after the evaluation of a number of possible tools and approaches, it was decided to use EDS as the means of determining composition and to base explanations of the electrical properties, in part, on the relative amounts on aluminium present in the ruthenium alloys. In Chapter Four and Chapter Five the ability of the apparatus to accurately reflect the dependence of electronic properties on temperature was shown and results were reported that enable the dependence of the electrical properties on temperature and composition to be discussed.

The discussion of the electrical properties of ruthenium-aluminium alloys will use the calculated variation of the density of states with energy for ruthenium aluminide[2] but the application is not direct. It can be appreciated that variations in processing could result in a different density of APB. A lower than stoichiometric composition of aluminium may result in a drop in the electron concentration and thus in the Fermi energy possibly leading to a different dependence of the density of states on electron energy at that Fermi energy. Off-stoichiometric compositions further disrupt the ideal structure due to vacancies and substitutions in the lattice which can effect the assumptions made in calculating the variation of the density of states with energy.

The dependence of resistivity on temperature in gold-palladium vs. that of platinum will be discussed as there is no direct comparison made in the literature reviewed. This discussion will prove useful as the dependence of resistivity on temperature in the ruthenium-aluminium system is similar to that of platinum.

For ease of reference the partial variation of the density of states with energy for ruthenium aluminide after Lin et al[2], the equilibrium phase diagram of the ruthenium-aluminium system after Boniface and Cornish[22], and the dependence of thermo-e.m.f. and resistivity on temperature in the ruthenium-aluminium system reported in the previous chapter are reproduced in this chapter. Also included are graphs of the dependence of thermo-e.m.f. and resistivity on composition in the ruthenium-aluminium system.

6.1 Resistivity

The temperature dependence of resistivity of ruthenium-aluminium is similar to that of platinum and some compositions exhibit resistivities close to that of platinum. The following sections will attempt to provide explanations firstly for the values of resistivity at room temperature of ruthenium-aluminium alloys vs. platinum and gold-palladium and secondly for the temperature dependences observed.

6.1.1 Room temperature resistivity values

The minimum resistivity of the ruthenium-aluminium alloys near 50 at.% is greater than that of platinum but less than that of gold-palladium. The ruthenium-aluminium alloys are more resistive than platinum partly because of the higher resistivity associated with alloying[7]. The contribution of alloying to resistivity also explains the relatively high resistivity of gold-palladium. This contribution should be highest near equi-atomic compositions where there is maximum disruption of the host lattice[7]. In the ruthenium aluminium system the ordered ruthenium aluminide phase exists near equiatomic

compositions as shown in Figure 6.1. The consequence of disorder in a crystal lattice is that electrons are more likely to be scattered causing an increase in resistivity. Ordering at the equiatomic composition in the ruthenium aluminide system should cause a drop in resistivity as shown in Figure 6.2 which offsets the increase in resistivity associated with alloying. This explains why some compositions of ruthenium-aluminium alloys near 50 at. % aluminium have resistivities close to that of platinum. The degree of order of the atomic structure is not the only contribution to resistivity, however.

Platinum, gold-palladium of composition $Au_{48.4}Pd_{51.6}$ and the ruthenium-aluminium alloys considered here are expected to have s-d scattering contributions to their resistivity. The electronic structure of platinum and gold-palladium was dealt with in Chapter Two. The variation of the density of states with energy of ruthenium aluminide also shows potential for s-d scattering in that the d band ovelaps the s band at the Fermi energy as shown in Figure 6.3 and Figure 6.4. It is expected that this contribution should decrease with increasing aluminium concentration as aluminium s and p electrons fill the ruthenium d band. Calculations made for this study indicate that this should occur near 80 at. % aluminium.

The resistivity of ruthenium-aluminium vs. composition exhibits a minimum over compositions which fall within the ordered ruthenium aluminide phase field as can be seen by comparing the dependence of resistivity on composition, shown in Figure 6.2., with the equilibrium phase diagram of the ruthenium aluminium system ,shown in Figure 6.1. The transition metal aluminide systems reviewed in Chapter Two all show ordering dependent resistivity phenomena near 50 at.% aluminium, and the aluminium concentration range over which the resistivity minimum is observed in the cobalt aluminium and nickel aluminium systems depends on the width of the aluminium concentration range over which the ordering takes place (i.e. the width of the aluminide's phase field)[18,19].

To illustrate this point the equilibrium phase diagram for the nickel aluminium system together with the dependence of the resistivity on compositon are reproduced in Figure 6.5 and Figure 6.6 respectively.

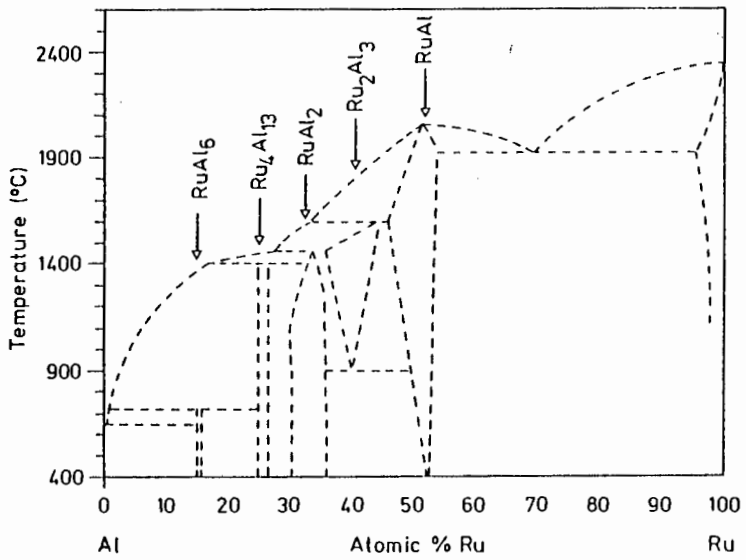

Figure 6.1: The equilibrium phase diagram of the ruthenium aluminium system (after Boniface and Cornish[22]).

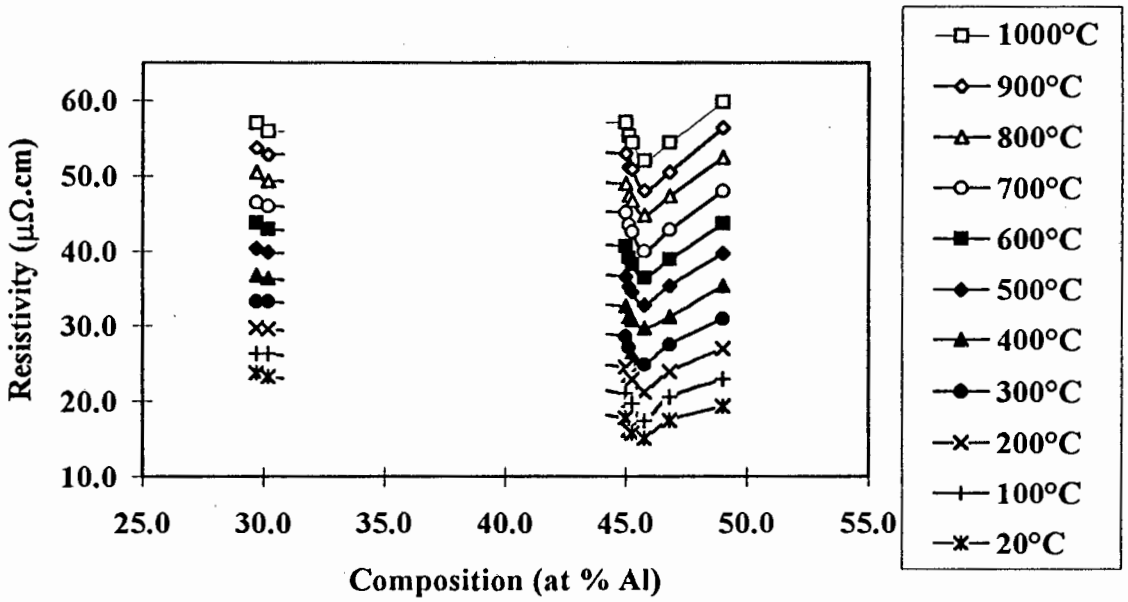

Figure 6.2: The dependence of resistivity on composiiton in the ruthenium-aluminium system at various temperatures showing a clear minimum near 50 at. % aluminium.

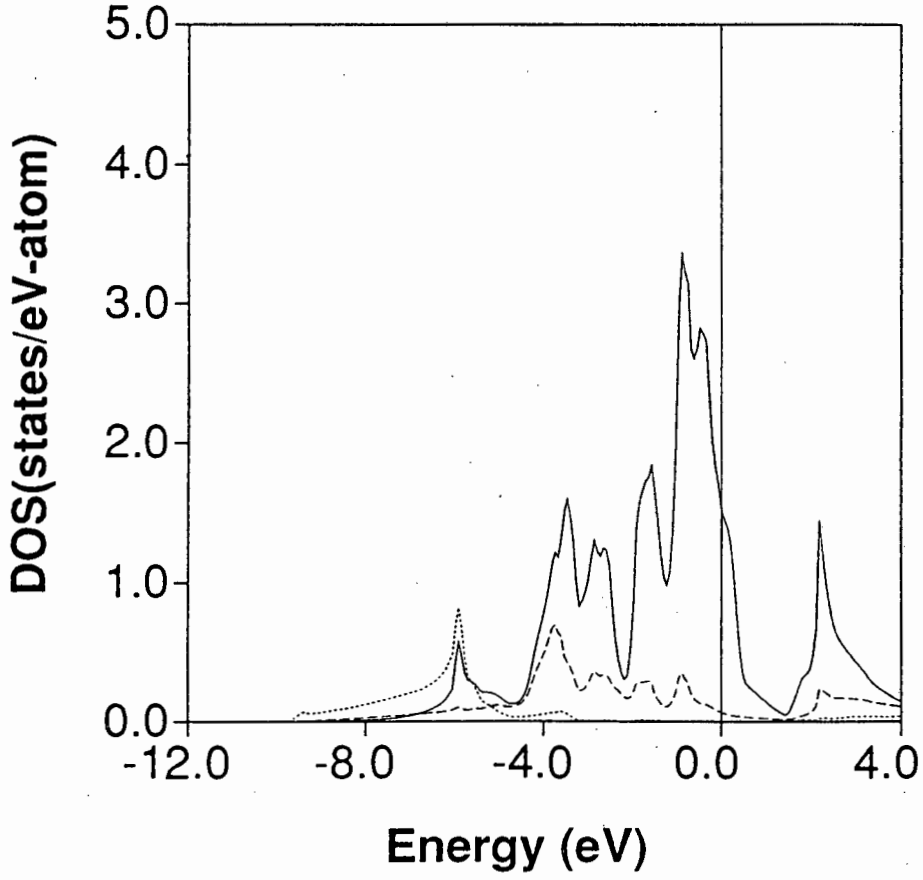

Figure 6.3: Calculated partial variation of the density of states with energy of ruthenium aluminide, without allowing for APB energy (after Lin et al[2]).

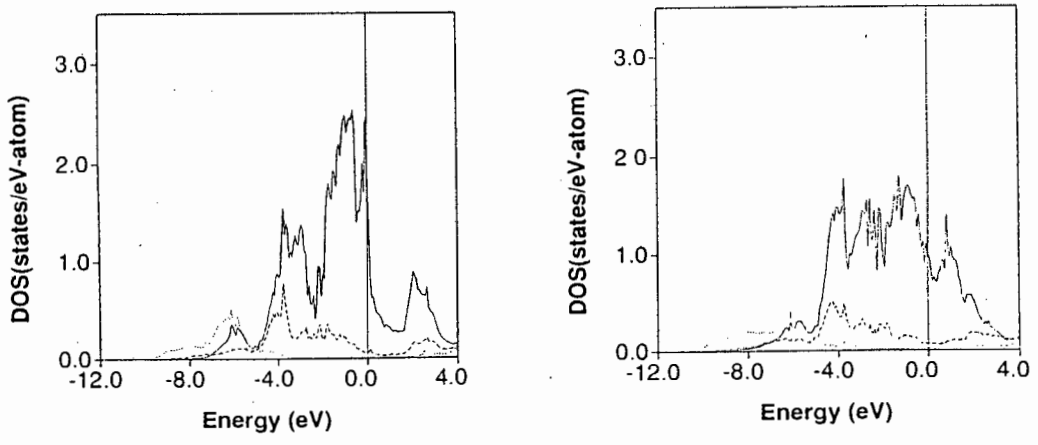

Figure 6.4: Calculated partial variation of the density of states with energy (with APB): a) Ru-site 1 and b) Ru-site 2 (after Lin et al[2]).

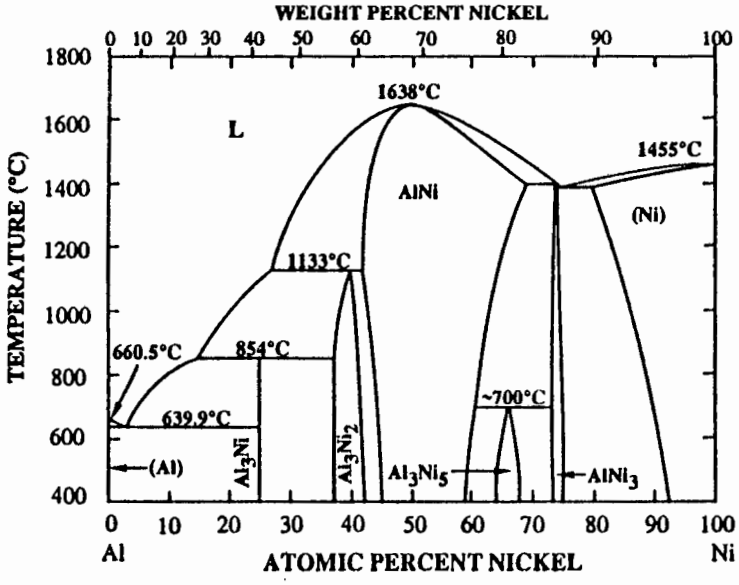

Figure 6.5: Equilibrium phase diagram of the nickel aluminium system (after Miracle[36]).

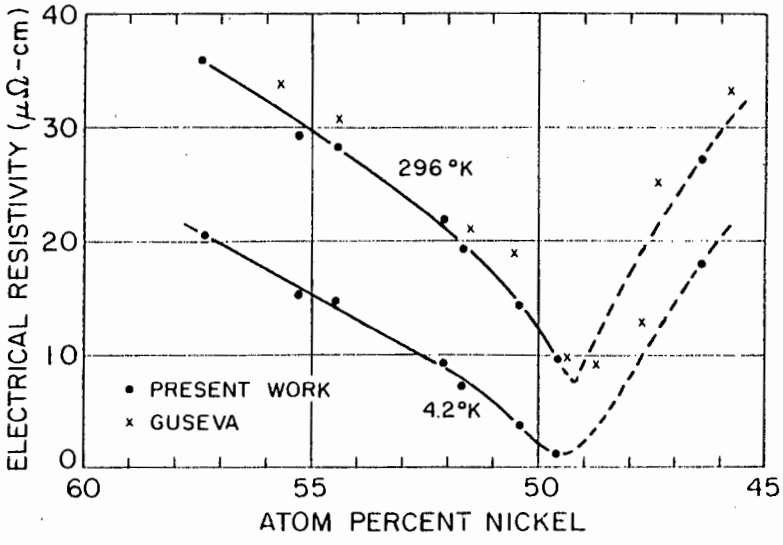

Figure 6.6: The dependence of resistivity on composition in the nickel aluminium system near 50 at. % aluminium (after Sellmyer et al[18]).

In the cobalt-aluminium system the cobalt aluminide phase field exists from approximately 47 at. % aluminium to 57 at. % cobalt[19]. A comparison with the dependence of resistivity on composition shown in Figure 6.7 shows that the aluminium concentration range over which the resistivity minimum occurs corresponds with these compositions.

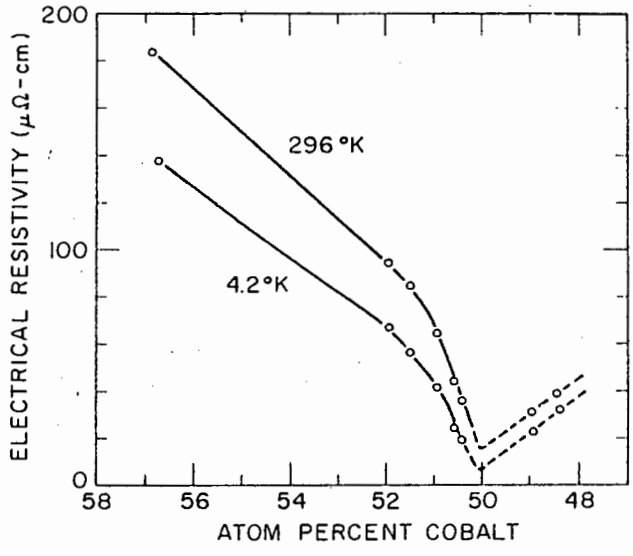

Figure 6.7: The dependence of resistivity on composition in the cobalt-aluminium system near 50 at. % aluminium (after Sellmyer et al[19]).

The depth of the resistivity minimum observed is dependent on the degree of order at the stoichiometric composition and the electronic structure at that composition. Nickel aluminide approximates a 3/2 electron compound[18], has a high degree of order and has a wide phase field. The contribution of s-d scattering to resistivity in nickel aluminide is expected to be relatively small in view of the low density of d-states at the Fermi energy. The combination of the wide phase field and the low resistivity at the stoichiometric composition cause a deep wide minimum to be observed in the resistivity vs. composition curve. Cobalt aluminide's resistivity minimum is less deep than that of nickel aluminide as

it has some electron compound features in its atomic structure but it also has a higher density of unfilled d states so that s-d scattering is expected to increase the resistivity[19]. Iron aluminide is more disordered and has the least filled d-band of the three and no minimum is observed but rather an inflection point on the resistivity vs. composition curve[18]. Ruthenium-aluminium's relatively narrow resistivity minimum over a range of 5 at.% aluminium corresponds to the narrow ruthenium aluminide phase field. The shallow minimum could be because the drop in resistivity owing to ordering is offset by the s-d scattering still occuring at that composition. or that the ruthenium aluminide phase field is less ordered.

In the previous chapter in section 5.1.2.2 reference was made to the anomalous results obtained for the 45.7 at. % aluminium sample. This sample was from a longitudinal section of the end of a hot isostatically pressed cylindrical bar as opposed to other samples which are transverse sections from the center of the bar. The processing route followed, which includes an exothermic reaction at 650°C, can be expected to influence the degree of order. It is possible that the temperatures experienced by the part of the bar from which the 45.7 at. % aluminium sample was cut were at variance with those experienced during the processing by the rest of the bar, resulting in a difference in the degree of order. Ruthenium-aluminium alloys are not sensitive to heat treatment after processing, as is borne out by the linear dependence of resistivity on temperature, so it is assumed that the anomalous result has its origin in the processing route. The work by Sellmyer et al[18,19] is a study of a collection of results by various workers and some of the values measured for the same compositions vary by as much as 20-30%. This is attributed by Sellmyer et al to varying sample purity and order. The significance of this is that optimizing ruthenium-aluminium alloys for low resistivity not only requires careful composition control in view of the narrow phase field but also a good understanding of the processing route and possible variables within it.

Atomic configuration in the homogenous phase fields influences the slopes of the resistivity vs. composition curves on either side of the minima near 50 at. % aluminium in

transition metal aluminide systems. This behaviour can be seen in both the nickel-aluminium system and the cobalt-aluminium system. In nickel aluminide the excess aluminium atoms are accomodated at nickel sites initially (up to 50.76 at. % aluminium) thereafter vacancies substitute for the nickel at nickel sites[18]. Excess nickel is accomodated at aluminium sites in nickel-rich concentrations. This results in a nickel atom having eight like nearest neighbours. Cobalt-aluminium behaves in a similar fashion, with vacancies substituting cobalt in compositions of more than 50 at.% aluminium[19] while iron aluminium does accomodate excess aluminium at iron sites[18]. It is expected that different types of defects will scatter electrons with different strengths[19]. The difference in defect structure on either side of the stoichiometric compositions can be expected to lead to different dependences of resistivity on composition on either side of the resistivity minima. Fleischer finds that the ruthenium-aluminium system follows a hybrid of the two mechanisms mentioned above with both aluminium and vacancies occuring at ruthenium sites[3]. This accounts for the different slopes observed in the dependence of resistivity on composition near 50 at. % aluminium as shown in Figure 6.8.

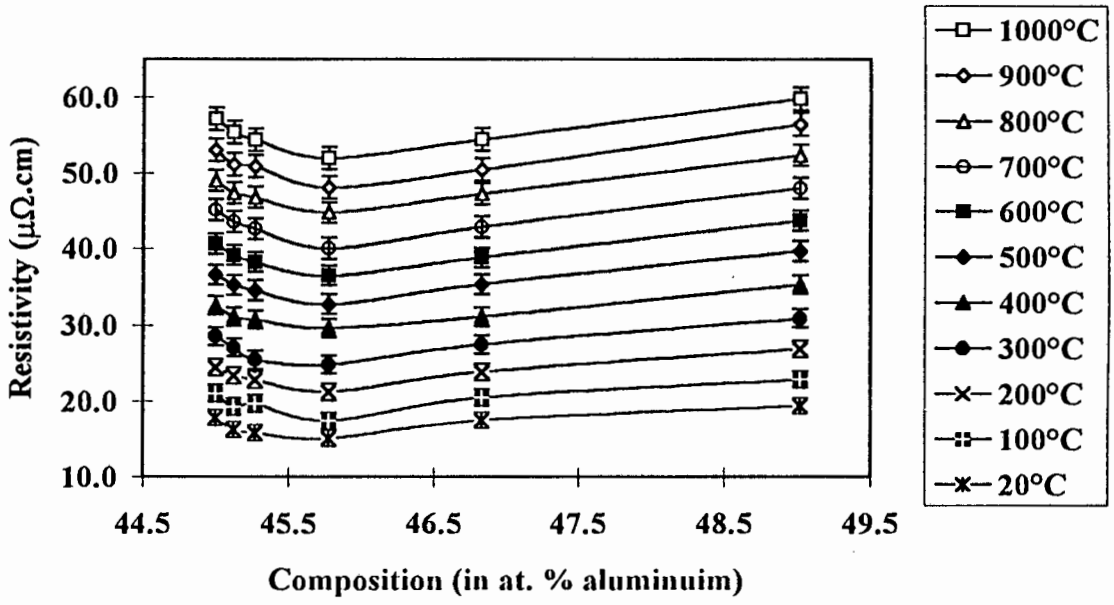

Figure 6.8: The dependence of resistivity on composition in the ruthenium-aluminium system near 50 at. % aluminium.

6.1.2 Dependence of resistivity on temperature of ruthenium-aluminium vs. platinum and gold-palladium

The most striking features of the dependence of resistivity on temperature in the materials examined is the weak dependence of resistivity on temperature in gold-palladium, shown in Figure 5.1, and the similarity in the dependence of resistivity on temperature in ruthenium-aluminium and platinum, shown in Figure 6.9. The resistivity of ruthenium-aluminium is seen to have a linear dependence on temperature. The plots in Figure 6.9 were made with measurements taken from two ramps to high temperature. The stability of the atomic structure of ruthenium aluminium and its lack of susceptibility to heat treatment is evident from the linearity and absence of hysteresis in these plots.

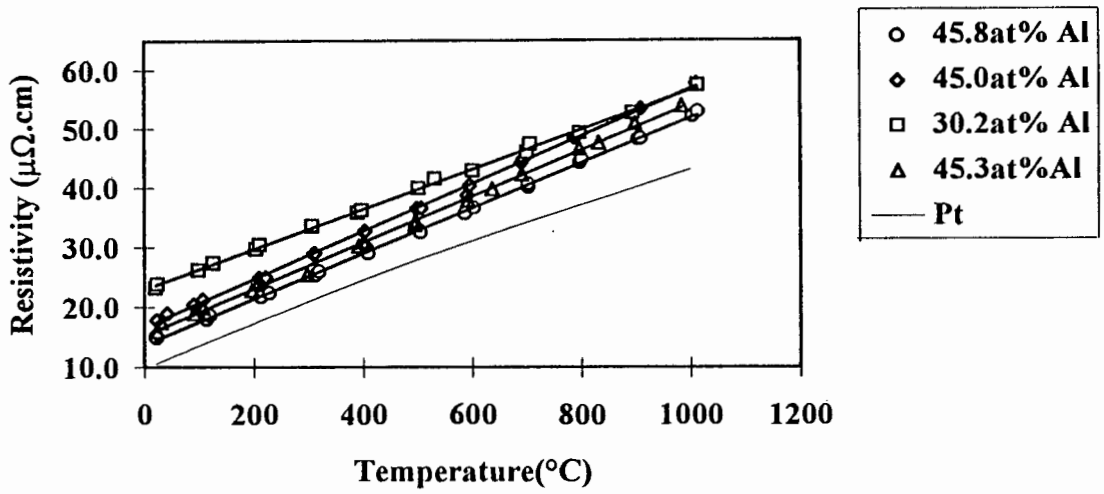

Figure 6.9: Dependence of resistivity on temperature for platinum[4] and selected compositions of ruthenium-aluminium.

Consistent resistivity behaviour with repeated cycling to high temperatures is an important feature required for high temperature electrical applications. Pure metals not subject to allotropic changes are generally considered the best candidates, particularly if low resistivity is required, but ruthenium-aluminium alloys are seen in Figure 6.9 to compare favourably with platinum, one of the most commonly used high temperature conductors.

The weak dependence of resistivity on temperature in gold-palladium as compared to that of platinum can be rationalized by comparing two similar equations which hold for these metals. These equations link the resistivities of platinum and gold-paladium to temperature and to their density of d and s electron states at the Fermi energy[15,16].

Platinum's electrical properties vary with temperature in a similar way to that of palladium which has been modelled[15] with the following equation:

$$\rho \approx LN_s(E_F)T + MN_d(E_F)T(1 - AT^2) \qquad \text{Equation 6.1}$$

where L and M are constants, $N_s(E_F)$and $N_d(E_F)$ are the densities of states for the s and d bands and the E_F is the Fermi energy. The factor A allows for the thermal energy kT that is available to the electrons at the Fermi energy resulting in the value of $N_d(E_F)$ varying appreciably over the range E_F - kT to E_F + kT. This is only important at high temperatures and can result in the slight downward curvature of the Pt resistivity temperature curve. The factor A is calculated as follows:

$$A = \frac{\pi^2 k^2}{6}\left[3\left(\frac{1}{N(E)}\frac{dN(E)}{dE}\right)^2 - \frac{1}{N(E)}\frac{d^2N(E)}{dE^2}\right] \qquad \text{Equation 6.2}$$

where $N_d(E_F)$ is written N(E). The first term within the brackets in equation 6.2 will increase as kT increases with temperature as illustrated in Figure 6.10. The second term is a second derivative that reflects the nature of the curvature of the $N_d(E_F)$ curve e.g. an approximately linear variation with energy will result in a zero value and an increasingly downward curvature of the $N_d(E_F)$ curve will result in a large positive value. The larger $N_d(E_F)$ is, the smaller the effect of A.

The variation of the density of d states with energy in platinum[10] is shown in Figure 6.11 (band 5) and the potential for a large A coefficient can be seen in the linear region adjacent to the Fermi energy.

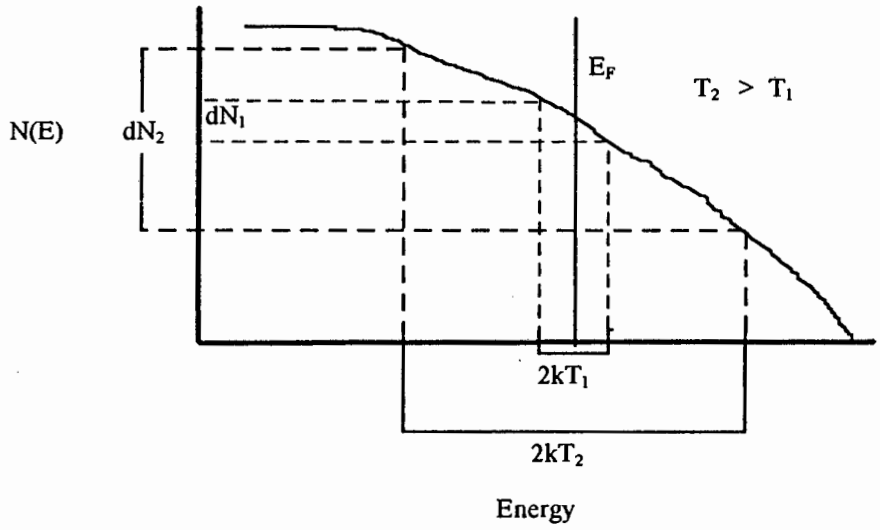

Figure 6.10: Schematic diagram showing the dependence of the variation of N(E) on width of thermal energy 2kT around the Fermi energy.

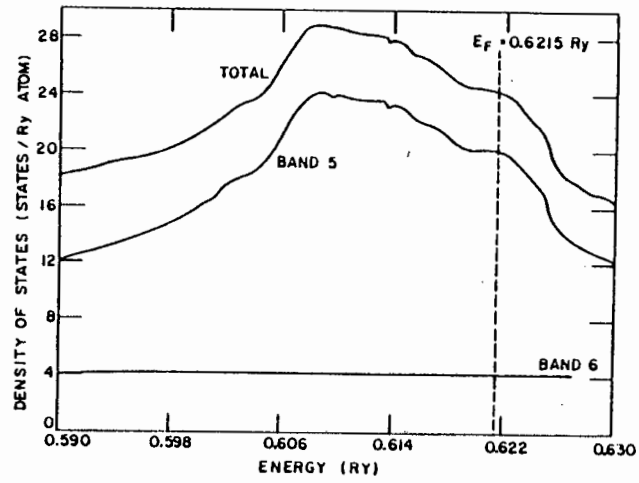

Figure 6.11: Variation of density of states with energy for platinum. Band 5 represents $N_d(E)$ (after Fradin et al[10]).

Gold-palladium's dependence of resistivity on temperature is similar to silver-palladium and is analysed on this basis by Rowland[16] after the study by Dugdale and Guenalt[15]. The resistivity can be written:

$$\rho = LN_s T + MN_d T\left(1 - AT^2\right) + \rho_{sd}\left(1 - AT^2\right) + \rho_{ss} \qquad \text{Equation 6.3}$$

The meaning of the terms is similar to that of equation 6.1. The third term in equation 6.3 dominates the first two terms, but these terms are the source of the linear temperature dependence. The density of d states is expected to be lower in gold-palladium than in platinum as the s electrons from gold fill the palladium d bands causing a shift in the Fermi energy relative to the d band resulting, in a lower density of d states at the Fermi energy[15]. The density of d states is also expected to be much higher than the density of s states and the second term is therefore expected to contribute most to the linear temperature dependence observed in gold-palladium. This contribution should be less than that from the similar term in equation 6.1 due to the expected lower density of d states in gold-palladium relative to platinum. This explains the weaker dependence of gold-palladium's resistivity on temperature.

Figure 6.11 shows the platinum d band (band 5) dominating the variation of the density of states for platinum. In ruthenium aluminide a similar dominance is observed in Figure 6.3 showing that the density of d states is much greater than the density of s states in both materials. This implies the dominance of the second term (in equations such as equation 6.1 and 6.3) over the first term in determining the temperature dependence. If an equation such as equation 6.3 could be applied to ruthenium-alumininium then a strong temperature dependence similar to that of platinum, originating from a large second term which in turn depends on the density of d states, could be rationalized. Also the high density of d states would keep the A factor in equation 6.3 low predicting a linear dependence on temperature as is observed for ruthenium-aluminium samples.

Eutectic ruthenium-aluminium alloys have a slightly lower dependence of resistivity on temperature. The changes in band structure with addition of aluminium may result in a different ratio of d to s states at ≈30 at. % aluminium. In the absence of information about electronic structure at these compositions it is not possible to explain the trend in terms of the reasoning above.

6.2 Thermo-e.m.f.

The two most noticeable features of the thermo-e.m.f. results are the positive sign of thermo-e.m.f. of ruthenium-aluminium as shown in Figure 6.12 and the peak in thermo-e.m.f. for ruthenium-aluminium as shown in Figure 6.13 at a composition which corresponds to a minimum in resistivity.

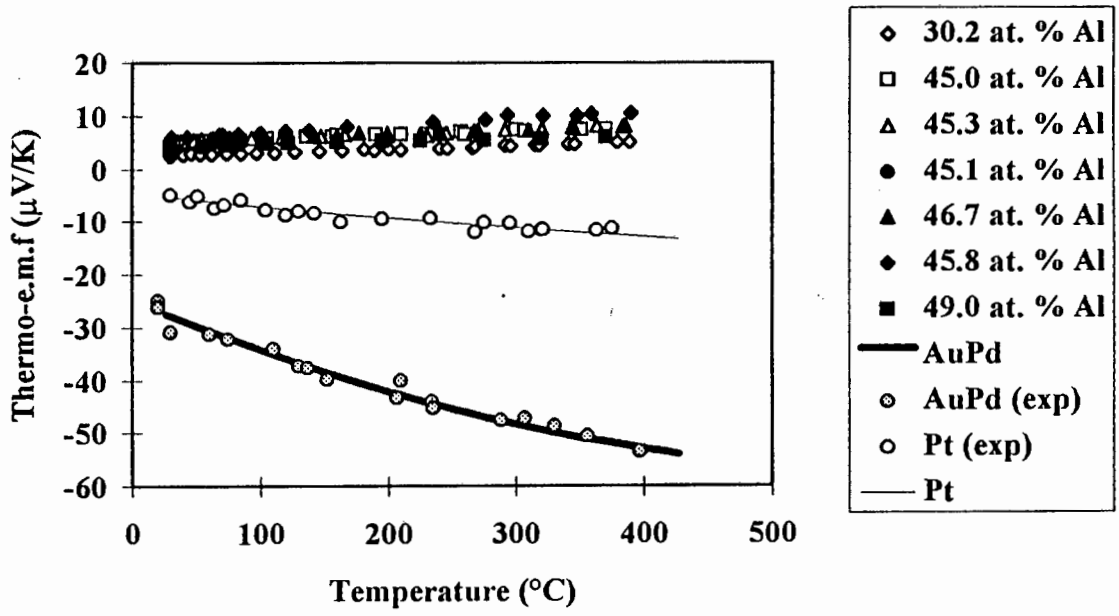

Figure 6.12: The dependence of thermo-e.m.f. on temperature for platinum, gold-palladium and ruthenium-aluminium. The thin and thick solid lines represent published results for platinum[6] and $Au_{50}Pd_{50}$,[14] while (exp) signifies results from the present work.

6.2.1 Sign of thermo-e.m.f. in ruthenium aluminium vs. platinum and gold palladium

The Mott equation introduced in Chapter Two is reproduced here to aid discussion:

$$S = \frac{-\pi^2 kT}{3|e|}\left[\frac{\partial \ln \sigma(E)}{\partial E}\right]_{E=E_F} \qquad \text{Equation 6.4}$$

The conductivity derivative can be written as follows:

$$\frac{\partial \ln \sigma(E)}{\partial E} = \frac{\partial \ln \Lambda}{\partial E} + \frac{\partial \ln \mathbf{A}}{\partial E} \qquad \text{Equation 6.5}$$

If the material is susceptible to s-d scattering then, the Λ being shorter for a higher probability of scattering, it is found that:

$$\Lambda \propto \frac{1}{N_d(E_F)} \qquad \text{Equation 6.6}$$

The variation of the density of d states with energy shown in Figure 6.3 for ruthenium aluminide shows it to have the potential for s-d scattering. According to Equation 6.6, Λ should be dependent on the density of d states. Near the Fermi energy at 50 at.% aluminium the density of d states is generally falling with energy. This should result in a negative contribution to the thermo-e.m.f from the first term in Equation 6.5. This reasoning is valid for both platinum and gold palladium which have a decreasing density of d states at Fermi energy and have negative thermo-e.m.f.'s.

Sellmyer et al[18,19] rationalized the thermo-e.m.f.'s of cobalt-aluminium and iron-aluminium solely in terms of the dependence of the thermo-e.m.f. on the density of d-states as information about the Fermi surface of cobalt aluminide and iron aluminide was not available. The Fermi surface of ruthenium aluminide has not been calculated yet but if it

were positioned near the Brillouin zone then the interaction between the Fermi surface and the Brillouin zone could give a positive contribution to the thermo-e.m.f, strong enough to result in a overall small positive thermo-e.m.f. Information on the Fermi surface of pure ruthenium is available but cannot be related to the ruthenium aluminide structure as pure ruthenium has a hexagonally close packed crystal structure and ruthenium aluminide has the B2 (BCC) CsCl structure.

The possibility of the density of d states increasing with energy at the Fermi energy exists when considering the variation of the density of d states with energy for ruthenium aluminide. Near the Fermi energy the small peak that exists, as shown in Figure 6.3 and Figure 6.4, could result in a positive contribution as the density of d states is increasing over a small energy interval. This explanation is not favoured as the Fermi energy will be moved relative to this peak by changes in composition or ordering. The possibility that the Fermi energy should always be within an energy interval where the density of d states is increasing with energy, leading to a positive contribution to the thermo-e.m.f., and that this condition be duplicated at 30 at.% aluminium (but to a lesser degree) resulting in a slightly smaller positive value, is small.

6.2.2 Dependence of thermo-e.m.f on composition in ruthenium-aluminium

The peak in thermo-e.m.f with respect to composition shown in Figure 6.13 is associated with the formation of the ruthenium aluminide ordered structure. This weights the argument in favour of the origin of the positive contribution being the interaction of the ruthenium aluminide compound's Fermi surface with the Brillouin zone boundary. This assumes that the composition at which there is a resistivity minimum represents the closest approach to the ordered B2 structure intermetallic compound ruthenium aluminide. This is a reasonable assumption as this is the trend for both cobalt-aluminium and nickel-aluminium[18,19].

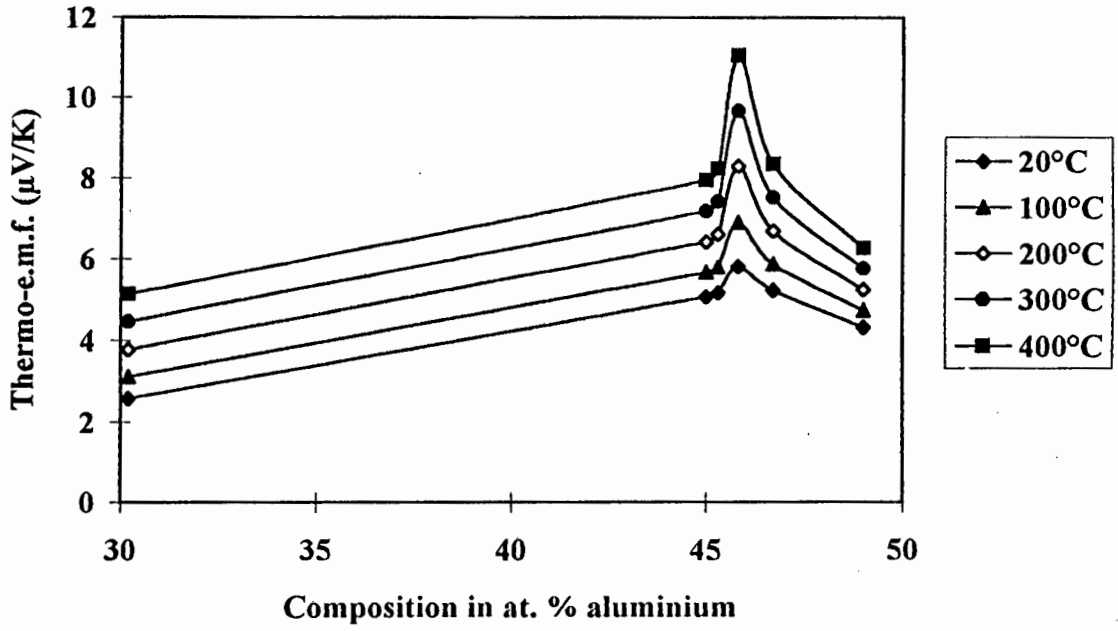

Figure 6.13: The dependence of thermo-e.m.f. on composition in the ruthenium-aluminium system at various temperatures.

A lack of information about the Fermi surface of ruthenium aluminide precludes an explanation based on the exact nature of the interaction but the interaction is expected to make its maximum contribution when the atomic structure of the samples are closest to that of the B2 ruthenium aluminide structure. In compositions further away from the composition of maximum order the B2 structure will be disrupted and the interaction will not be as strong leading to a decrease in the thermo-e.m.f.

Changes in the lattice parameter will effect the dimensions of the brillouin zone moving it closer to or further away from the Fermi surface. The Fermi surface is expected to be complicated due to the presence of d electrons at the Fermi energy as shown in Figure 6.3. Because of this complexity it is not easy to use data on the change in the lattice parameter to determine whether the change in the Brillouin zone dimensions will strengthen or weaken a positive contribution to the thermo-e.m.f.. Fleischer finds that the lattice parameter is constant on the ruthenium-rich side of the equiatomic composition and

increases on the aluminium-rich side[3]. The dependence of thermo-e.m.f on composition in the ruthenium-aluminium system as shown in Figure 6.13 does not reflect this behaviour.

An alternative explanation is that if it is the formation of the ordered structure that causes a positive contribution to thermo-e.m.f, the decrease in the thermo-e.m.f. to either side of the ruthenium aluminide phase field could be ascribed to the expected decrease in volume fraction of the B2 phase as the composition moves away from the ruthenium aluminide phase field, leading to a decrease in the positive contribution to the thermo-e.m.f. Studies have shown that in aluminium-poor compositions an intergranular ruthenium-α phase forms and in aluminium-rich compositions an intergranular phase consisting of various aluminium-rich intermetallics forms[1].

The dual phase eutectic has some ruthenium aluminide and ruthenium-α present and shows a small positive value for thermo-e.m.f. The contribution to a positive thermo-e.m.f will be diminished as B2 ruthenium aluminide is not the bulk phase.

6.3 Summary

The dependence of resistivity on composition in the ruthenium-aluminium system can be explained in terms of the effects of ordering at the equiatomic composition and the contribution of s-d scattering to resistivity. The dependence of resistivity on temperature for the ruthenium-aluminium system is similar to that of platinum and is attributed to the high density of d-states. The resistivity behaviour of the ruthenium-aluminium system is seen to be stable and not sensitive to repeated cycling to high temperatures.

The positive sign of thermo-e.m.f and the dependence of thermo-e.m.f. on composition in the ruthenium-aluminium system cannot be explained on the basis of the existing knowledge about the electronic structure of ruthenium aluminide. It is thought likely that the interaction of the Fermi surface with the Brillouin zone makes a positive contribution

to the thermo-e.m.f., overshadowing likely negative contributions from the variation of the density of d-states with energy.

7. Summary and Conclusion

- Apparatus appropriate to the accurate measurement of resistivity and thermo-e.m.f. of intermetallics has been constructed.
- The resistivity and thermo-e.m.f. of ruthenium-aluminium alloys have been measured to elevated temperatures for the first time.
- The dependence of resistivity on temperature for ruthenium-aluminium between 20°C and 1000°C is linear and remains linear after repeated cycles to high temperatures, implying microstructural stability, which is important in high temperature conductors.
- Ruthenium-aluminium has a minimum in resistivity dependent on composition which corresponds to a maximum in thermo-e.m.f.
- The minimum resistivity of ruthenium-aluminium and the dependence of this resistivity on temperature is similar to that of platinum.
- Optimizing ruthenium-aluminium alloys for low resistivity not only requires careful compositional control in view of the narrow ruthenium aluminide phase field but also a good understanding of the processing route and possible variables within it.
- The resistivity minimum is associated with the formation of the ordered ruthenium aluminide structure as is the maximum thermo-e.m.f.
- The maximum in thermo-e.m.f suggests that the ruthenium aluminide phase contributes positively to thermo-e.m.f. and the reason is expected to be the interaction of the Fermi surface with the Brillouin zone which dominates any negative contribution from a density of d states that is generally decreasing with increasing energy.

8. References

[1] R.L. Fleischer, R.D. Field and C.L. Briant
Metall. Trans. A. **22** 403 (1991)

[2] W. Lin, Jian-hua Xu and A.J. Freeman
J. Mater. Res. 7 592 (1992)

[3] R.L. Fleischer
Acta Metall. Mater. **41** 863 (1993)

[4] *Metals Reference Book*
Ed: C.J. Smithells
Butterworths London 1976

[5] R.J. Weiss
Physics of Materials
Hemisphere Publishing Corporation New York 1990

[6] N. Cusack and P.W. Kendall
Proc. Phys. Soc. 72 898 (1958)

[7] P.L. Rossiter
The Electrical Resistivity of Metals and Alloys
Cambridge University Press 1987

[8] J.M. Ziman
Electrons and Phonons
Cambridge University Press London 1972

[9] J.B. Ketterson and L.R. Windmiller
Phys. Rev. B **2** 4813 (1970)

[10] F.Y. Fradin, D.D. Koelling, A.J. Freeman and T.J. Watson-Yang
Phys Rev. B **12** 5570 (1975)

[11] N.F. Mott and H. Jones
The Theory of the Properties of Metals and Alloys
Clarendon, Oxford 1936

[12] J.S. Dugdale
The Electrical Properties of Metals and Alloys
Edward Arnold London 1977

[13] C.Y. Ho, M. W. Ackerman, K.Y. Wu, T.N. Havill, , R.A. Matula, S.G. Oh and H.M. James
J. Phys. Chem. Ref. Data **12** 183 (1983)

[14] C.Y. Ho, R.H. Bogaard, T.C. Chi, T.N. Havill and H.M. James
Thermochimica Acta **218** 29 (1993)

[15] J.S. Dugdale and A.M. Guenault
Phil. Mag. **13** 503 (1966)

[16] T. Rowland, N.E. Cusack and R.G. Ross
J. Phys. F: Metal Phys. **4** 2189 (1974)

[17] M.J. Kim and W.F. Flanagan
Acta Met. **15** 735 (1967)

[18] D.J. Sellmyer, G.R. Caskey and J.M. Franz
J. Phys. Chem. Solids **34** 1179 (1973)

[19] D.J. Sellmyer, G.R. Caskey and J.M. Franz
J. Phys. Chem. Solids **33** 561 (1972)

[20] M.C. Lovell, A.J. Avery and M.W. Vernon
Physical Properties of Materials
Van Nostrand Reinhold Company New York 1981

[21] A. Cottrell
Introduction to the Modern Theory of Metals
The Institute of Metals
London 1988

[22] T.D. Boniface and L.A. Cornish
Submitted to *Journal of Alloys and Compounds*

[23] D.W.McKee and R.L. Fleischer
High-Temperature Ordered Intermetallic Alloys IV
Materials Research Soceity Symp. Proc. **213** 969 (1991)
L.A.Johnson, D.P.Pope, and J.O. Stiegler, eds.
Materials Research Soceity , Pittsburgh P.A.

[24] R.L. Fleischer and D.W.McKee
Met. Trans. A **24A** 759 (1993).

[25]R.L. Fleischer
ISIJ International **31** 1186 (1991).

[26] L.J. van der Pauw
Philips. Res. Repts. **13** 1 (1958).

[27] D.Cahen, J.R. Hahn and J.R. Anderson
Rev. Sci. Instrum. **44** 1567 (1973).

[28] J.Papaioannou and J.L. Dye
Rev. Sci. Instrum. **59** 496 (1988).

[29] L. Plomp, J.A.M. van Rossmalen and E.H.P. Cordfunke
Rev. Sci. Instrum. **61** 1949 (1990).

[30] M. Futamata
Meas. Sci. Technol. **3** 919 (1992).

[31] Y. Sun, O. Ehrmann, J. Wolf and H. Reichl
Rev. Sci. Instrum. **63** 3752 (1992)..

[32] Y. Sun, O. Ehrmann, J. Wolf and H. Reichl
Rev. Sci. Instrum. **63** 3757 (1992).

[33] J.D.Hodge and H.K. Bowen
J. Am. Ceram. Soc. **64** 431 (1981).

[34] P.C. Ecklund and A.K. Mabatah
Rev. Sci. Instrum. **48** 775 (1977).